

ER 8275

N 66-17 077

FACILITY FORM 602

(ACCESSION NUMBER)	(THRU)
124	1.
(PAGES)	(CODE)
CR 70.304	28
(NASA CR OR TMX OR AD NUMBER)	(CATEGORY)

Final Report

STUDY OF FUNDAMENTALS
OF
PRESSURANT DISTRIBUTOR DESIGN
NAS8-5416

January 1966

GPO PRICE \$

CFSTI PRICE(S) \$

Hard copy (HC) 4.00

Microfiche (MF) 1.00

Prepared For: ff 653 July 66

GEORGE C. MARSHALL SPACE FLIGHT CENTER

Prepared By:

LOCKHEED GEORGIA NUCLEAR LABORATORY

LOCKHEED GEORGIA NUCLEAR LABORATORY
Lockheed-Georgia Company - A Division of Lockheed Aircraft Corporation

FOREWORD

This report summarizes the work performed under Contract NAS8-5416, Study of Fundamentals of Pressurant Distributor Design, for the George C. Marshall Space Flight Center, NASA, Huntsville, Alabama.

TABLE OF CONTENTS

	Page
FOREWORD	i
TABLE OF CONTENT	ii
LIST OF TABLES AND FIGURES	v
1.0 SUMMARY	1
2.0 INTRODUCTION	3
3.0 — ANALYSES	4
3.1 FREE CONVECTION	4
3.2 FORCED CONVECTION	17
3.3 TEST TANK	29
3.4 FLIGHT TANK	33
3.5 SCALING ANALYSIS	33
3.6 DESCRIPTION OF SYMBOLS	<u>40</u>
4.0 EXPERIMENTS	42
4.1 SMOKE TEST CHAMBER	42
4.2 — SELECTION OF GOOD DISTRIBUTOR	42
4.3 SELECTION OF POOR DISTRIBUTOR	44
4.4 FLUID DYNAMICS SYSTEM	<u>48</u>
4.5 LIQUID TRANSFER SYSTEM	48
4.6 PROPELLANT STORAGE AND SUPPLY	51
4.7 INSTRUMENTATION	52
4.8 CALIBRATION	55
4.9 TEST RESULTS	57
5.0 CONCLUSIONS AND RECOMMENDATIONS	66

TABLE OF CONTENTS

(Continued)

		Page
APPENDIX I	CALCULATION OF TURBULENT FREE CONVECTION DATA USING ECKERT AND JACKSON EQUATIONS RECOMP III PROGRAM NO. L-00072	68
I.1	SUMMARY	69
I.2	ANALYSIS	69
I.3	INPUT	70
I.4	OUTPUT	71
I.5	SAMPLE CASE	71
I.6	DESCRIPTION OF SYMBOLS	75
APPENDIX II	SCALING OF TANK PRESSURIZATION DATA RECOMP III PROGRAM NO. L-00090	76
II.1	SUMMARY	77
II.2	ANALYSIS	77
II.3	INPUT	78
II.4	OUTPUT	78
II.5	SAMPLE CASE	79
II.6	DESCRIPTION OF SYMBOLS	83
APPENDIX III	RADIAL DISTRIBUTOR WEIGHT DATA	84
III.1	SUMMARY	85
III.2	MATERIAL SELECTION	86
III.2.1	Short Time Tensile Values - Values In Kips	86
III.3	HEAD SELECTION	87
III.3.1	Dished Head Stress Calculations	87
III.3.2	Hemispherical Head Stress Calculations	91
III.3.3	Flat Unstayed Heads Stress Calculations	91
III.4	SHELL SELECTION (ACTIVE AREA)	93

TABLE OF CONTENTS

(Continued)

(Continued)		Page
III.4.1	Shell Stress Calculations	93
III.4.2	Shell Material: Sintered Stainless Type 316	95
III.4.3	Shell Material 60 X 60 X .011 Screen, Type 316	97
III.4.4	Shell Material 12 X 64 Rigimesh - 316 S.S. _____	100
III.4.5	Shell Material Perforated Screen 40 Mesh	102
III.4.6	Shell Material Efficiency	104
III.5	WEIGHT ANALYSIS	104
III.5.1	Weight Analysis, General	104
III.6	STRENGTH TO WEIGHT	106
III.6.1	Strength To Weight - General	115
III.7	DIMENSIONS	115
III.7.1	Dimensions, General _____	116
REFERENCES		118

LIST OF TABLES AND FIGURES

Tables		Page
TABLE 1	CORRELATION DATA	38
TABLE 2	TEST CONDITIONS	58
TABLE 3	TEMPERATURE PROFILES	59
TABLE 4	TANK PRESSURE HISTORY - psia	63
TABLE 5	MANIFOLD CONDITIONS	64
Figures		
FIGURE 1	GRASHOF NUMBER FOR HYDROGEN	5
FIGURE 2	GRASHOF NUMBER FOR HELIUM	6
FIGURE 3	GRASHOF NUMBER FOR OXYGEN	7
FIGURE 4	GRASHOF NUMBER FOR NITROGEN	8
FIGURE 5	CHARACTERISTIC VELOCITY FOR HYDROGEN	9
FIGURE 6	CHARACTERISTIC VELOCITY FOR HELIUM	10
FIGURE 7	CHARACTERISTIC VELOCITY FOR OXYGEN	11
FIGURE 8	CHARACTERISTIC VELOCITY FOR NITROGEN	12
FIGURE 9	HEAT TRANSFER COEFFICIENT FOR HYDROGEN	13
FIGURE 10	HEAT TRANSFER COEFFICIENT FOR <u>HELIUM</u>	14
FIGURE 11	HEAT TRANSFER COEFFICIENT FOR OXYGEN	15
FIGURE 12	HEAT TRANSFER COEFFICIENT FOR NITROGEN	16
FIGURE 13	MAXIMUM VELOCITY IN RADIAL WALL JET	19
FIGURE 14	MASS FLOW IN RADIAL WALL JET	22
FIGURE 15	POROSITY COMPARISON	24
FIGURE 16	EFFECT OF INTERNAL GAS-TO-WALL HEAT TRANSFER COEFFICIENT ON PRESSURANT GAS REQUIREMENT - 500 GALLON TEST TANK	30
FIGURE 17	EFFECT OF HEAT TRANSFER COEFFICIENT ON GAS REQUIREMENTS - FLIGHT TANK	31

LIST OF TABLES AND FIGURES (Continued)

Figures		Page
FIGURE 18	EFFECT OF INLET GAS TEMPERATURE ON PRESSURANT REQUIREMENT - TEST TANK	32
FIGURE 19	CORRELATION DATA	39
FIGURE 20	SMOKE TEST CHAMBER	43
FIGURE 21	PLENUM AND BAFFLE DISTRIBUTOR	45
FIGURE 22	DISCHARGE PATTERN OF PLENUM AND BAFFLE DISTRIBUTOR	46
FIGURE 23	PLENUM AND BAFFLE DISTRIBUTOR DESIGN	47
FIGURE 24	FLUID TEST SYSTEM SCHEMATIC	49
FIGURE 25	500-GALLON TEST TANK	50
FIGURE 26	INSTRUMENTATION LAYOUT	53
FIGURE 27	CALIBRATION, THERMOCOUPLE NO. 1	56
Appendix Figures		
FIGURE I-1	FORTTRAN PROGRAM	72
FIGURE I-2	INPUT DATA FOR SAMPLE CASE	73
FIGURE I-3	REPRODUCTION OF OUTPUT SHEET FOR SAMPLE CASE	74
FIGURE II-1	PROGRAM LISTING	80
FIGURE II-2	SAMPLE INPUT	81
FIGURE II-3	SAMPLE OUTPUT	82
FIGURE III-1	SHORT TIME TENSILE STRENGTH - MAXIMUM STRESS VALUE	88
FIGURE III-2	ASPECT RATIO FOR GIVEN AREA AND HEIGHT	89
FIGURE III-3	DISHED HEAD THICKNESS	90
FIGURE III-4	HEMISPHERICAL HEAD THICKNESS	92
FIGURE III-5	FLAT UNSTAYED HEAD THICKNESS	94
FIGURE III-6	SHELL THICKNESS FOR SOLID TYPE 316 STAINLESS STEEL - REFERENCE	96

LIST OF TABLES AND FIGURES (Continued)

Appendix Figures	Page
FIGURE III-7 SHELL THICKNESS FOR TYPE "C" POROUS STAINLESS STEEL	98
FIGURE III-8 SHELL THICKNESS FOR TYPE "D" POROUS STAINLESS STEEL	99
FIGURE III-9 SHELL THICKNESS FOR 60 X 60 X .011 SCREEN	101
FIGURE III-10 SHELL THICKNESS FOR 12 X 64 RIGIMESH	103
FIGURE III-11 SHELL THICKNESS FOR 40 MESH PERFORATED SCREEN	105
FIGURE III-12 WEIGHT OF HEMISPHERICAL HEAD	107
FIGURE III-13 WEIGHT OF DISHED HEAD	108
FIGURE III-14 WEIGHT OF FLAT HEAD	109
FIGURE III-15 WEIGHT OF 60 X 60 X .011 SCREEN SHELL	110
FIGURE III-16 WEIGHT OF 12 X 64 RIGIMESH SHELL	111
FIGURE III-17 WEIGHT OF 40 MESH PERFORATED SCREEN SHELL	112
FIGURE III-18.A WEIGHT OF TYPE "C" SINTERED SHELL	113
FIGURE III-18.B WEIGHT OF TYPE "D" SINTERED SHELL	114
FIGURE III-19 HEIGHT OF FLANGED AND DISHED HEAD	117

1.0 SUMMARY

17077
The results of an analytical and experimental study of pressurant distributor design fundamentals are presented.

The results of expulsion tests employing gaseous nitrogen over liquid nitrogen clearly show that a means of limiting the velocity with which condensable pressurants impinge on the liquid surface is required if massive condensation is to be avoided. It was found, using a "poor" distributor, that when the gas inlet velocity reached a critical value for the current location of the liquid surface, a sudden drop in ullage pressure occurred indicating a great increase in condensation rate brought about by disturbance of the liquid surface. No such collapse of ullage pressure was found in the six expulsion tests with the "good" distributor. The only test completed with the "poor" distributor required approximately twice as much pressurant as any of the other tests even though collapse of the ullage pressure was successfully avoided.

An analysis of turbulent free convection heat transfer based on the equations developed by Eckert and Jackson (Reference 1) is presented. Curves of Grashof number, characteristic velocity, and heat transfer coefficient as functions of gas-to-wall temperature difference with length of boundary layer run and with wall temperature as parameters are presented for gaseous hydrogen, oxygen, helium, and nitrogen all at 30 psia. A computer program used to generate some of the free convection data is included along with a sample case.

An analysis of forced convection is made on the basis of the radial wall jet. Theoretical and experimental investigations of the radial wall jet have shown that the maximum velocity in the jet decreases rapidly with distance while the entrainment of secondary fluid increases quite rapidly. The rapid decay of maximum velocity is indicative of a rapid decay in heat transfer coefficient which is a desirable characteristic in a pressurant distributor. The high rate of secondary fluid entrainment is

also a desirable characteristic because it tends to reduce the bulk temperature of the jet thereby reducing the gas-to-wall temperature difference which is the driving potential of the convective heat transfer and consequently the magnitude of that heat transfer.

Rigimesh screen was found to have a much higher strength-to-weight ratio than any other material tested. Since it presents no straight through flow paths, effective turning of the flow is assured. The porosity of the screen can be varied over a wide range with little change in strength or weight.

Multiple radial distributors are shown to be lighter than a single distributor when total active surface area and internal pressure are the same. The weight of additional plumbing required for multiple inlets is not considered.

2.0 INTRODUCTION

Since the weight of the pressurization system can be a significant portion of the weight of the vehicle, it is necessary to optimize the system so that a minimum payload penalty will be imposed. The optimization must consider both the weight of the pressurant required and the weight of system hardware.

To minimize the weight of pressurant required, it is necessary to provide for a high average final gas temperature and to minimize condensation. The role of the pressurant distributor is to introduce the pressurant into the tank in a manner which will promote these objectives.

A pressurant distributor capable of eliminating forced convection effects at the tank wall and liquid surface probably would impose a considerable net payload penalty on the vehicle. It is, therefore, necessary to optimize the weight of the total pressurization system.

The test program, in which liquid nitrogen was pressurized and discharged from a 500 gallon test tank, demonstrated the necessity for having at least a minimum distributor when a condensable pressurant is employed. In these tests, it was found that almost total collapse of the pressurant occurred when the "poor" distributor was used and little collapse was found when the "good" distributor was used.

3.0 ANALYSES

3.1 FREE CONVECTION

The present study is largely concerned with heat transfer from the pressurizing gas to the tank wall and to the liquid in a liquid propellant tank. Since this transfer, assuming a good distributor, will be primarily due to free convection, it is necessary to determine the free convection heat transfer characteristics for a range of representative conditions. To this end, curves of Grashof number, characteristic velocity, and heat transfer coefficient were generated for various boundary layer runs, wall temperatures, and gas-to-wall temperature differences for gaseous hydrogen, helium, oxygen, and nitrogen all at 30 psia. These curves are Figures 1 through 12. The computations are based on vertical flat plate theory. The equations for turbulent flow were used since almost all of the computed Grashof numbers exceed 10^9 which is the usually accepted value for transition from laminar to turbulent flow.

The characteristic velocity is the free stream velocity of a forced convection flow which would give the same velocity profile near the wall as does the free convection flow. It seems probable that little would be gained by enlarging the pressurant distributor beyond the point at which its exit velocity is of the order of the free convection characteristic velocity. When the exit velocity is less than the free convection induced velocity, free convection effects will determine the heat transfer coefficient at the wall. Thus, the characteristic velocity is indicative of the minimum practical distributor discharge velocity.

The calculated free convection curves presented herein can be expected to predict only approximately the conditions in an emptying tank. The theory was developed for a steady-state vertical flat plate at constant temperature and with a sharp leading edge; whereas, the test tank is an enclosed volume with conditions varying over time and position. However, they are useful for establishing trends and probable

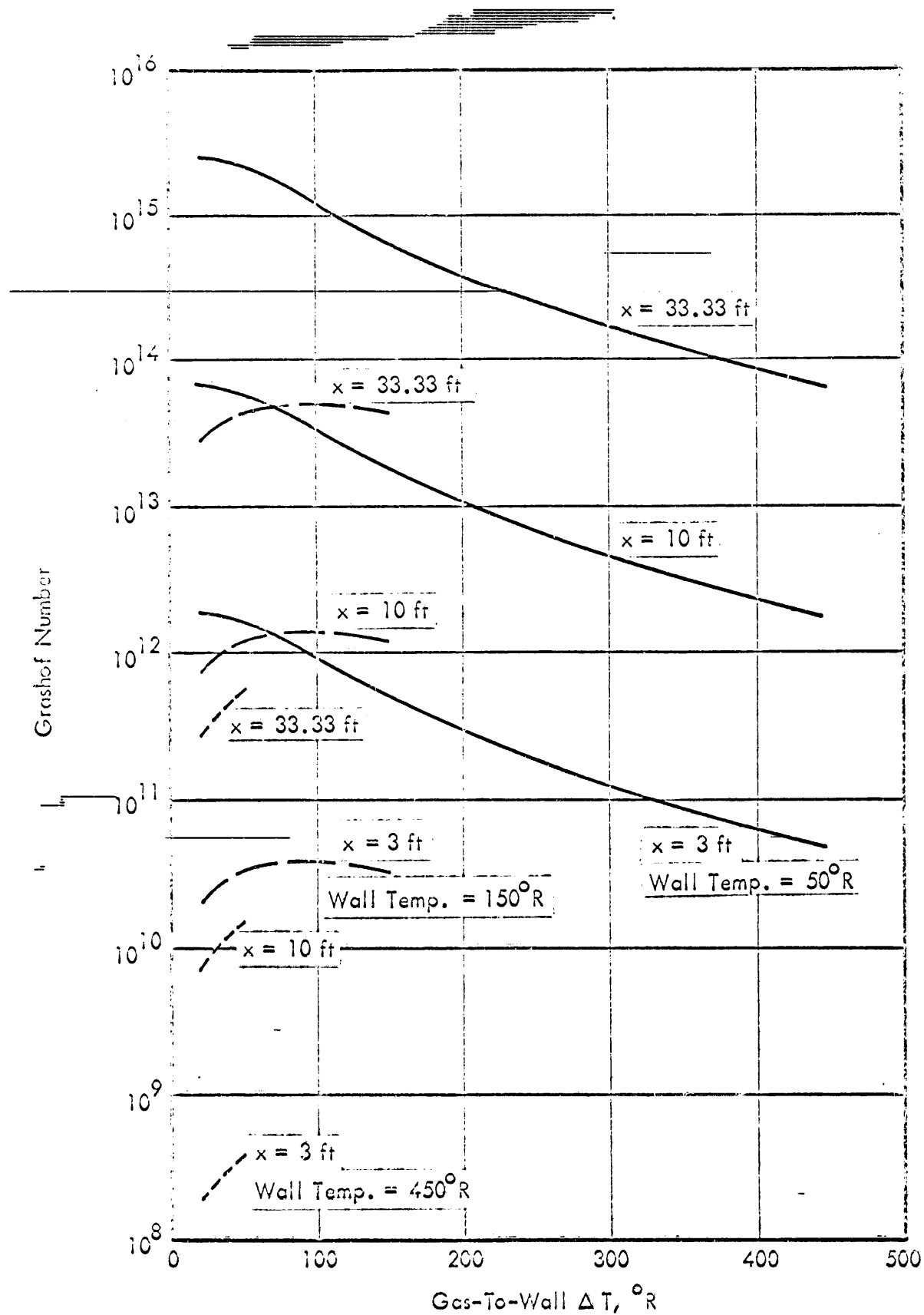


FIGURE 1 GRASHOF NUMBER FOR HYDROGEN

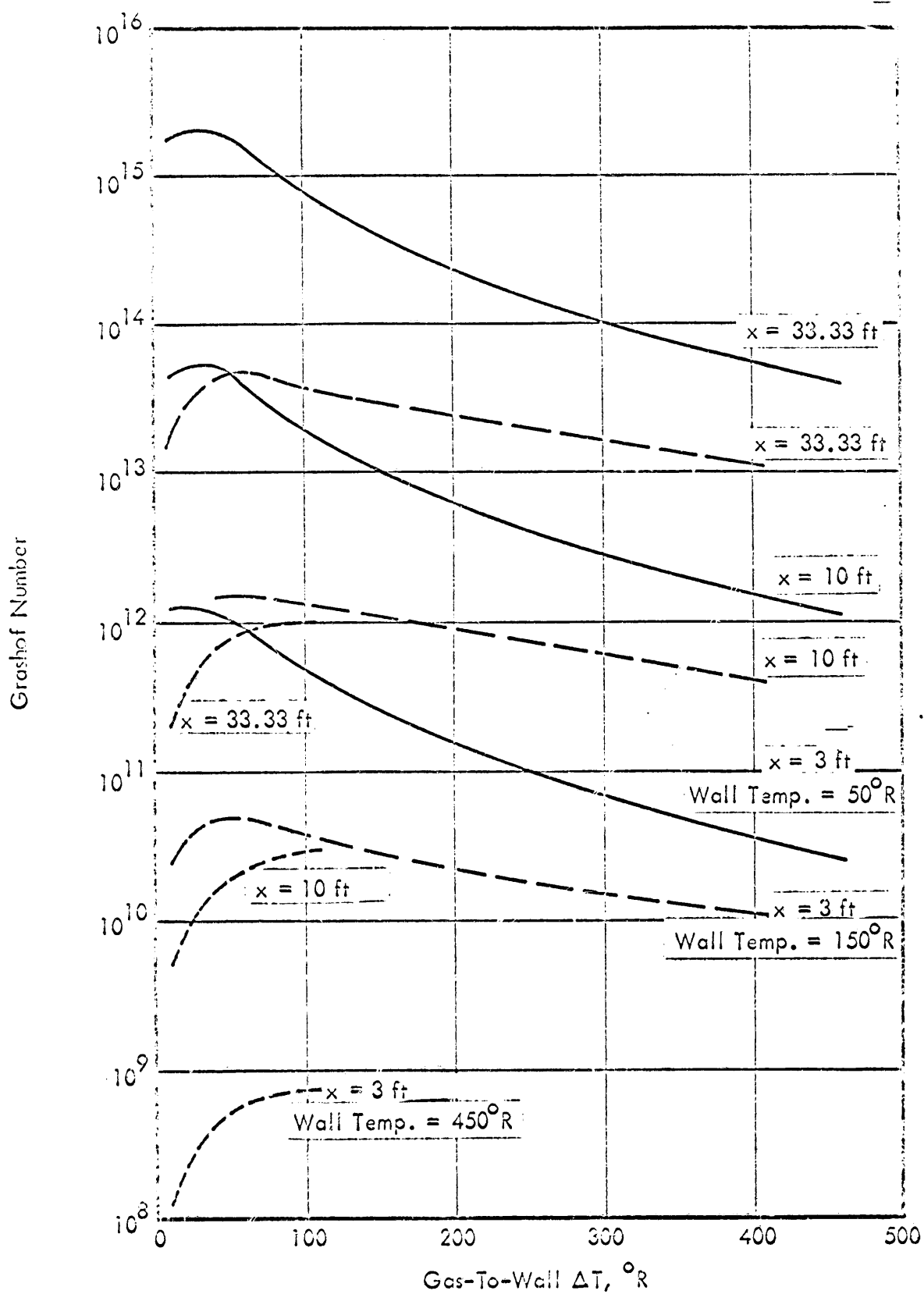


FIGURE 2 GRASHOF NUMBER FOR HELIUM

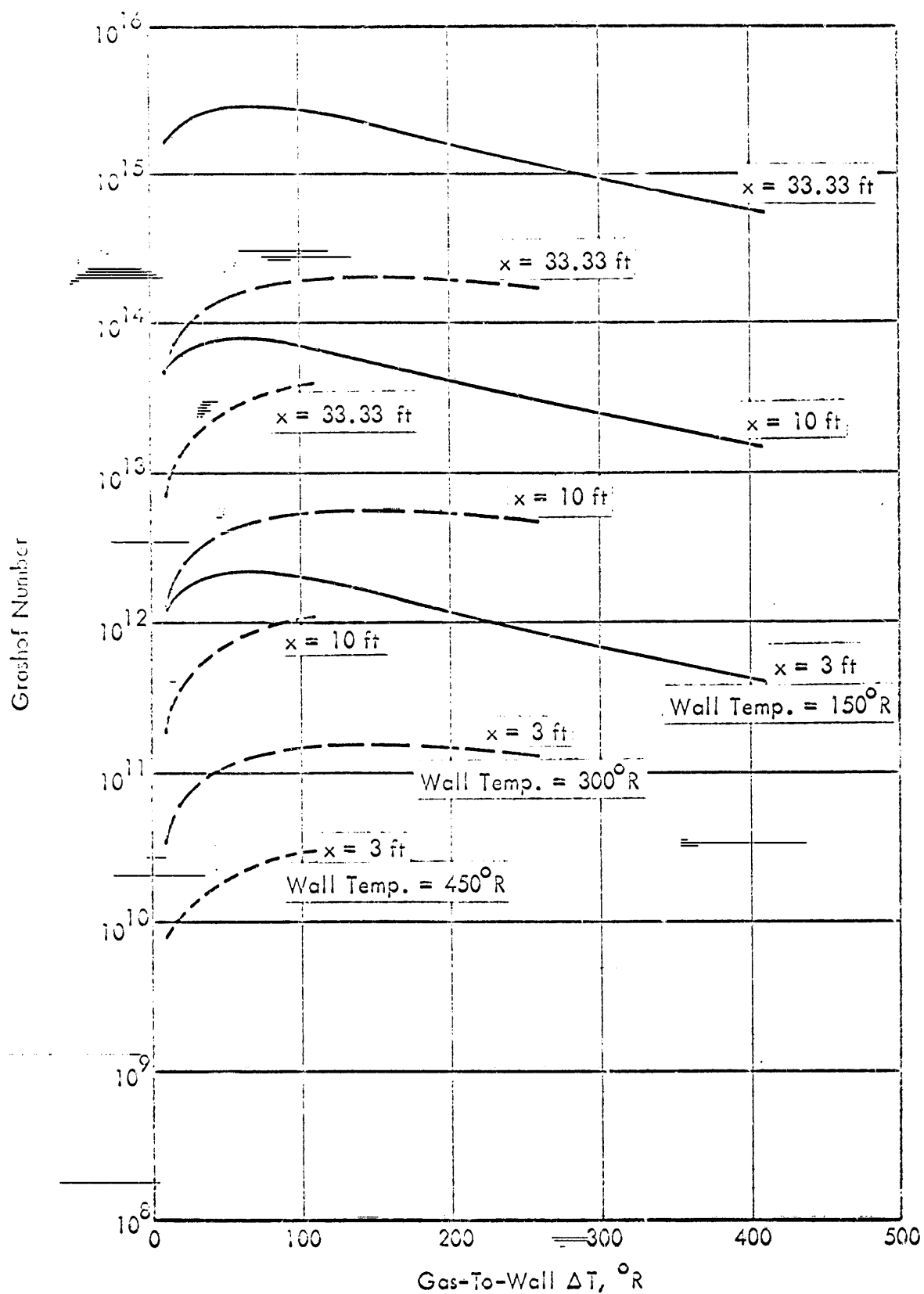


FIGURE 3 GRASHOF NUMBER FOR OXYGEN

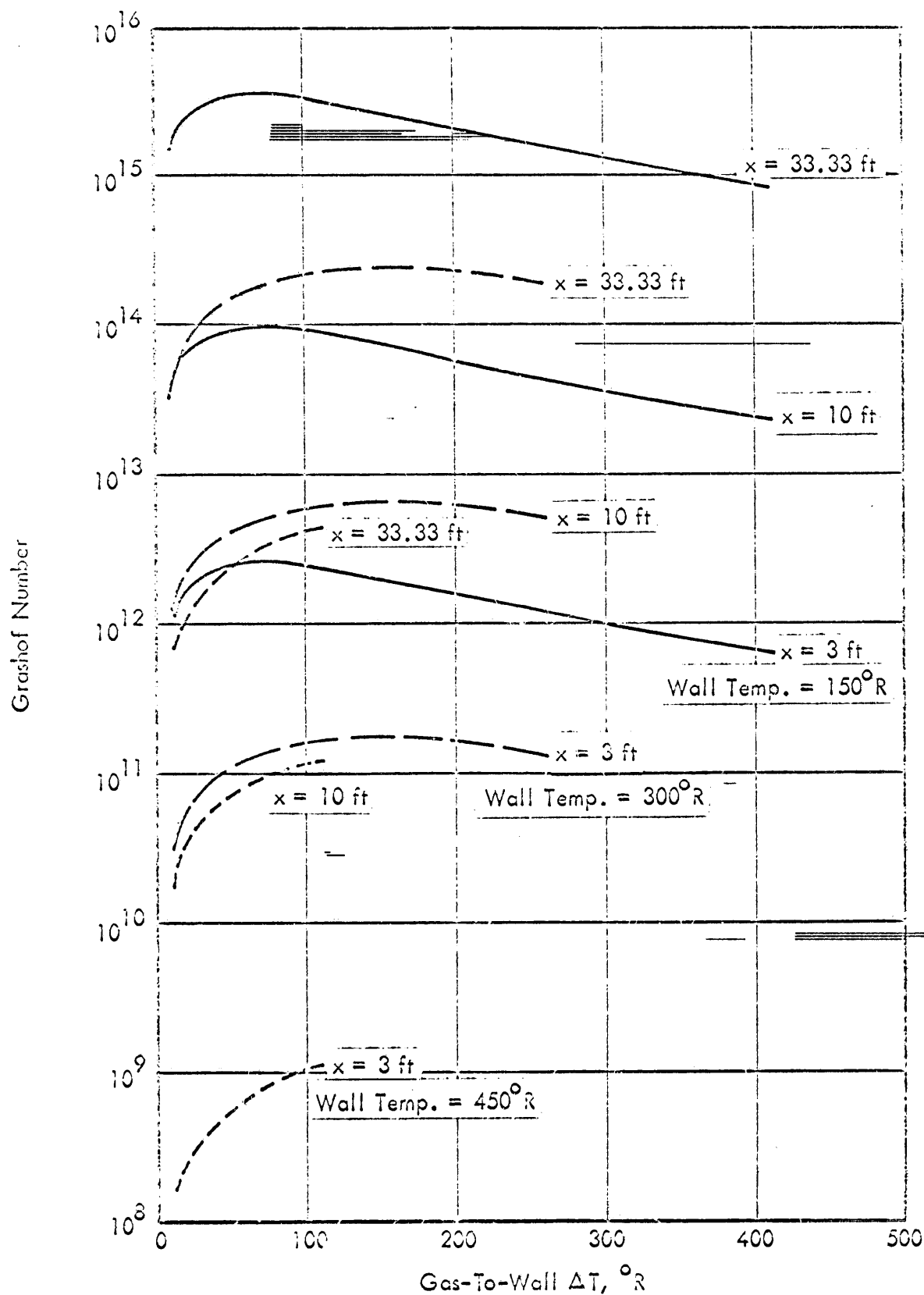


FIGURE 4 GRASHOF NUMBER FOR NITROGEN

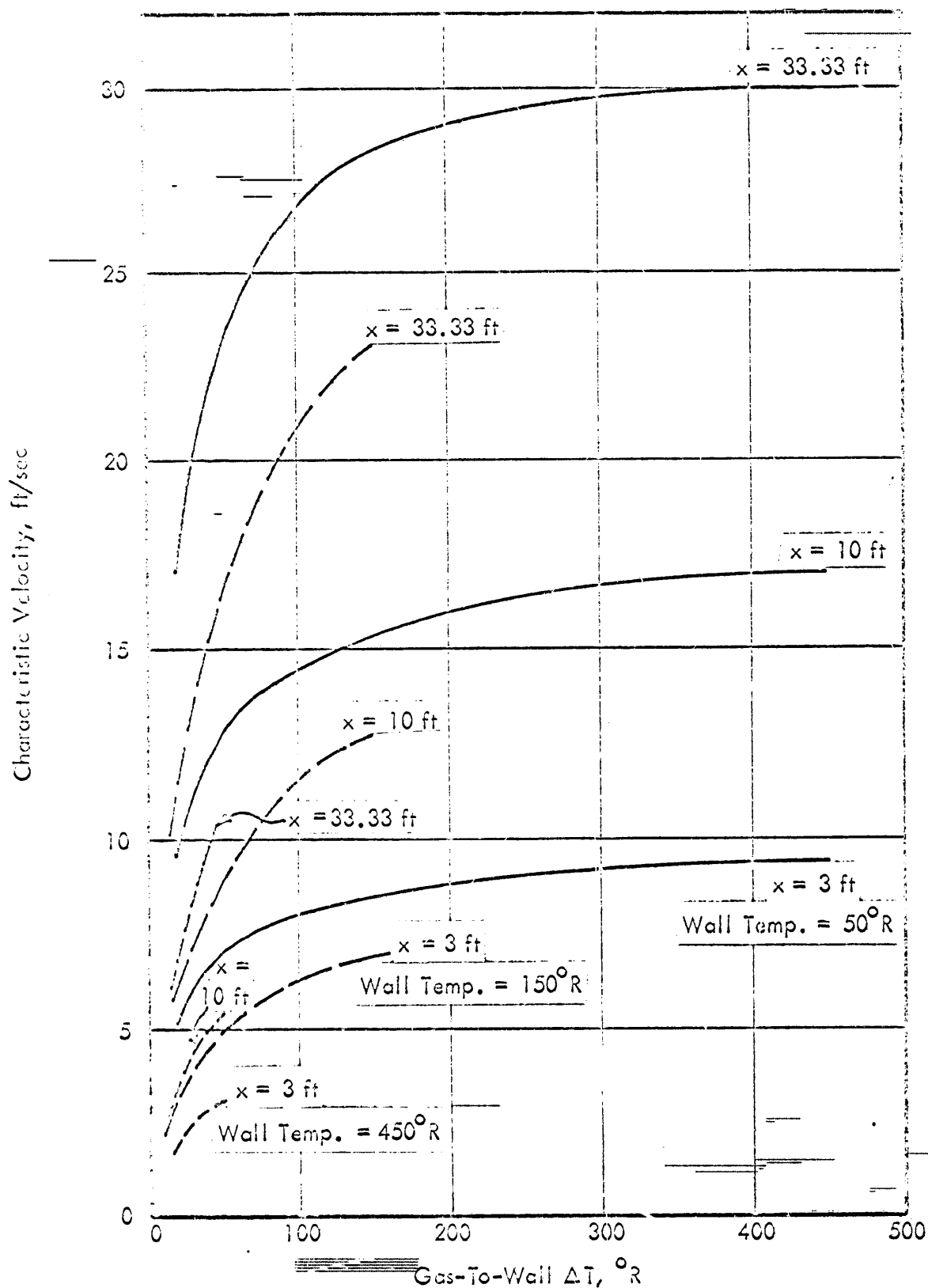


FIGURE 5 CHARACTERISTIC VELOCITY FOR HYDROGEN

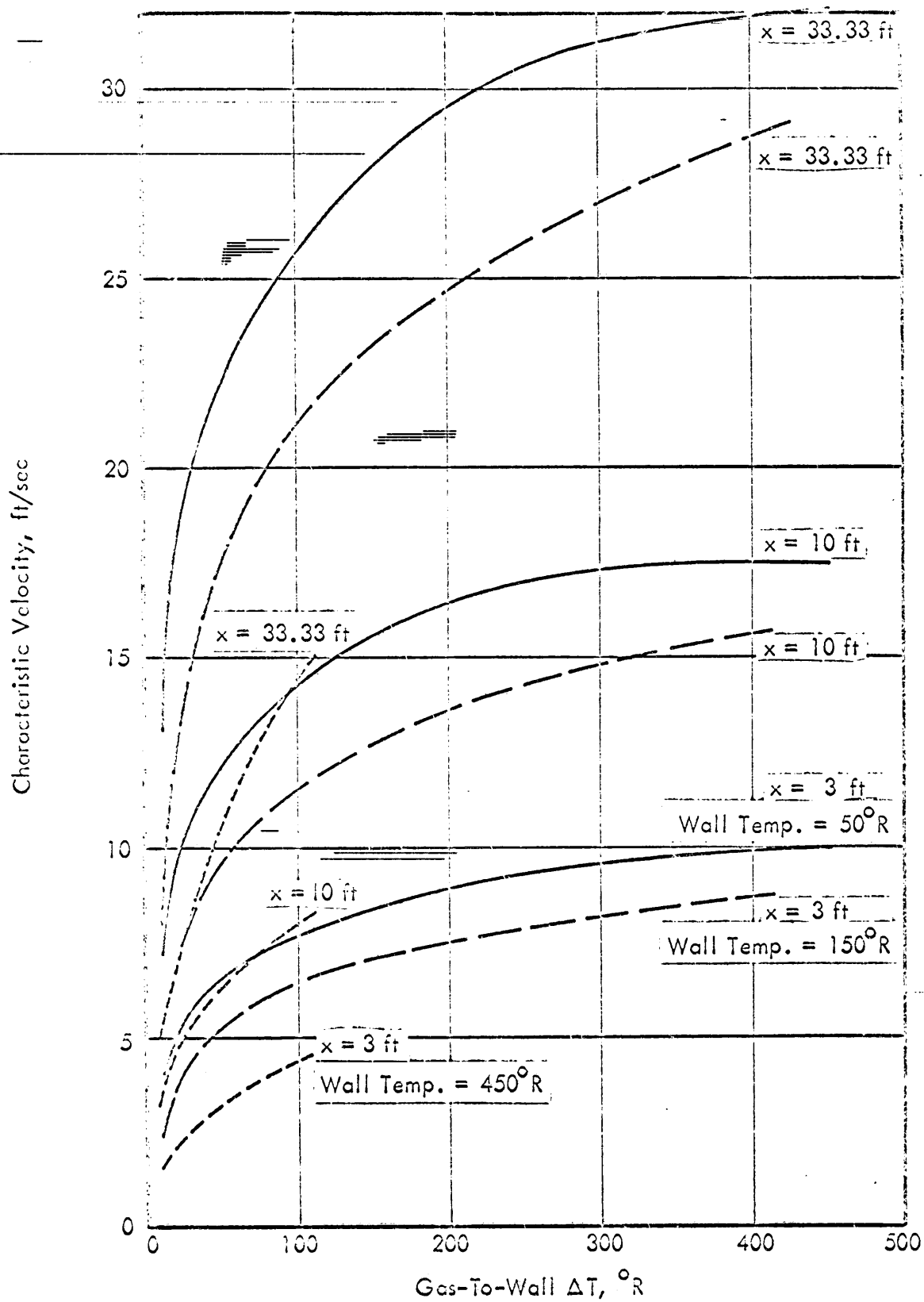


FIGURE 6 CHARACTERISTIC VELOCITY FOR HELIUM

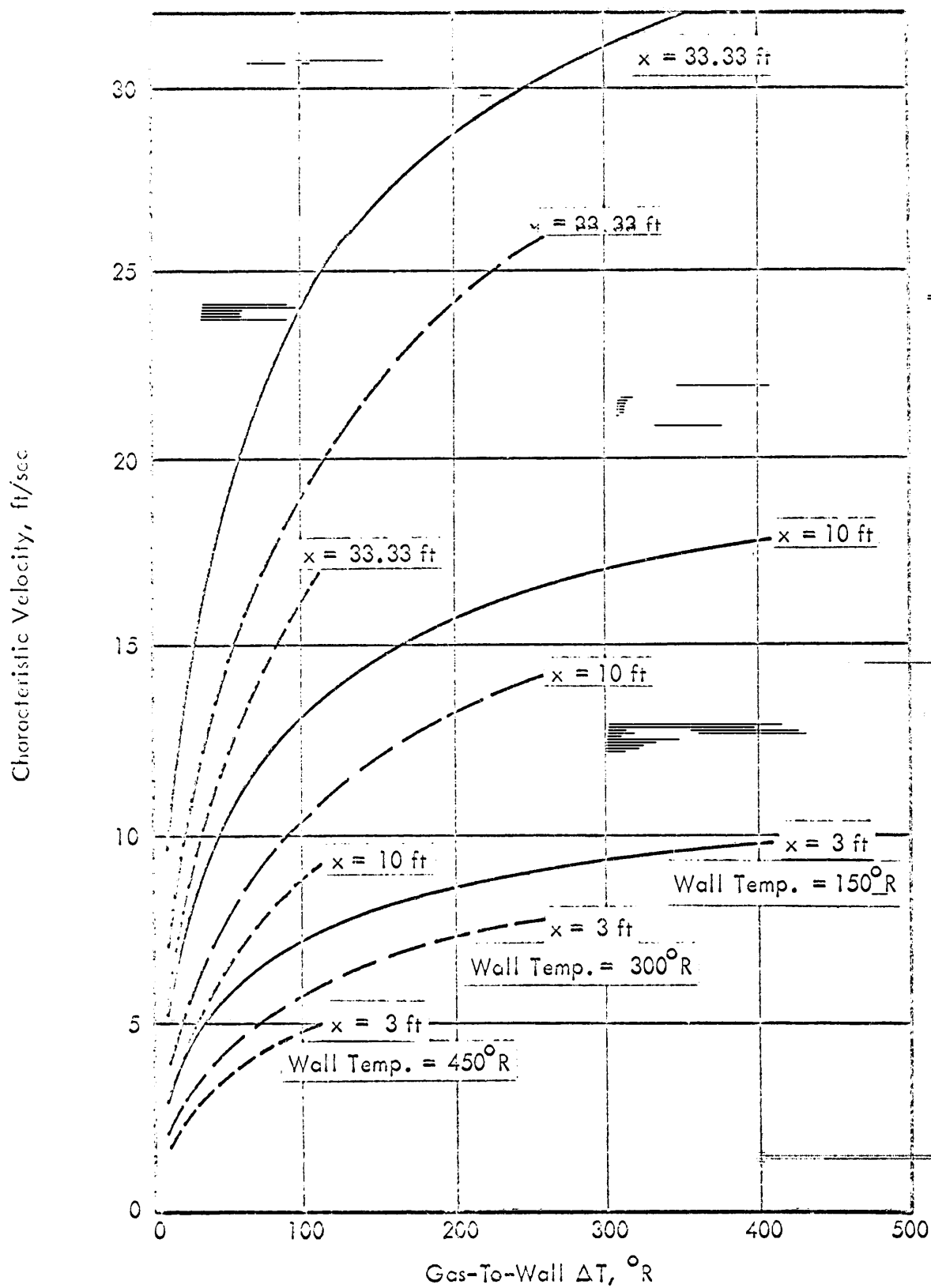


FIGURE 7 CHARACTERISTIC VELOCITY FOR OXYGEN

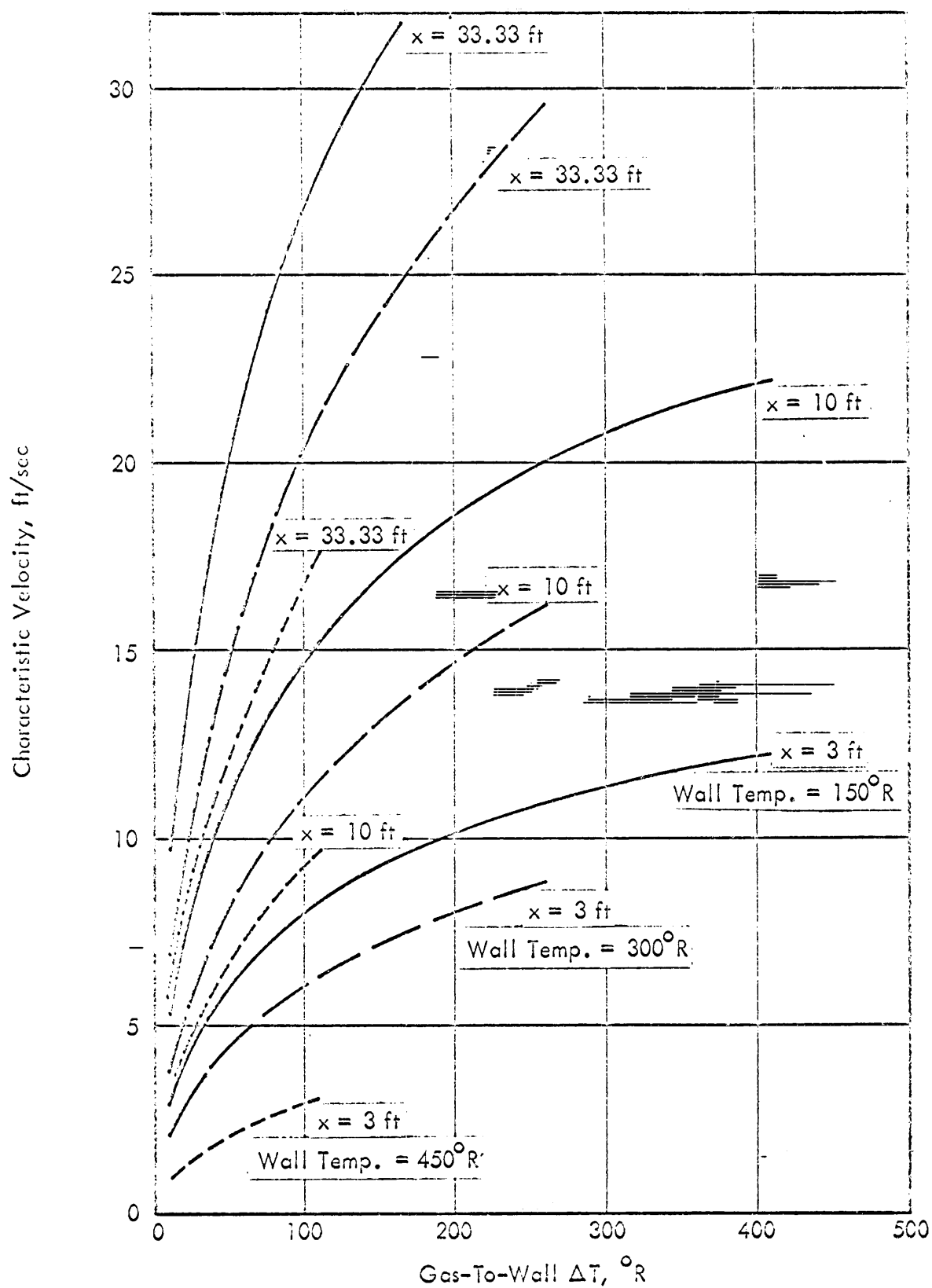


FIGURE 8 CHARACTERISTIC VELOCITY FOR NITROGEN

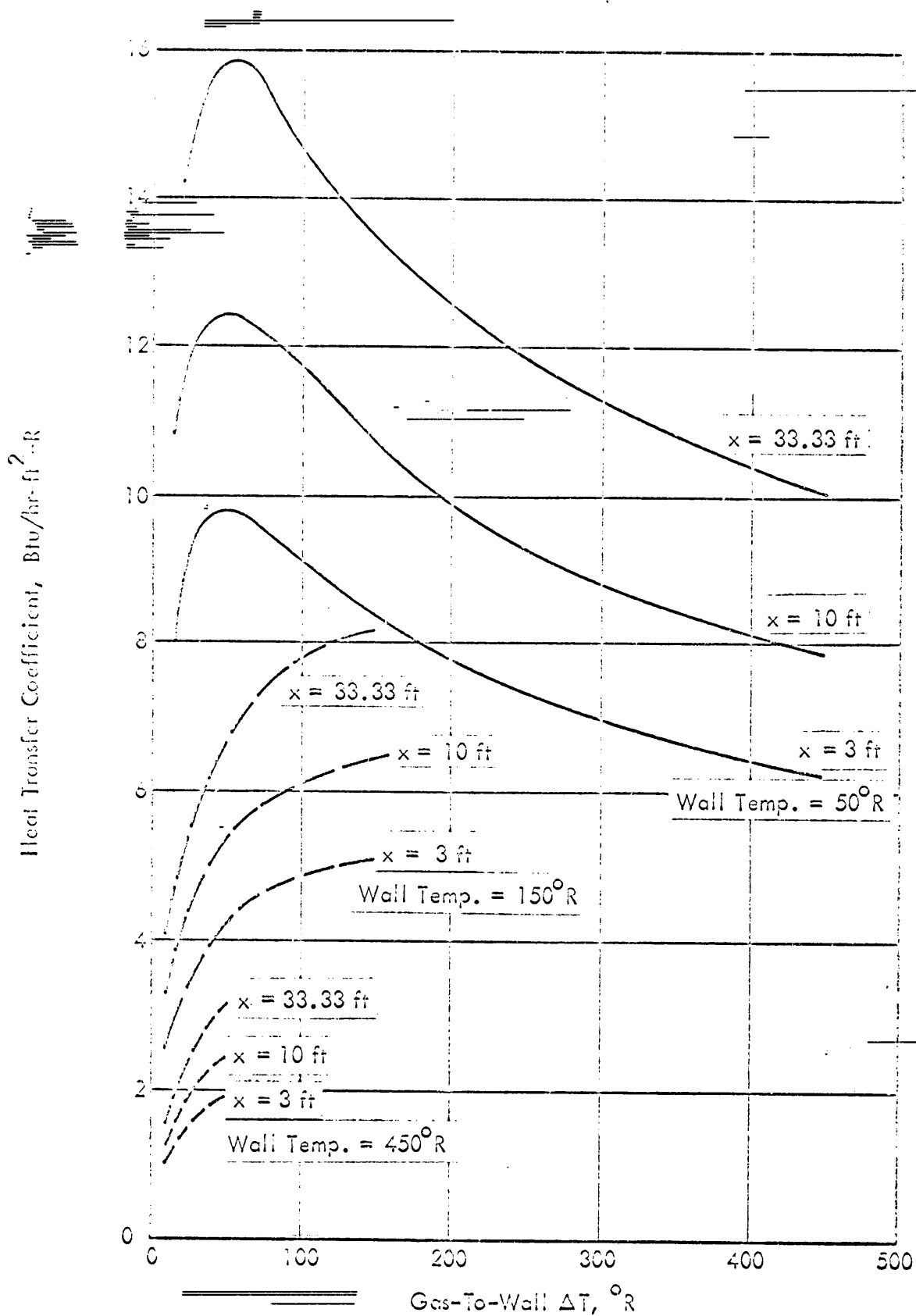


FIGURE 9 HEAT TRANSFER COEFFICIENT FOR HYDROGEN

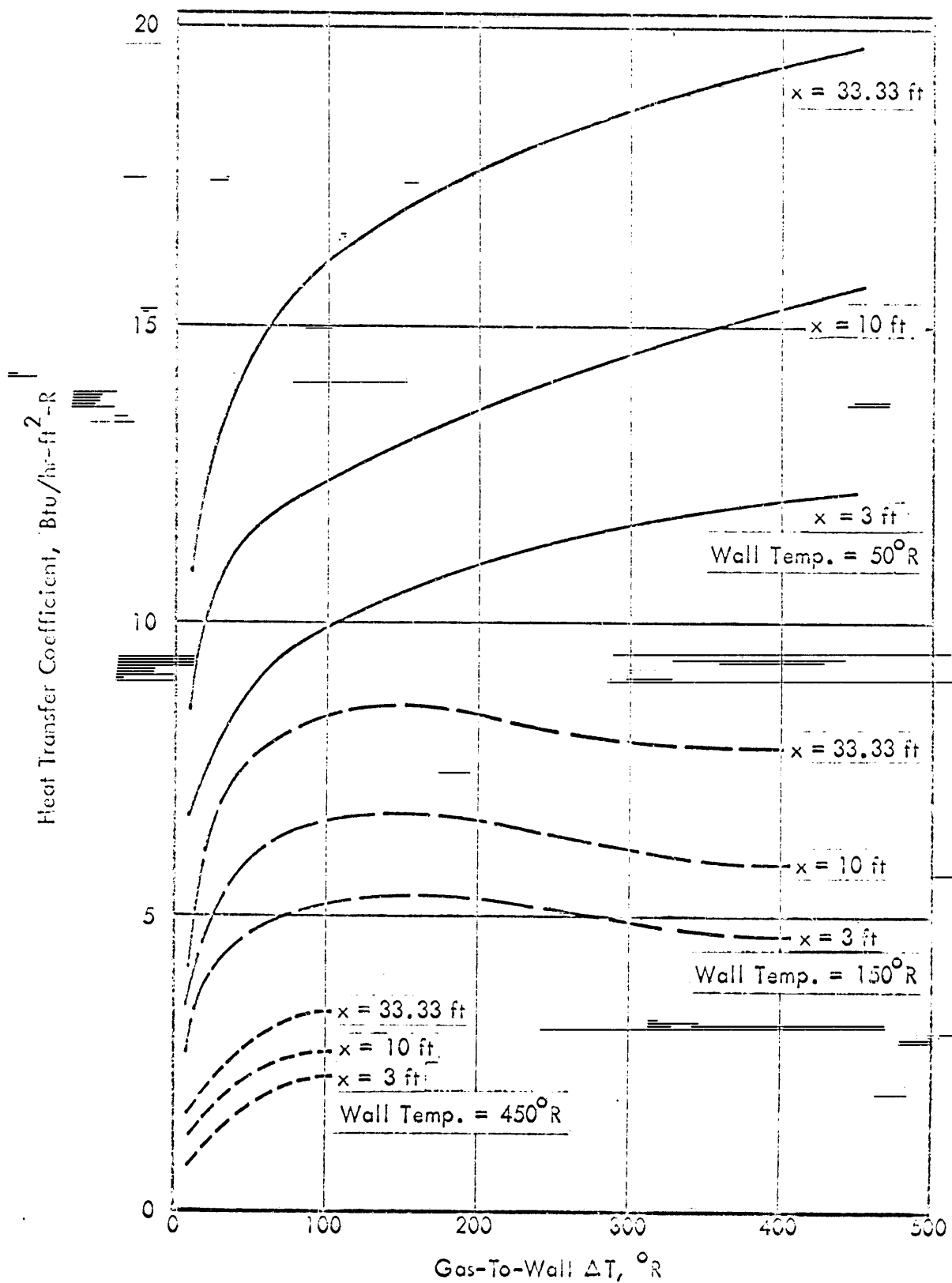


FIGURE 10 HEAT TRANSFER COEFFICIENT FOR HELIUM

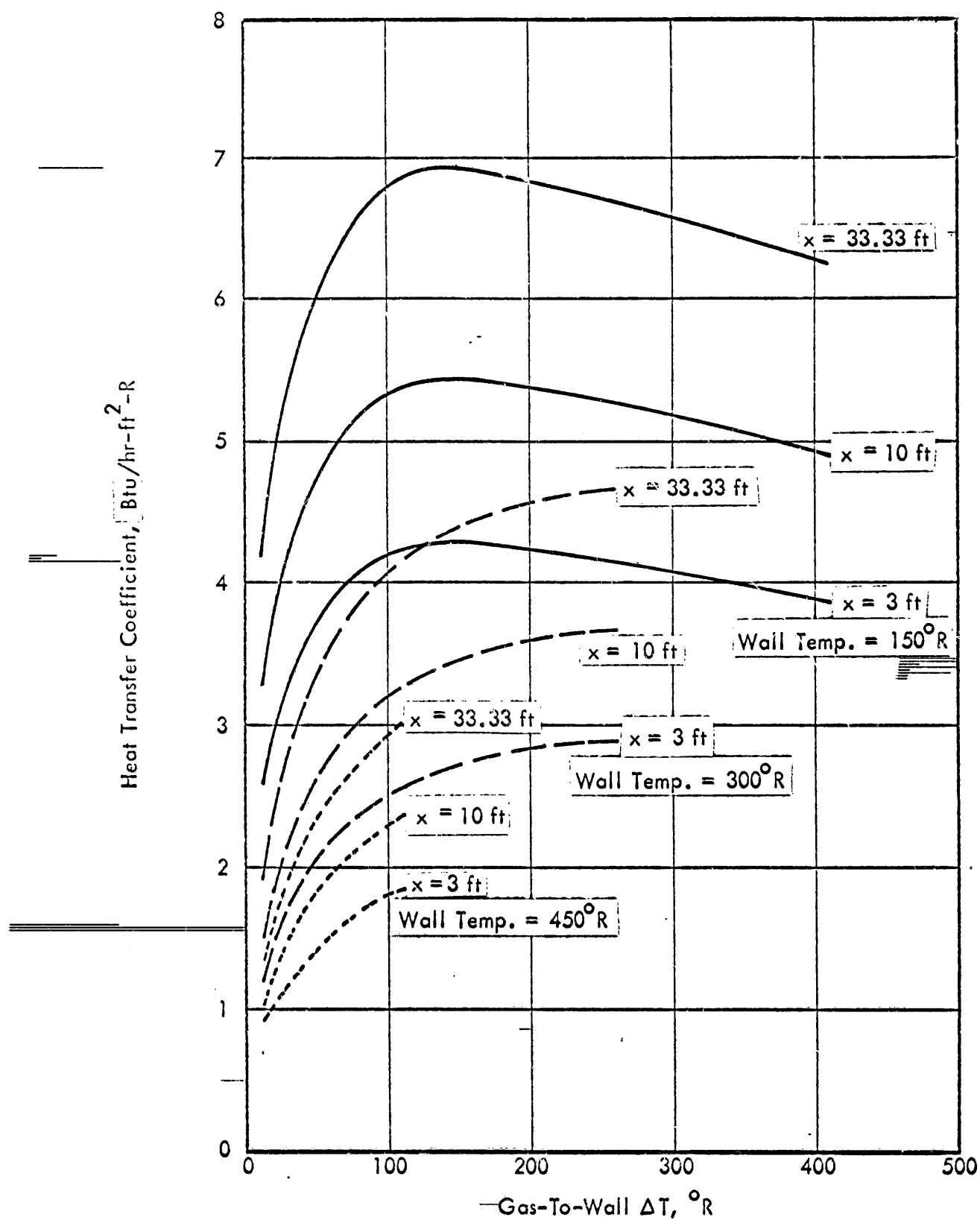


FIGURE 11 HEAT TRANSFER COEFFICIENT FOR OXYGEN

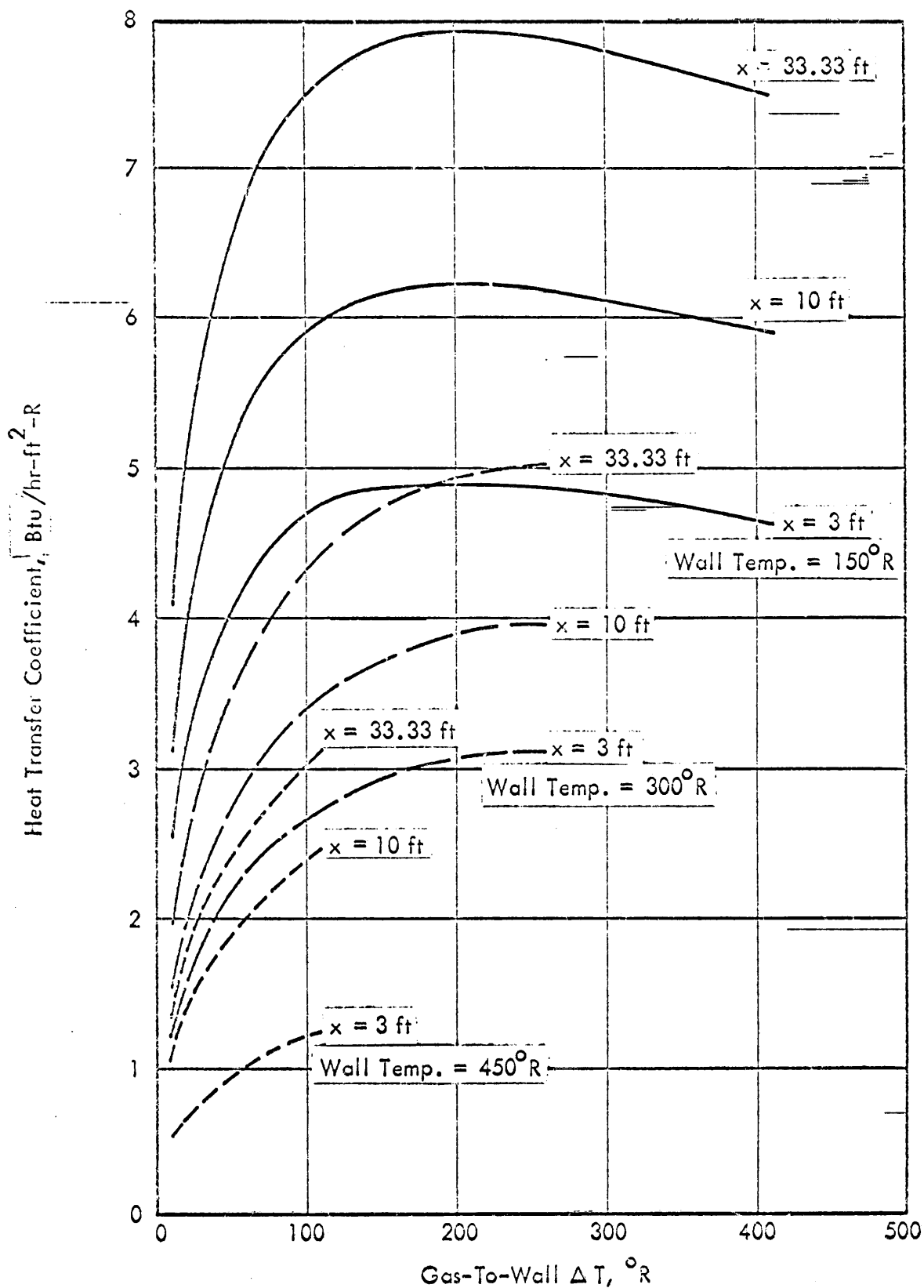


FIGURE 12 HEAT TRANSFER COEFFICIENT FOR NITROGEN

ranges of conditions to be encountered. Past experience has shown results to agree surprisingly well with predicted values.

A Recomp III computer program was used to facilitate the computation of the free convection data for oxygen and nitrogen. The program, with a sample case, is described in Appendix I. It is included as an aid to the computation of data for conditions not included in this report.

3.2 FORCED CONVECTION

Forced convection in the ullage region of a missile propellant tank is too complex to permit a general solution. The principal impediments to the analytical solution of the mixed forced and free convection in this case arise from the time and space dependence of boundary temperatures, the time dependence of the physical boundaries of the convective region, and on the existence of a compound boundary condition in which a flow may be bounded on two sides by temperatures which differ from each other and from that of the bulk flow. This latter complication is apparent in the case of a wall jet in which the hot flow of gas is bounded on one side by a cold wall and on the other side by the cool bulk ullage gas.

A radial wall jet on a flat plate in quiescent surroundings is representative of a radially discharging pressurant distributor which is mounted coaxially with the propellant tank on the upper bulkhead of the tank. The flow properties of such a wall jet have been studied both analytically and experimentally by several investigators (see for example, Reference 2). The results of these studies are important even though they do not directly provide heat transfer data.

Ludwig and Brady (Reference 2) studied the phenomena associated with the impingement of a uniform jet on a flat plate. After turning, the flow in this case behaves as would a wall jet. In the region where the flow is behaving as a wall jet, these

authors found the non-dimensional maximum velocity in the jet to be proportional to the non-dimensional radius raised to the -1.143 power. Similarly, they found the non-dimensional distance from the plate to the point at which the velocity is one-half maximum velocity to be proportional to the 1.028 power of the non-dimensional radius.

The velocity and distances are non-dimensionalized by dividing by the uniform velocity of the initial jet and by the radius of that jet, respectively. These correlations are shown in Figure 26 of Reference 2.

In a true wall jet, the exit surface or slot is the origin of the flow and no radius adjustment is required in the equation for maximum velocity. That equation is:

$$\frac{u_m}{U_\infty} = \left(\frac{r}{R}\right)^{-1.143}$$

where u_m = local maximum velocity at r ,
 U_∞ = initial velocity at R ,
 r = radius from nozzle centerline, and
 R = radius of nozzle.

This equation can be put into a more convenient form by defining $r^* = \frac{r - R}{R}$ in which case

$$\frac{u_m}{U_\infty} = (1 + r^*)^{-1.143}$$

Figure 13 shows the very rapid decay in maximum velocity as a function of distance from the nozzle surface.

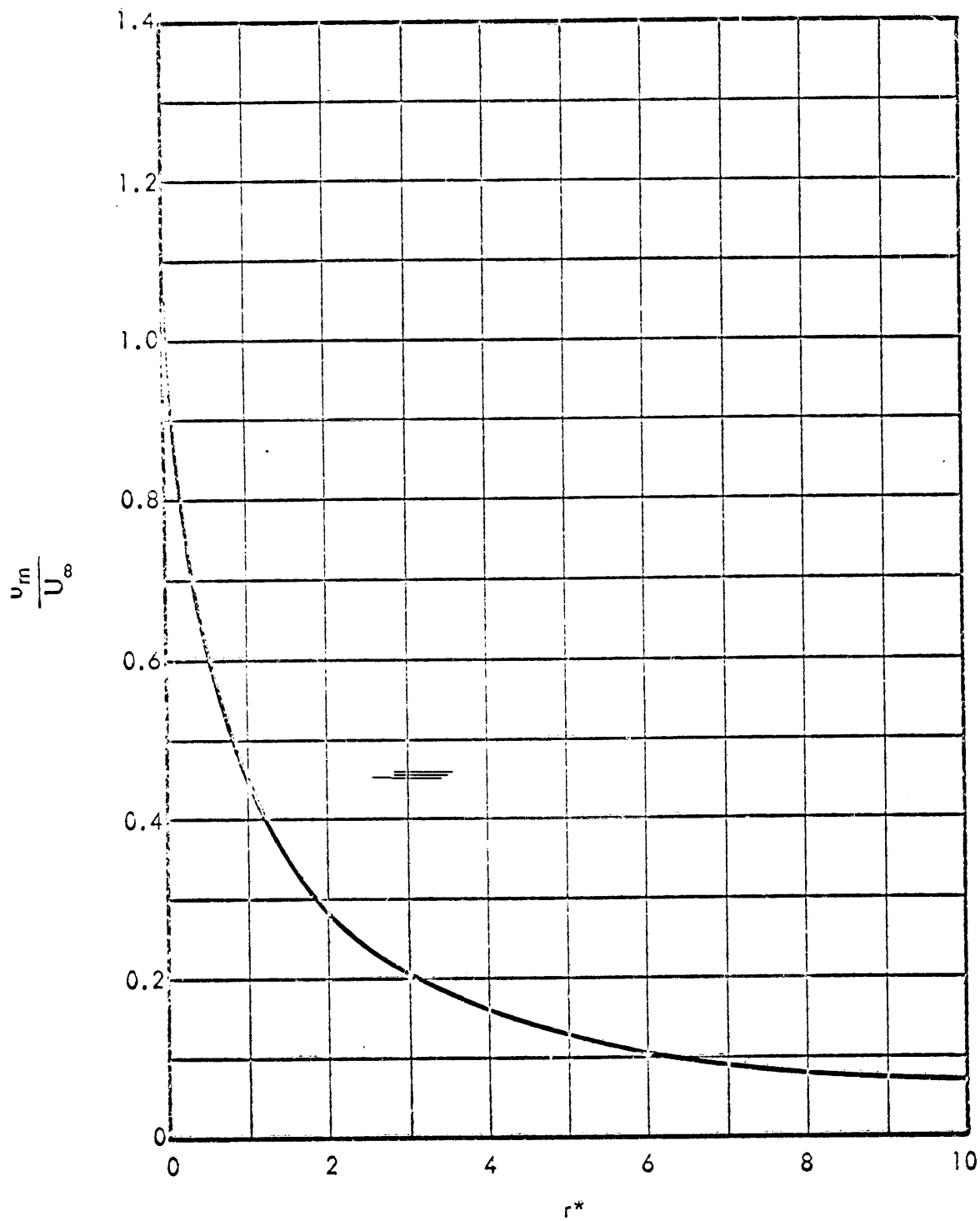


FIGURE 13 MAXIMUM VELOCITY IN RADIAL WALL JET

As seen in Figure 26 of Reference 2, $\frac{Y_{1/2}}{R}$ increases as the 1.028 power of r/R after wall jet flow is established. Since boundary layer growth by entrainment of secondary fluid begins at the origin, $Y_{1/2} = H$ at $r = R$. The corresponding equation for $Y_{1/2}$ becomes:

$$\frac{Y_{1/2}}{H} = \left(\frac{r}{R}\right)^{1.028}$$

where H = nozzle height, and
other terms previously defined.

Ludwig and Brady also correlated mass flow as a function of radial position in the jet. They found the following equation to hold true:

$$Q_r = 2.22 \pi \rho r u_m Y_{1/2}$$

where Q_r = radial mass flow rate at r ,
 ρ = jet density, and
 $r, u_m, Y_{1/2}$ as previously defined.

Substituting the equations for u_m and $Y_{1/2}$ into this equation yields:

$$Q_r = 2.22 \pi \rho U_\infty H r \left(\frac{r}{R}\right)^{-0.015}$$

Non-dimensionalizing this equation by the mass flow at the origin gives:

$$\frac{Q_r}{Q_R} = \left(\frac{r}{R}\right)^{0.985}$$

again, using $r^* = \frac{r - R}{R}$,

$$\frac{Q_r}{Q_r} = (1 - R^*)^{0.985}.$$

For this flow, the entrainment of secondary mass is shown in Figure 14. Note that a mass approximately equal to the initial mass is entrained for each nozzle radius of flow path outside the nozzle.

The very rapid decay in maximum velocity with distance from the nozzle implies a relatively small range of strong forced convection effects even at rather high nozzle exit velocities. This conclusion is further justified by the fact that pressurant gas requirements computed on the basis of free convection only, in general, agree quite well with corresponding test results.

The high rate of secondary fluid entrainment also tends toward the establishment of free convection conditions from the initial forced convection conditions by reducing the difference between the bulk temperature of the jet and that of the surrounding gas. Thus, the initial temperature of the jet is reduced by mixing to a value more nearly that of the bulk ullage gas, thereby permitting the use of wall temperature and bulk gas temperature on the calculation of free convection heat transfer.

For a given discharge area, the minimum velocity is attained when a uniform velocity profile is achieved. Since forced convection heat transfer coefficients increase with velocity, it is desirable to obtain reduced velocities by smoothing the velocity profile across the diffuser exit. This smoothing of the velocity profile is accomplished by increasing the pressure drop in the radial direction relative to that in the axial direction. A porous surface, such as a screen, placed over the discharge of the distributor is the best way of increasing radial pressure gradient substantially independently of the axial pressure gradient. Several porous materials were investigated to

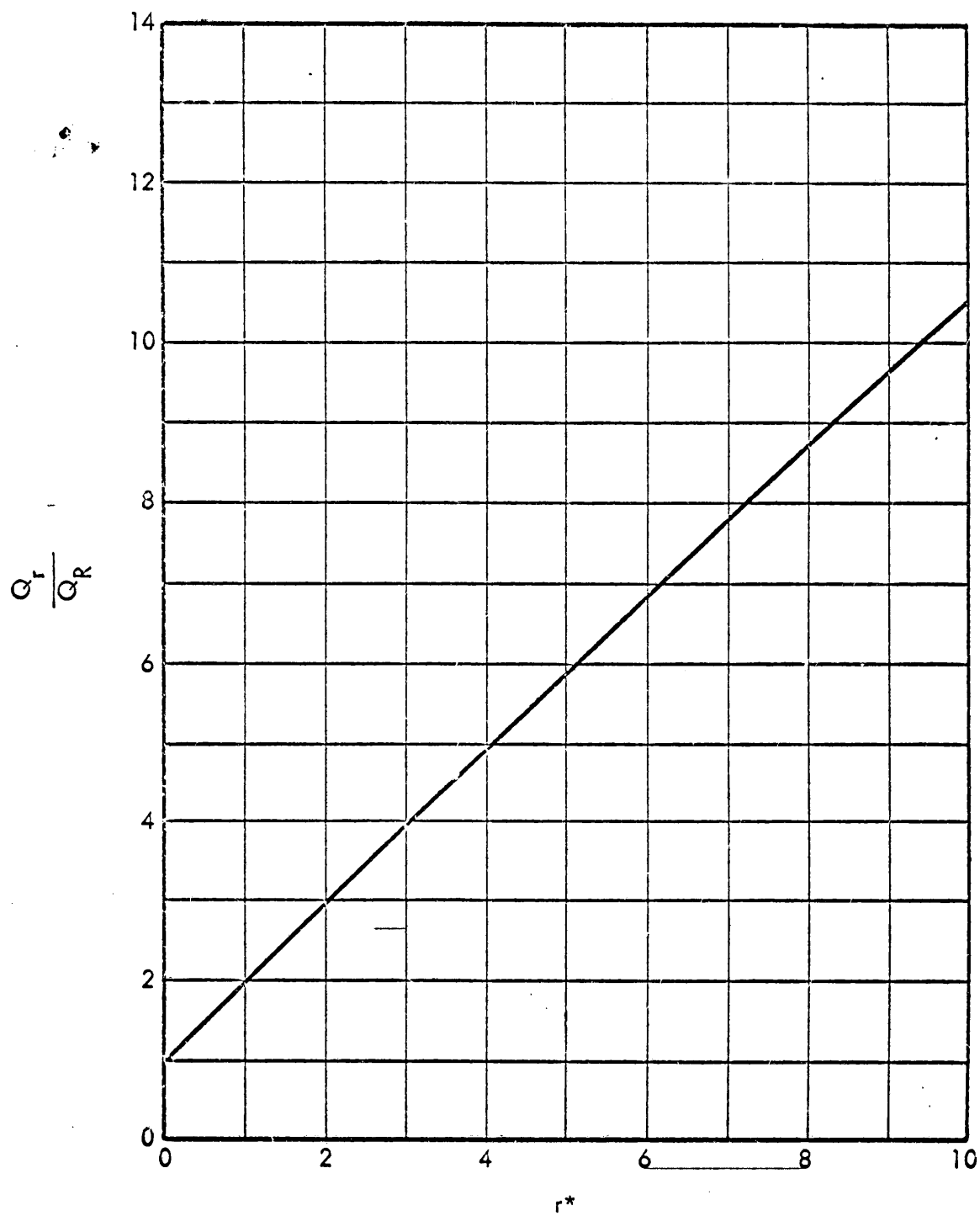


FIGURE 14 MASS FLOW IN RADIAL WALL JET

determine their suitabilities in this application.

Pressure drops across several active surface materials of the flow rate of air at 70°F into an atmospheric plenum are shown in Figure 15. The data for Rigimesh and Porous Stainless Steel were obtained from References 3 and 4, respectively. The data for the 40 mesh perforated screen and for the 60X60X .011 woven screen were computed from pressure drop correlations presented in References 5 and 6, respectively.

The two curves for Rigimesh illustrate the wide range of porosity which can be achieved for substantially the same weight of material or with substantially the same strength. For small diameter distributors where the weight of the distributor is determined by considerations other than pressure induced stress, a more uniform velocity profile can be obtained by using a higher pressure drop at no increase in distributor weight. For large diameter distributors where pressure induced stresses are significant, it is evident that the weight of the distributor can be reduced perhaps substantially by the selection of a higher porosity material. It is realized, of course, that the flow orienting ability of a material is related to its porosity. This is discussed elsewhere in this report.

For a given required active surface area and allowable length L , the weight of the active surface is:

$$W_s = \pi D L \rho_s t_s$$

where ρ_s = weight of active surface material per unit area, and
 t_s = thickness.

The end closure of the distributor will have a weight:

$$W_e = K \pi D^2 \rho_e t_e$$

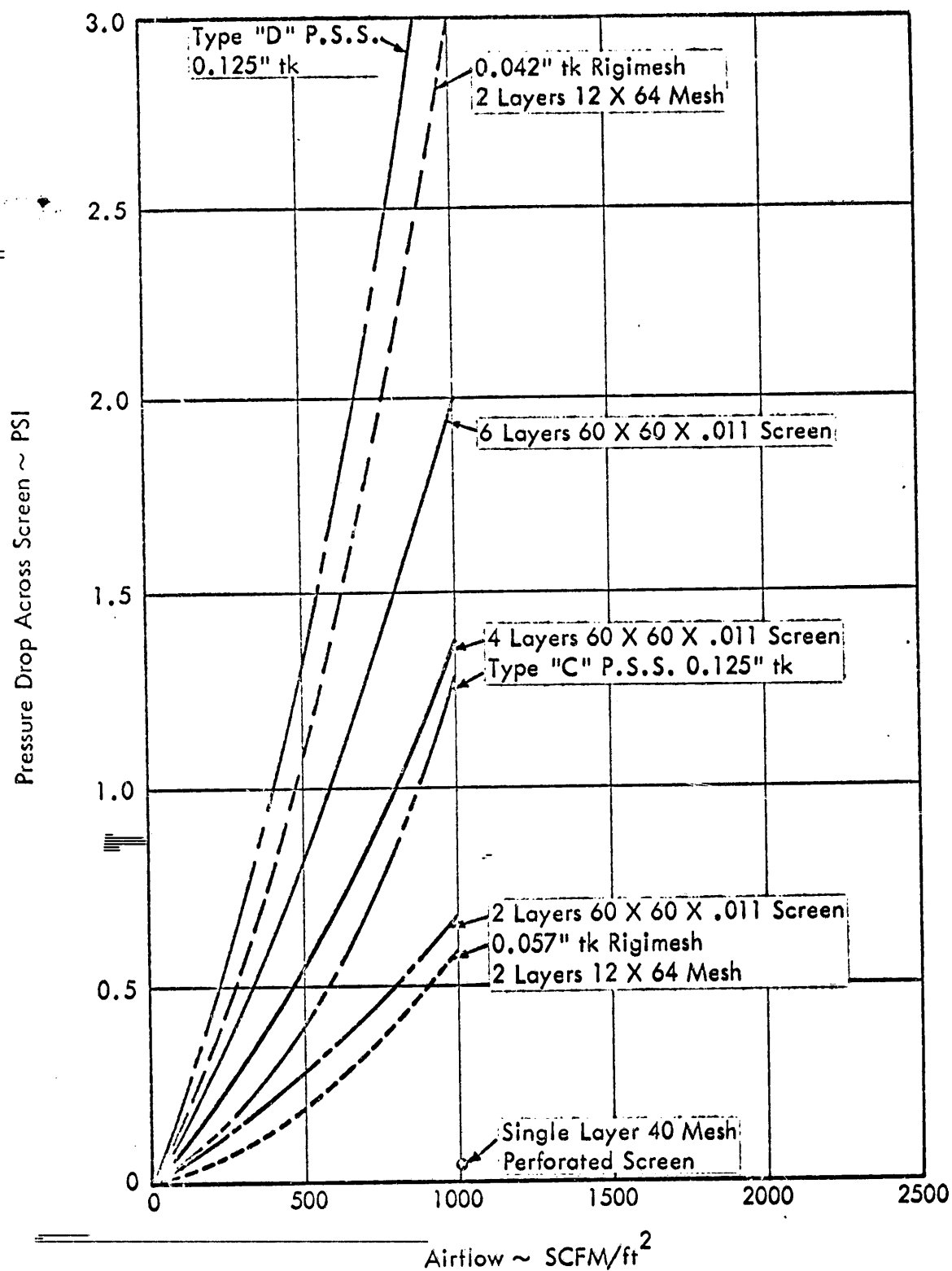


FIGURE 15 POROSITY COMPARISON

where the constant K depends upon the particular configuration employed.

Using N identical distributors of the required total active surface area, the active surface weight is:

$$W_{sn} = W_s = N \pi D_n L_n \rho_s t_{sn} = \pi D L \rho_s t_s.$$

But, $N \pi D_n L_n = \pi D L$ and $t \sim D$.

Of course, the proportionality between t and D holds only when t is determined by internal pressure.

$$\frac{W_{sn}}{W_s} = \frac{t_{sn}}{t_s} = \frac{D_n}{D}$$

The weight of the end closure is:

$$W_{en} = K N \pi D_n^2 \rho_e t_{en}$$

$$\frac{W_{en}}{W_e} = \frac{N D_n^2 t_{en}}{D^2 t_e}$$

again, $t \sim D$ so:

$$\frac{W_{en}}{W_e} = \frac{N D_n^3}{D^3}.$$

Consider a fixed L/D ratio:

$$\pi D L = N \pi D_n L_n$$

$$D^2 L/D = N D_n^2 \frac{L N}{D_n} = N D_n^2 L/D$$

$$D^2 = N D_n^2$$

$$\frac{D_n}{D} = \left(\frac{1}{N}\right)^{1/2}$$

Then,

$$\frac{W_{sn}}{W_s} = \frac{D_n}{D} = \left(\frac{1}{N}\right)^{1/2}$$

$$\frac{W_{en}}{W_e} = \frac{N D_n^3}{D^3} = N \left(\frac{1}{N}\right)^{3/2} = \left(\frac{1}{N}\right)^{1/2}$$

Consider total weights:

$$W_{tn} = W_{sn} + W_{en}$$

$$W_t = W_s + W_e$$

$$W_s = N^{1/2} W_{sn}, \quad W_e = (N^{1/2}) W_{en}$$

So

$$\frac{W_{tn}}{W_t} = \frac{W_{sn} + W_{en}}{W_s + W_e} = \frac{W_{sn} + W_{en}}{N^{1/2} (W_{sn} + W_{en})} = \left(\frac{1}{N}\right)^{1/2}$$

Consider a fixed length L :

$$\pi D L = N \pi D_n L_n$$

$$D = N D_n, \quad \frac{D_n}{D} = \frac{1}{N}$$

Therefore,

$$\frac{W_{sn}}{W_s} = \frac{1}{N}$$

$$W_{en} = N \left(\frac{1}{N} \right)^3 = \left(\frac{1}{N} \right)^2$$

$$\frac{W_{tn}}{W_t} = \frac{W_{sn} + W_{en}}{N W_{sn} + N^2 W_{en}} = \frac{W_{sn} + W_{en}}{N W_{sn} + N^2 W_{en}}$$

In both examples $\frac{W_{tn}}{W_t}$ decreases as N is increased. However, an increase in external plumbing required to supply multiple distributors will somewhat offset the apparent saving.

The foregoing analysis has shown that multiple distributors are advantageous from the viewpoint of distributor weight. The effect of multiple distributors on forced convection is now considered. For purposes of this analysis, it is assumed that the local heat transfer coefficient is directly proportional to the local maximum velocity. Total forced convective heat transfer, then, is proportional to the integral of $h \, dA$ over the area of influence. For simplification this area is taken from the outlet to an arbitrary minimum velocity when a common outlet velocity is assumed.

The maximum local velocity is given by:

$$u_m = U_\infty \left(\frac{r}{R} \right)^{-1.143}$$

The differential area is given by:

$$dA = 2\pi r \, dr$$

To obtain a given decrease in maximum local velocity, it is necessary only to specify the radius ratio $\frac{r}{R} = \alpha$.

The integral of $u_m \, dA$ is evaluated between the limits of R and r where $r = \alpha R$.

$$\int_R^{\alpha R} u_m \, dA = 2\pi U_\infty \int_R^{\alpha R} \left(\frac{r}{R} \right)^{-1.143} r \, dr$$

$$= \frac{2\pi U_\infty}{0.857} \left[\alpha^{0.857} - 1 \right] R^2$$

For constant L/D , $\frac{R_n}{R} = \left(\frac{1}{N} \right)^{1/2}$ and N differential areas are required. These substitutions reduce the above integral to itself thereby showing that no heat transfer advantage is to be gained by multiple distributors of constant L/D ratio.

For constant length L , $\frac{R_n}{R} = \frac{1}{N}$ and N differential areas are required. These substitutions reduce the integral to the following:

$$\left(\int_R^{\alpha R} u_m \, dA \right)_L = \frac{1}{N} \frac{2\pi U_\infty}{0.857} \left[\alpha^{0.857} - 1 \right] R^2$$

Therefore, it is concluded that N distributors of the same length L as a single distributor

will have $\frac{1}{N}$ times the total heat transfer of the single distributor.

3.3 TEST TANK

Figure 16 shows the effect of film coefficient on pressurant requirements in the 500-gallon test tank. Pressurizing gas changes by a factor of four for a change in film coefficient from 30 Btu/hr-ft²-R to zero. This is a much larger percentage change than in a flight tank (Figure 17).

The difference is due primarily to two factors, radius and structural safety factor. For a given pressure, tank wall thickness is proportional to radius but tank volume is proportional to radius squared, so the ratio of gas weight to wall weight increases in direct proportion to radius. Thus, wall heat capacity has an inherently smaller gas cooling potential in a large tank than in a small tank. Furthermore, the 500-gallon tank was designed for operation at 100 psia with the increased structural margins normally associated with test tanks as compared to flight tanks. Thus, the test tank again has a relatively large gas cooling capacity.

In actuality, the effect of film coefficient on pressurant requirements is likely to be somewhat more pronounced than is indicated by Figure 16. The difference will be due to the assumption of no interface heat or mass transfer and to the higher actual mass of the dome area of the tank. The additional mass of material associated with the flange and lid of the manhole substantially increases the wall heat capacity in the dome region thereby increasing the gas cooling rate in that region. This effect was not included in the development of Figure 16.

The effect of inlet gas temperature on pressurant requirement, shown in Figure 18, is presented only to show the relatively small variation that can be expected and, therefore, the accuracy with which this quantity must be measured during the test operation.

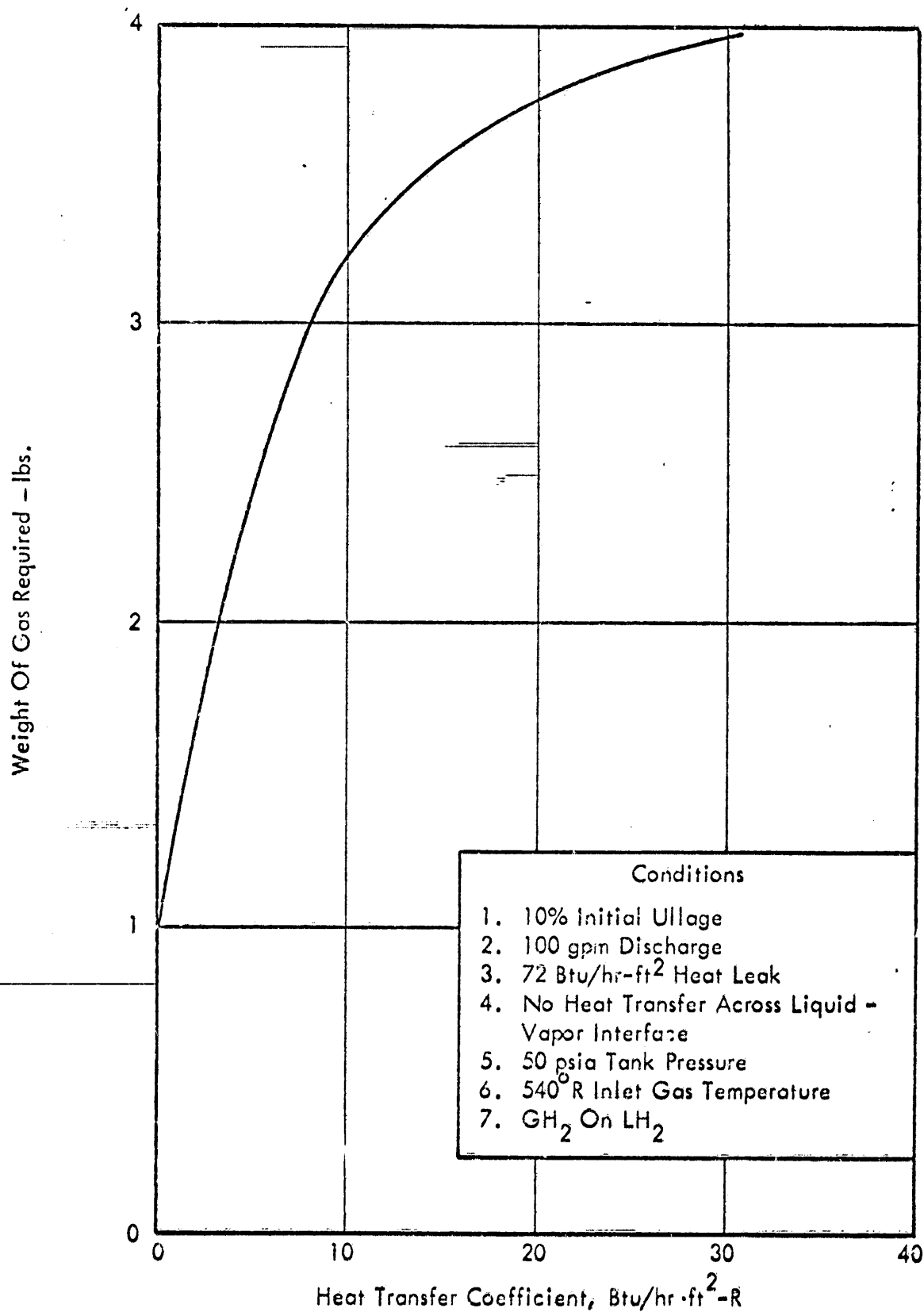


FIGURE 16 EFFECT OF INTERNAL GAS-TO-WALL HEAT TRANSFER COEFFICIENT ON PRESSURANT GAS REQUIREMENT - 500 GALLON TEST TANK

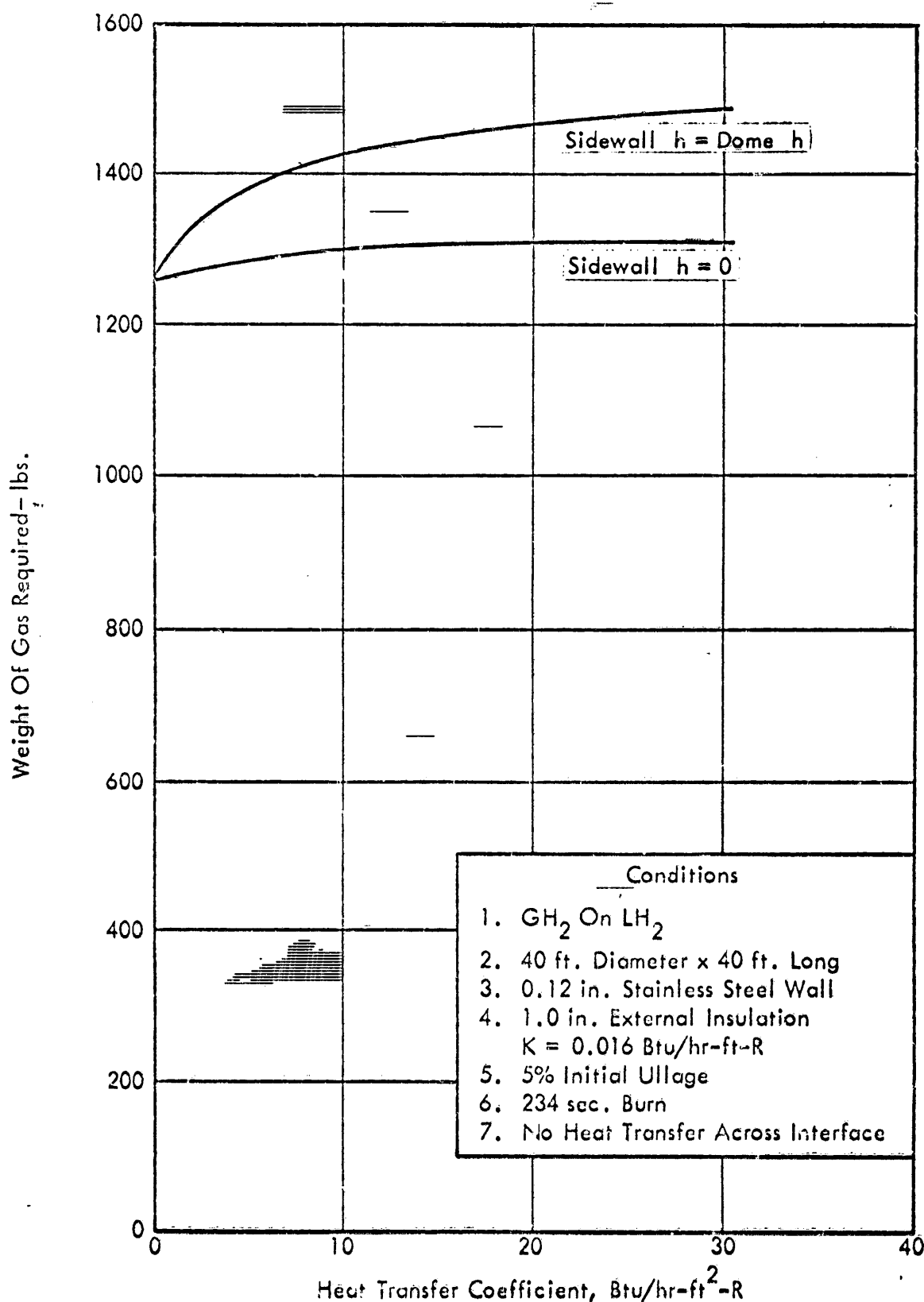


FIGURE 17 EFFECT OF HEAT TRANSFER COEFFICIENT ON GAS REQUIREMENTS - FLIGHT TANK

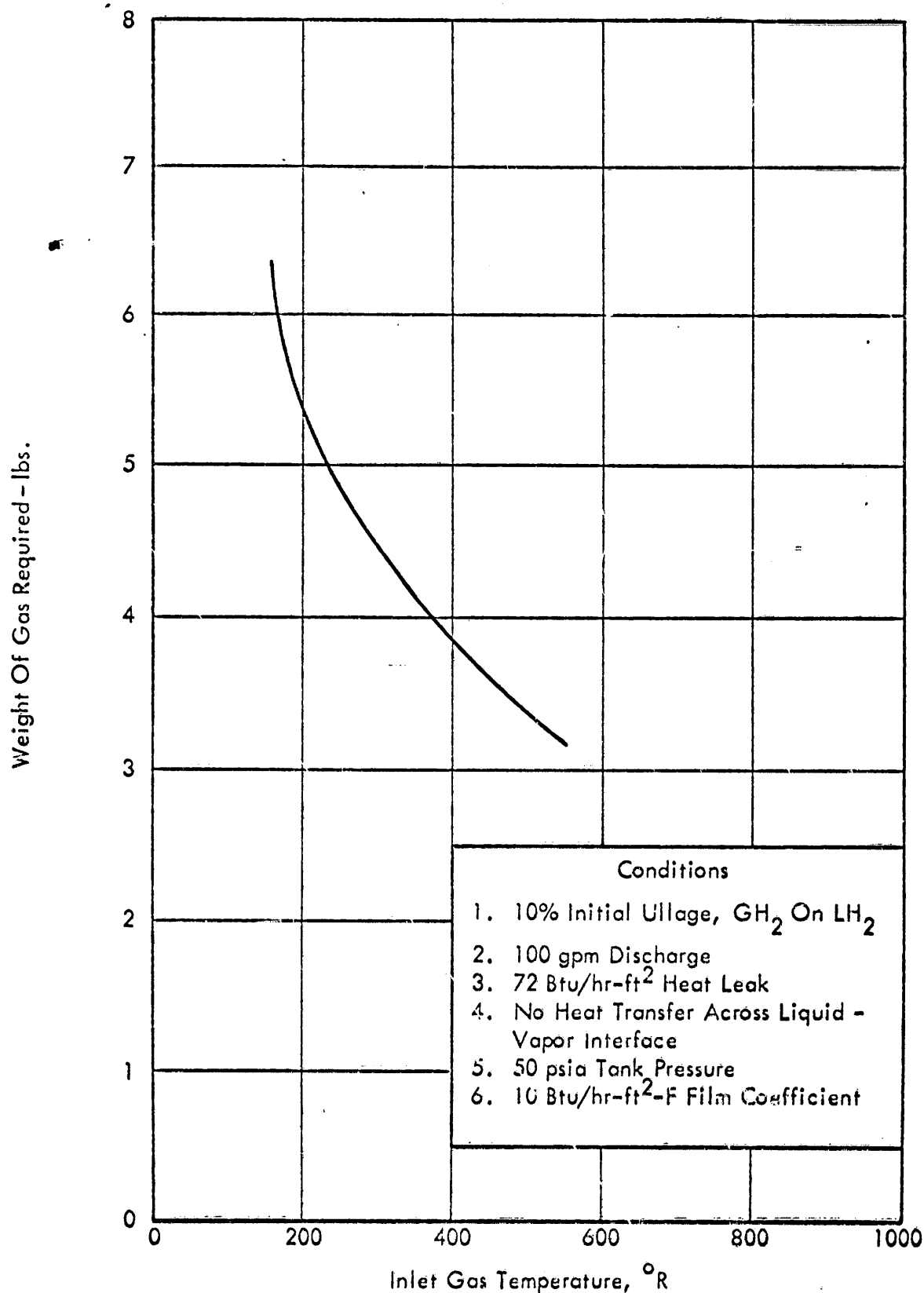


FIGURE 18 EFFECT OF INLET GAS TEMPERATURE ON PRESSURANT REQUIREMENT - TEST TANK

3.4 FLIGHT TANK

To obtain an indication of the possible weight savings to be realized by proper distribution of the pressurant gas at the inlet, calculations were made for a flight size tank. Using the Lockheed-Georgia Company Tank Pressurization and Aerodynamic Heating Program for the IBM 7090 computer (Reference 7), the required inlet gas flow history was determined for a representative large hydrogen tank. On the basis of free convection data for similar conditions, it seemed reasonable to size the distributor for a velocity of 10 ft/sec based on gross active surface area. For the maximum inlet flow rate of 6.21 lb/sec, this gave an area of 32.25 ft².

The potential gain due to reduced wall heat transfer coefficients can be seen from Figure 17, which is the pressurizing gas requirements computed in the IBM runs for the conditions indicated on the figure. If both the sidewall coefficient and the dome coefficient are reduced from 30 Btu/hr - ft² - R to zero, the saving in pressurizing gas weight is 230 lbs. However, if the distributor is assumed to affect only the dome coefficient, the saving would be 50 lbs for complete elimination of dome heat transfer or 10 lbs if h is reduced from 30 to 10 Btu/hr - ft² - R.

The effect of heat and mass transfer across the liquid-vapor interface was not included in the computer runs because sufficient data relative to these processes were not available at the time. However, it seems reasonable to assume that these effects would tend to increase the potential saving due to proper propellant distribution in which heat and mass transfer coefficients are reduced at the interface as well as along the tank boundaries. This assumption is verified by the results of the 500-gallon tank tests with nitrogen in which severe condensation of the pressurant occurred as the result of poor inlet gas distribution.

3.5 SCALING ANALYSIS

Of necessity, all of the data collected in the course of this program are from tanks

of much smaller size than the ones to which the information or results are to be applied. It is for the purpose of determining the applicability of data collected in this program to flight systems that the following analysis was performed. Specifically, the intent of the analysis is the determination of those variables, or groups of variables, which have a significant influence on the total pressurant gas requirements and of the degree to which they influence these requirements.

The pressurizing gas requirements of any system are determined by balancing the rate of change of energy in the gas space with the rate of change of energy in the wall. The rate of change of energy in the gas space is equal to the rate at which energy enters the system minus the rate at which energy leaves the system. That is,

$$\begin{array}{rcl}
 \text{RATE OF CHANGE OF} & & \text{RATE OF ENERGY ENTERING} \\
 \text{ENERGY IN GAS SPACE} & = & \text{IN INLET GAS} \\
 \\
 - \text{RATE OF ENERGY} & & - \text{RATE OF HEAT TRANSFER} \\
 \text{ENTERING WALL} & & \text{FROM GAS TO LIQUID} \\
 \\
 - \text{RATE OF ENERGY TRANSFER FROM} & - & \text{RATE OF WORK} \\
 \text{GAS TO LIQUID BY CONDENSATION} & & \text{DONE BY GAS}
 \end{array}$$

The rate of energy entering the wall is equal to the net rate of energy transfer to the wall from the pressurizing gas and from external heating. That is,

$$\begin{array}{rcl}
 \text{RATE OF ENERGY} & & \text{RATE OF HEAT TRANSFER} \\
 \text{ENTERING WALL} & = & \text{FROM GAS TO WALL} \\
 \\
 + \text{RATE OF AERODYNAMIC} & + & \text{NET RADIANT ENERGY} \\
 \text{HEAT TRANSFER TO WALL} & & \text{FLUX TO WALL}
 \end{array}$$

For the present, it is assumed that the heat and mass transfer between the gas and the liquid is negligible compared to other effects and, therefore, they are dropped from the analysis. If it should later be shown that they are generally important and if the magnitudes of the coefficients governing the interchange can be determined,

these terms can readily be included. Heating of the wall from the outside is omitted in this development.

The approach for determining the dimensional groups is that described in References 8 and 9. The dimensionless groups are determined by dividing the governing differential equation by one term of the equation as follows:

$$W_g C_p \frac{dT}{d\tau} = C_p (T_i - T_g) \frac{dW_g}{d\tau} - hA (T_g - T_w) + \frac{V_t}{J} \frac{dP}{d\tau}$$

Refer to the end of this section for definitions of terms.

Setting

$$\begin{aligned} dT &= T_g \\ d\tau &= \tau \\ dW_g &= W_g \\ dP &= \Delta P \end{aligned}$$

and rearranging terms gives:

$$\frac{W_g C_p T_g}{\tau} = \frac{W_g C_p (T_i - T_g)}{\tau} - hA(T_g - T_w) + \frac{V_t \Delta P}{J \tau}$$

Dividing through by $\frac{W_g C_p T_g}{\tau}$ and setting $W_g = W_u + W_{sg}$ gives:

$$1 = \frac{T_i - T_g}{T_g} - \frac{\frac{T_g - T_w}{T_g} \frac{hA \tau}{C_p}}{W_u + W_{sg}} + \frac{V_t \Delta P}{J W_g C_p T_g}$$

Assuming that the gas behaves as a perfect gas and that the pressure change can be expressed as a power function of time, $P = C_K \tau^K$, the last term of the above equation can be reduced as follows:

$$\frac{V_t}{W_g T_g} \frac{\Delta P}{C_p J} = \frac{R \Delta P}{C_p P_g J} = \frac{C_K \tau^K}{P_g} \frac{R}{J C_p} = \frac{C_K \tau^K}{P_g} \left(1 - \frac{1}{\gamma}\right)$$

The term $\frac{\frac{T_g - T_w}{T_g} \frac{h A \tau}{C_p}}{W_u + W_{sg}}$ becomes more meaningful when W_u is replaced by $\rho_u V_i$ and the entire term is multiplied by $\frac{\rho_u V_t}{\rho_i V_t}$.

$$\frac{\frac{T_g - T_w}{T_g} \frac{h A \tau}{C_p}}{W_u + W_{sg}} = \frac{\frac{T_g - T_w}{T_g} \frac{h A \tau}{\rho_i V_t C_p}}{\frac{\rho_u V_i}{\rho_i V_t} + \frac{W_{sg}}{\rho_i V_t}}$$

When these substitutions are made the reduced differential equation becomes:

$$1 = \left(\frac{T_i}{T_g} - 1\right) - \frac{\left(1 - \frac{T_w}{T_g}\right) \frac{h A \tau}{\rho_i V_t C_p}}{\frac{\rho_u V_i}{\rho_i V_t} + \frac{W_{sg}}{\rho_i V_t}} + \frac{C_K \tau^K}{P_g} \left(1 - \frac{1}{\gamma}\right)$$

The energy rate equation for the wall,

$$m \rho_m C_{pm} \frac{dT_w}{d\tau} = h(T_g - T_w),$$

is readily reduced to:

$$1 = \frac{m \rho_m C_{pm}}{h \tau} \frac{T_w}{T_g - T_w}$$

by the technique applied to the energy rate equation for the gas.

Combining the two reduced energy rate equations and transposing the unknown groups to the left side yields:

$$\left[\frac{T_i}{T_g}, \frac{W_g}{\rho_i V_t}, \frac{W_{sg}}{\rho_i V_t} \right] = f \left[\frac{h A \tau}{\rho_i V_t C_p}, \frac{\rho_u V_i}{\rho_i V_t}, \frac{t m \rho_m C_{pm}}{h \tau}, \frac{C_K \tau^K}{P_g} \left(1 - \frac{1}{\gamma}\right) \right]$$

or

$$\frac{W_{sg}}{\rho_i V_t} = g_1 \left[\frac{h A \tau}{\rho_i V_t C_p}, \frac{\rho_u V_i}{\rho_i V_t}, \frac{t m \rho_m C_{pm}}{h \tau}, \frac{C_K \tau^K}{P_g} \left(1 - \frac{1}{\gamma}\right) \right]$$

$$\frac{W_g}{\rho_i V_t} = g_2 \left[\frac{h A \tau}{\rho_i V_t}, \frac{\rho_u V_i}{\rho_i V_t}, \frac{t m \rho_m C_{pm}}{h \tau}, \frac{C_K \tau^K}{P_g} \left(1 - \frac{1}{\gamma}\right) \right]$$

$$\frac{T_w}{T_g} = g_3 \left[\frac{h A \tau}{\rho_i V_t}, \frac{\rho_u V_i}{\rho_i V_t}, \frac{t m \rho_m C_{pm}}{h \tau}, \frac{C_K \tau^K}{P_g} \left(1 - \frac{1}{\gamma}\right) \right]$$

The term $\frac{W_{sg}}{\rho_i V_t}$ is the ratio of the weight of the pressurizing gas actually supplied to the weight of gas required to fill the tank assuming no initial ullage and no heat or mass transfer. The term $\frac{W_g}{\rho_i V_t} = \frac{T_i}{T_g}$ is the ratio of the actual weight of gas in the tank assuming the same conditions stated above.

The solution of the second of the above equations was obtained with the equation rewritten as:

$$\frac{T_i}{T_g} = \frac{W_g}{\rho_i V_t} = C_1 \left(\frac{h A \tau}{\rho_i D C_p} \right)^a \left(\frac{t m \rho_m C_{pm}}{h \tau} \right)^b \left(\frac{\rho_u}{\rho_i} \%U \right)^c \left(\frac{C_K \tau^K}{P_g} \frac{\gamma-1}{\gamma} \right)^d$$

The coefficients were determined for the case of hydrogen using the Lockheed-Georgia Company Tank Pressurization Program. The data available when the coefficient and exponents were obtained were for constant pressure runs and thus were insufficient to permit the determination of the exponent "d". The data used to determine the coefficient "C₁" and the other exponents are shown in Table 1 and are plotted in Figure 19. The slope of each curve is the exponent for that term. The coefficient "C₁" is found by dividing the temperature ratio $\frac{T_i}{T_g}$ by the product of all of the groups raised to the appropriate power. The resulting expression is:

TABLE 1 CORRELATION DATA

Run Number	Ti	$\frac{tm \rho_m C_{pm}}{h\tau}$	$\frac{h\tau}{\rho_i D C_p}$	$\frac{\rho_u}{\rho_i} \%U$	$\frac{W_{sg}}{\rho_i V_T \text{ Comp.}}$
1	500	0.433	0.437	0.248	1.41
2	500	0.0722	0.437	0.248	1.25
3	500	0.722	0.437	0.248	1.46
4	500	3.62	0.437	0.248	1.63
5	500	0.408	0.044	0.248	1.10
6	500	0.408	0.10	0.248	1.23
7	500	0.408	0.65	0.248	1.49
8	500	0.408	0.437	0.10	1.34
9	500	0.408	0.437	0.5	1.54
10	500	0.408	0.437	0.593	1.59
11	300	0.167	0.0264	0.149	1.1
12	300	0.167	0.06	0.149	1.12
13	300	0.167	0.39	0.149	1.27
14	300	0.167	0.26	0.06	1.17
15	300	0.167	0.26	0.3	1.30
16	700	0.513	0.0616	0.347	1.27
17	700	0.513	0.14	0.347	1.33
18	700	0.513	0.91	0.347	1.67
19	700	0.513	0.612	0.14	1.48
20	700	0.513	0.612	0.7	1.75

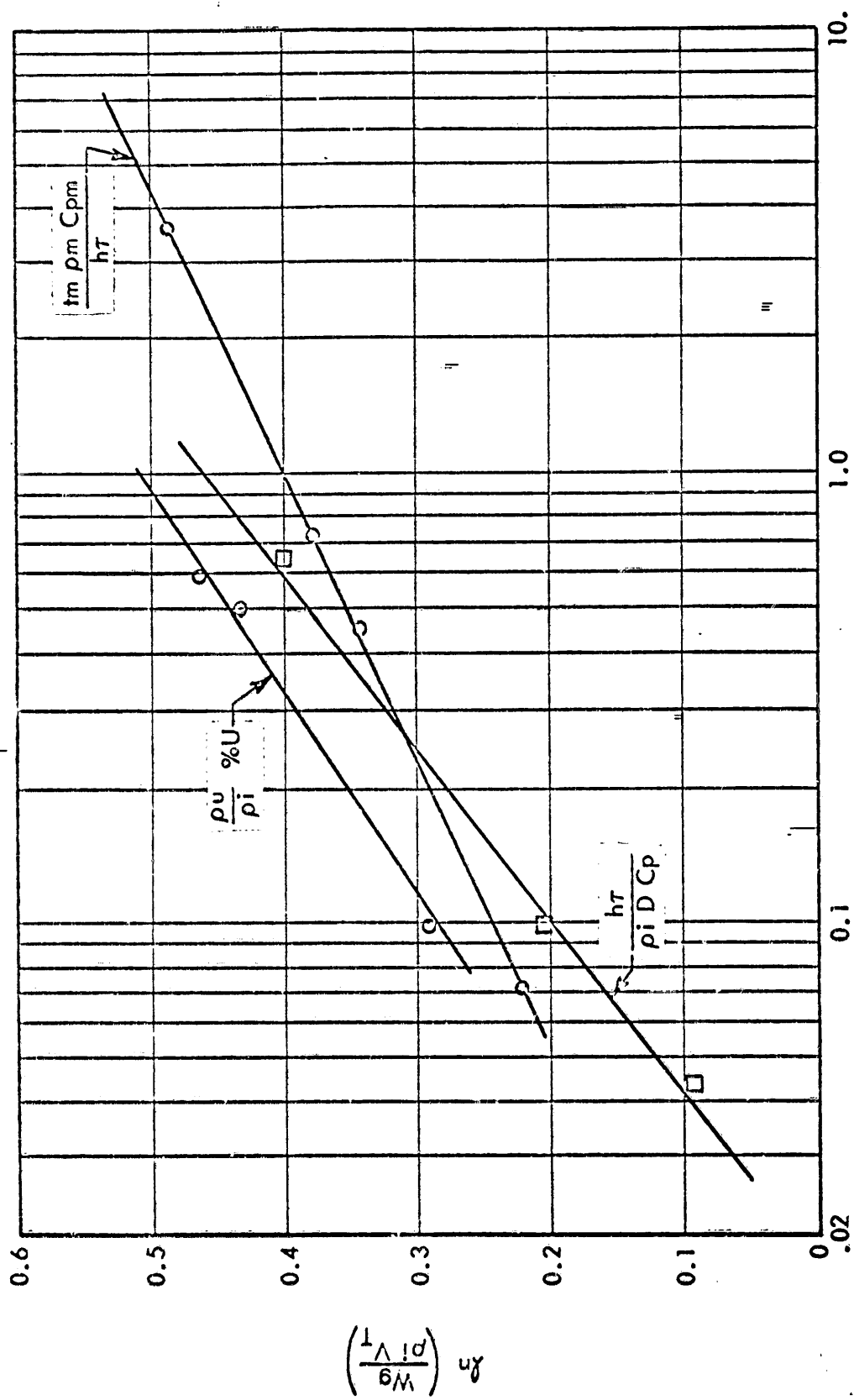


FIGURE 19 CORRELATION DATA

$$\frac{W_g}{\rho_i V_t} = 1.135 \left(\frac{h \tau}{\rho_i D C_p} \right)^{-0.113} \left(\frac{t_m \rho_m C_{pm}}{h \tau} \right)^{-0.0675} \left(\frac{\rho_u}{\rho_i} \%U \right)^{-0.098}$$

Assuming for the moment that in cases where the liquid is not expelled at constant pressure that the effect of the work term on the gas requirements is small or that at worst it is a constant additive, the possible reduction in the gas requirements of a flight system that could be obtained by using an effective pressurant distributor can be determined from this equation if the effect of distributor design on heat transfer coefficient is known. By substituting information from flight systems into the above expression, the test conditions for studying each flight system can be determined.

A computer program has been written to facilitate the use of the above expression in the computation and extrapolation of pressurant requirement data. The computer program is discussed in Appendix II.

3.6 DESCRIPTION OF SYMBOLS

Symbol	Description	Units
$A, \frac{W_g}{\rho_i V_t}$	Ratio of actual quantity of gas to that required if no heat or mass transfer occurred	-----
$C, c, \frac{h \tau}{\rho_i D C_p}$	Dimensionless parameter	-----
C_p, cp	Constant pressure specific heat of gas	Btu/lb-°F
C_{pm}, cpm	Specific heat of tank wall	Btu/lb-°F
D, d	Diameter of tank	Ft
$E, e, \frac{t_m \rho_m C_{pm}}{h \tau}$	Dimensionless parameter	-----

(Continued)

Symbol	Description	Units
$F, f, \frac{\rho_i}{\rho_u} \%U$	Dimensionless parameter	-----
h	Heat transfer coefficient in ullage region	Btu/hr-ft ² -°F
l_{max}, i_{max}	Number of data sets input	-----
P_i, p_i	Pressure of inlet gas	lb/ft ²
P_u, p_u	Initial ullage pressure	lb/ft ²
R, r	Gas constant	ft/°F
R_{hom}, ρ_m	Specific weight of tank wall	lb/ft ³
ρ_i	Specific weight of incoming gas	lb/ft ³
ρ_u	Specific weight of initial ullage gas	lb/ft ³
T_i, t_i	Temperature of incoming gas	°F
t_m	Thickness of tank wall	ft
T_u, t_u	Initial ullage gas temperature	°F
Time, time, τ	Emptying time of tank	hr
$U, u, \%U$	Ratio of initial ullage volume to total tank volume	-----
V_t	Total tank volume	ft ³

4.0 EXPERIMENTS

4.1 SMOKE TEST CHAMBER

The smoke test chamber shown in Figure 20 was used to obtain qualitative data on the discharge characteristics of real distributors. Visual and photographic observation of several configurations were made under flow conditions in the chamber.

The test chamber is a 42-inch diameter carbon steel cylinder with an ellipsoidal dome on one end and a removable perforated aluminum plate at the other end. The overall length of the chamber is 4.5 feet. A 1.5-inch diameter pressurizing gas line enters the dome end of the chamber from the side in the same manner as it enters the 500-gallon cryogenic test tank. Thus, the smoke chamber is essentially identical in size and shape to the upper half of the 500-gallon tank.

A dense, white, non-toxic smoke suitable for both visual and photographic observation was produced by passing air over olibanum gum which was heated in the gas generator. A nominal 100 psi, 1-inch diameter line from the shop air system supplied the test apparatus. It should be mentioned that the smoke, under certain conditions, is explosive.

Four windows are provided for observation: the three shown in Figure 20 and another which was added in the center of the removable end plate. Each of the windows has an 8-inch diameter viewing area. The three side windows were used primarily for visual observation while the end window was used primarily for photography. Use of the side windows for photography is limited by their proximity to the area of interest which severely reduces the depth of field.

4.2 SELECTION OF GOOD DISTRIBUTOR

The good distributor used in the cryogenic testing was selected on the basis of

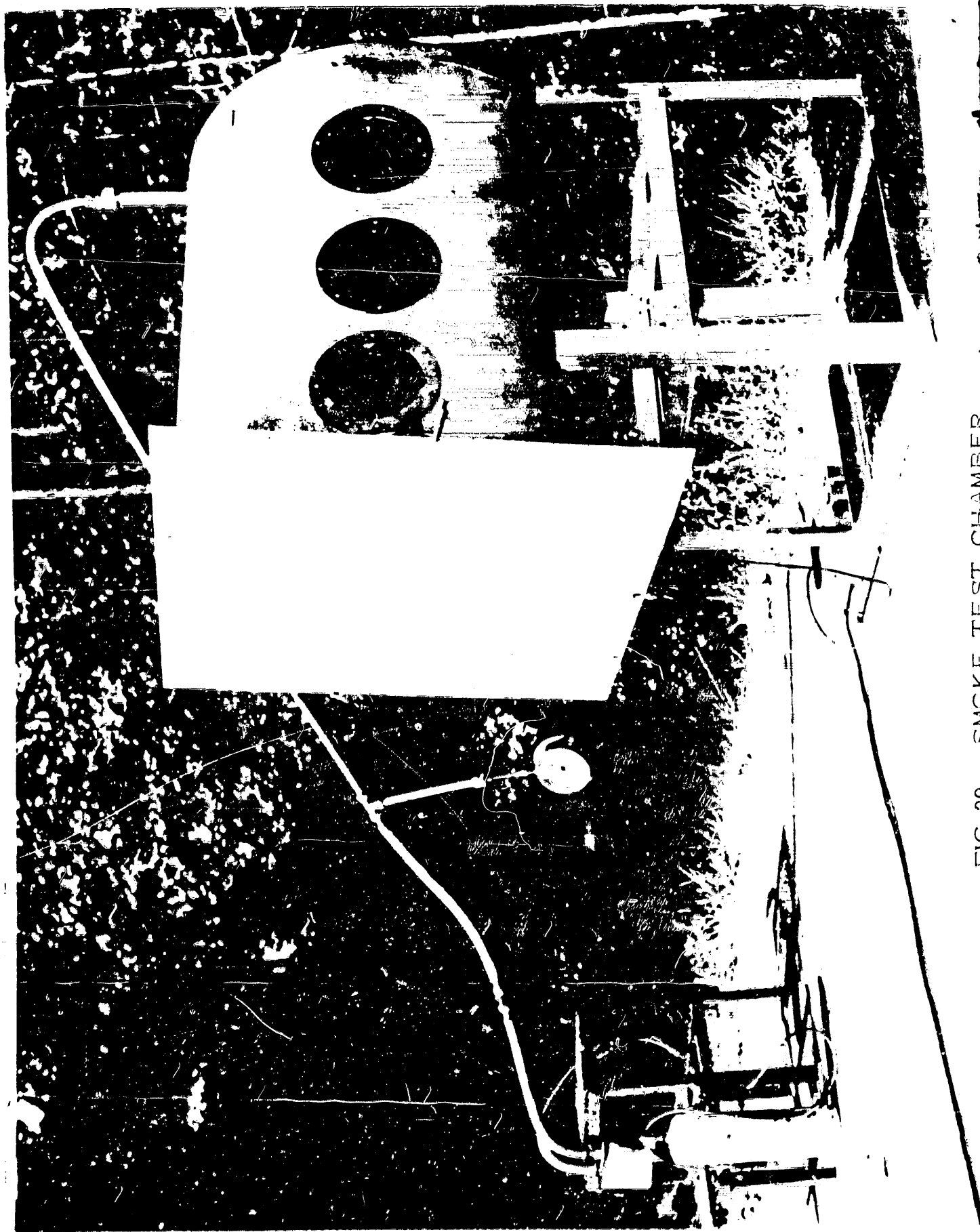


FIG. 20. SMOKE TEST CHAMBER

discharge patterns observed in the smoke test chamber. This distributor, shown on the right in Figure 21, has a nearly uniform discharge velocity with no noticeable non-normal components. The discharge pattern of the distributor is shown in end view in Figure 22. No side view photographs were attempted; but the flow was visually observed and noted to be uniform in profile.

The distributor is 10.0 inches in diameter by 2.5 inches deep as shown in Figure 23. It consists of a 2-inch deep plenum into which the incoming gas is initially dumped and a 0.5-inch deep normalizing chamber from which the gas is injected into the test tank. The plate which separates the two chambers (the inner baffle) and the bottom plate (the outer baffle) are both drilled with number 40 holes (0.098 dia.) on a square pattern of 0.5-inch centers but with the pattern in one baffle offset 0.25-inch in each direction from that of the other baffle. The material throughout is 0.040-inch thick aluminum and the fabrication is by welding.

The heat capacity of this distributor is approximately $0.375 \text{ Btu/}^{\circ}\text{R}$. Assuming that 3 lbs of hydrogen gas raises the temperature of the distributor by 500°R , the average temperature drop of the gas will be 14°R or approximately 3 percent of the available. The effect of this small temperature change on the quantity of pressurant gas required can be accounted for in the overall evaluation.

4.3 SELECTION OF POOR DISTRIBUTOR

The "poor" distributor to which the performance of the "good" distributor is compared was the best distributor which weighs no more than an open tube. An additional requirement was established to facilitate the analysis of the test data: the tube terminated in a sonic orifice. Consistent with these requirements a sonic orifice was placed in the end of the existing pressurant line in the test tank. The orifice extended approximately 6 inches into the tank at a point 4.5 inches below the tank top. It was directed radially toward the opposite wall.

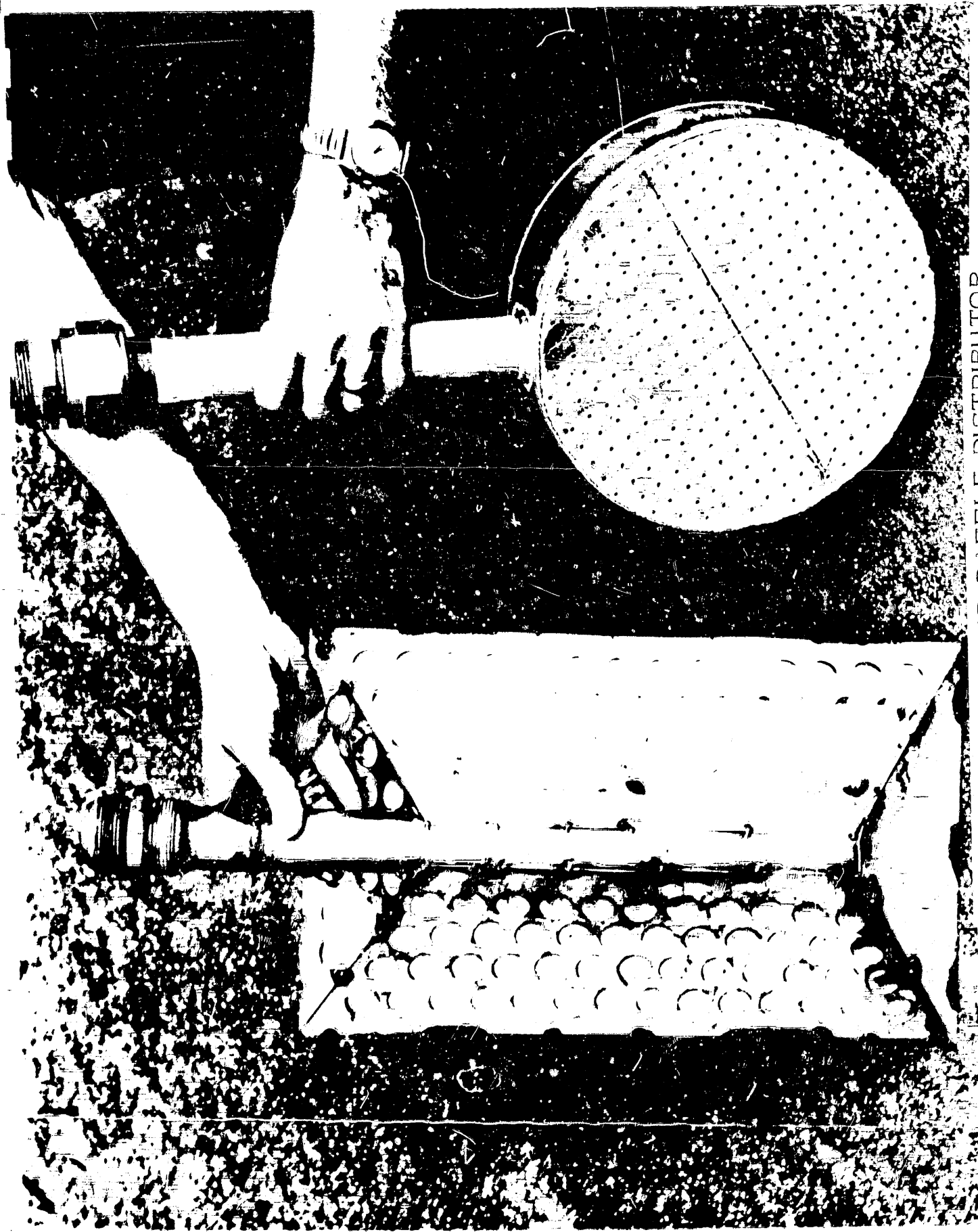
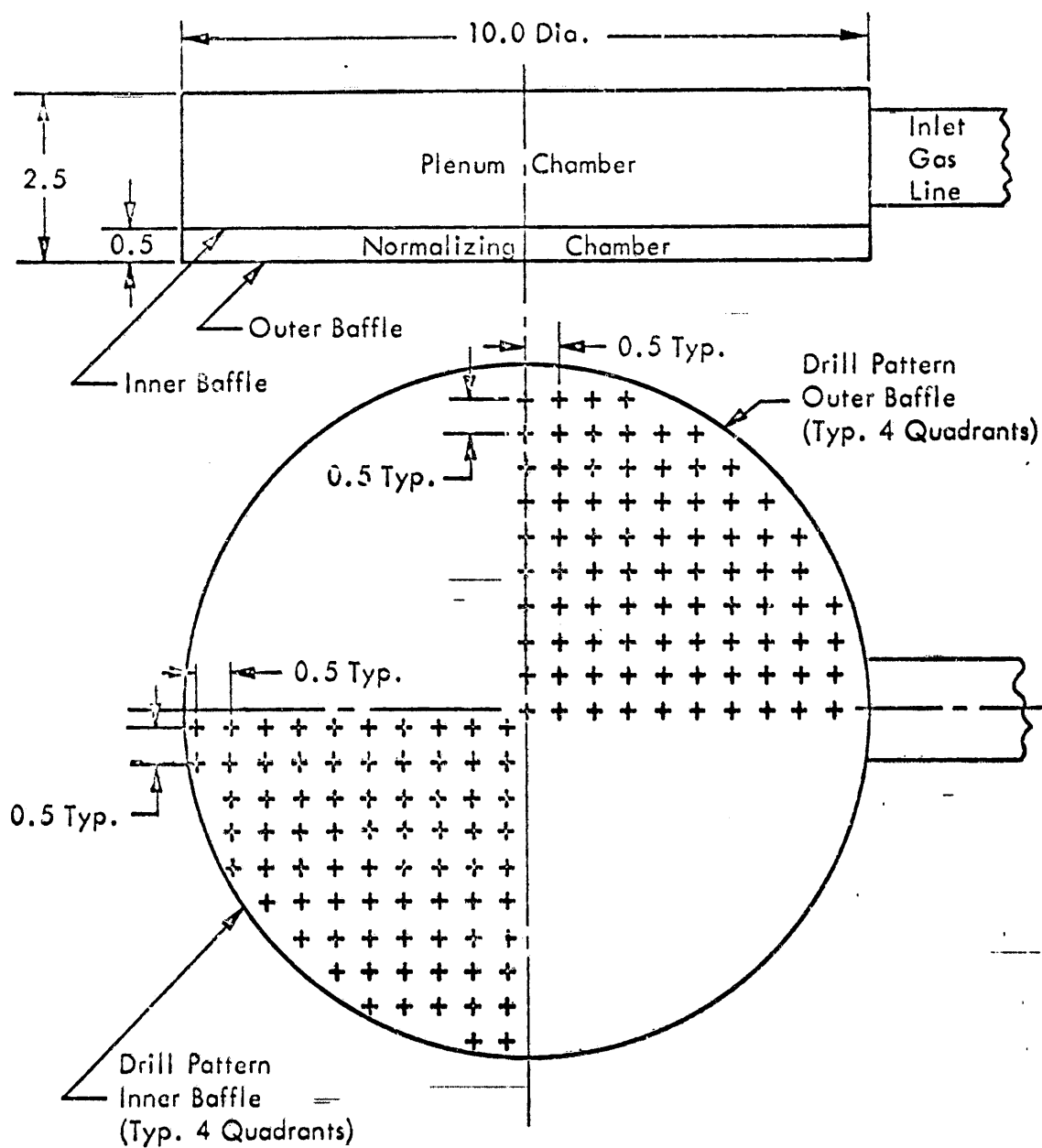


FIG 21 - PLENUM AND BAFFLE DISTRIBUTOR

FIG 22 - DISCHARGE PATTERN OF PLENUM AND
BAFFLE DISTRIBUTOR



Note: Front Side Removed
For Clarity

FIGURE 23 PLENUM AND BAFFLE DISTRIBUTOR DESIGN

4.4 FLUID DYNAMICS SYSTEM

The fluid dynamics system used in the test program is shown schematically in Figure 24.

The 500-gallon cryogenic test tank is shown in Figure 25. The inner vessel of the tank is 40 inches in diameter X 98 inches in length with ellipsoidal domes. The wall is 0.090-inch thick stainless steel.

The annular volume between the inner and outer shells of the tank is perlite filled in order to maintain a uniform and reasonably low heat leak into the tank. Localized heat leaks into the ullage region of the tank have been reduced to an estimated 80 Btu/hr for a 500°R temperature difference.

4.5 LIQUID TRANSFER SYSTEM

The liquid transfer system was composed of the line connecting the storage tank and the test tank and the valves which control the flow in that line.

Moving from the storage tank forward to the test tank, the following valves appear in the order listed:

- (1) A manually operated 2-inch gate valve which was used to isolate the storage tank and is normally closed.
- (2) A 0.25-inch relief valve used to vent the line between the 2-inch gate and positioning valves when both are closed.
- (3) An electrically operated 2-inch positioning valve used to meter the liquid flow during discharge and was normally open to prevent a pressure build-up due to the entrapment of evaporating liquid between it and the gate valve.

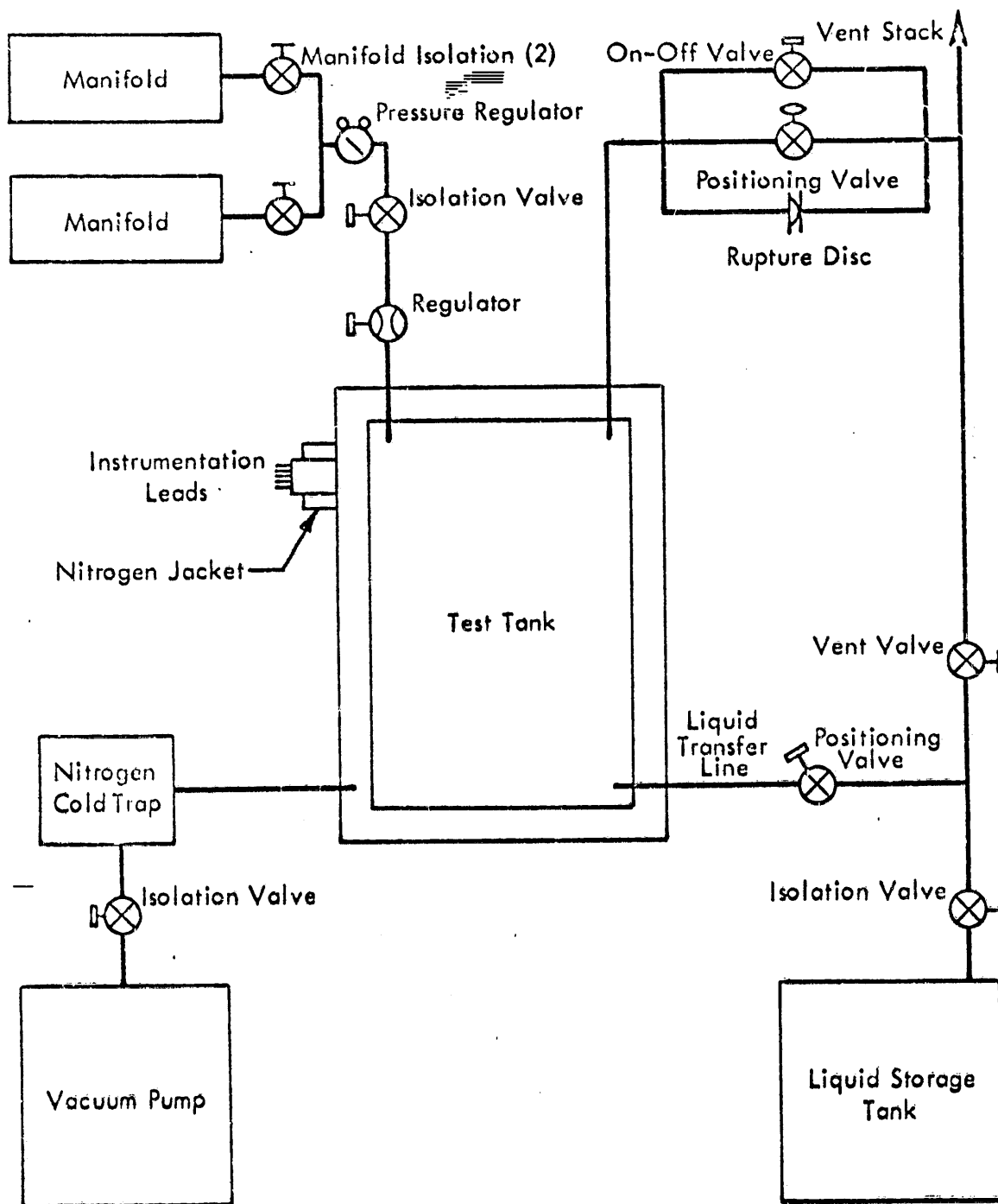
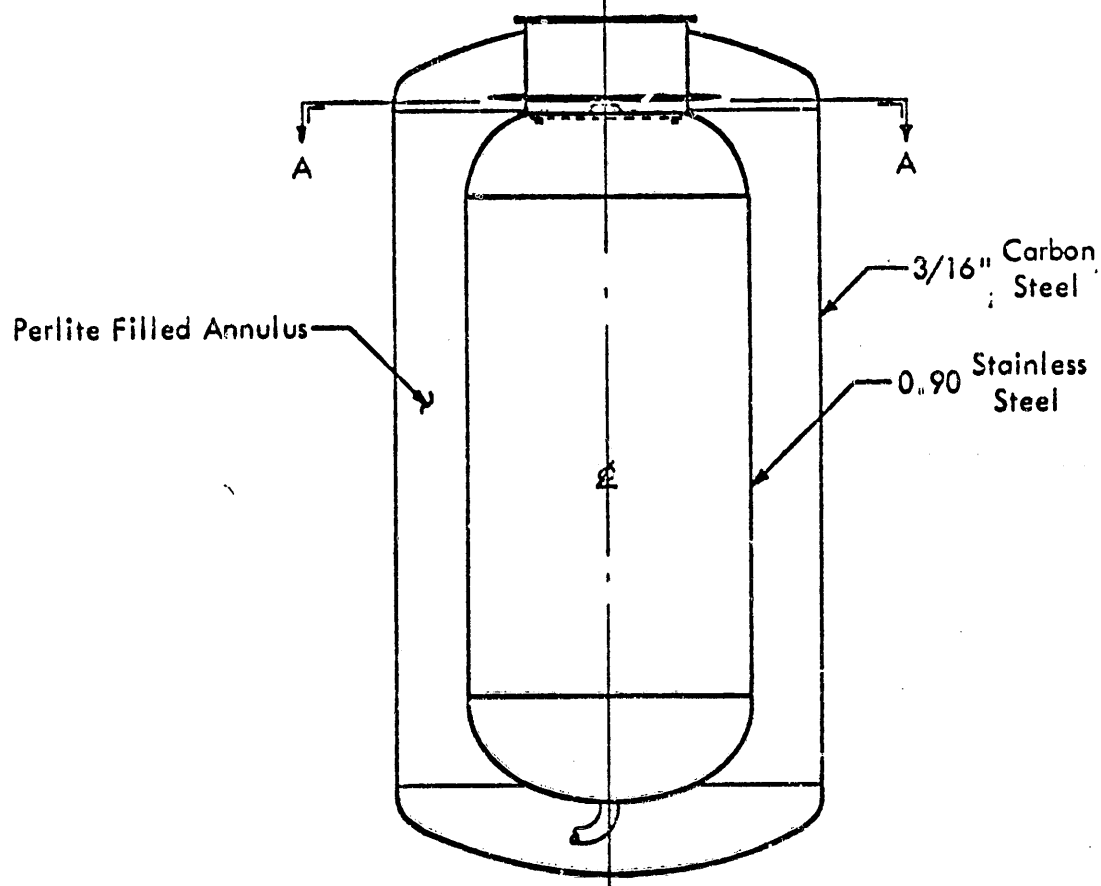
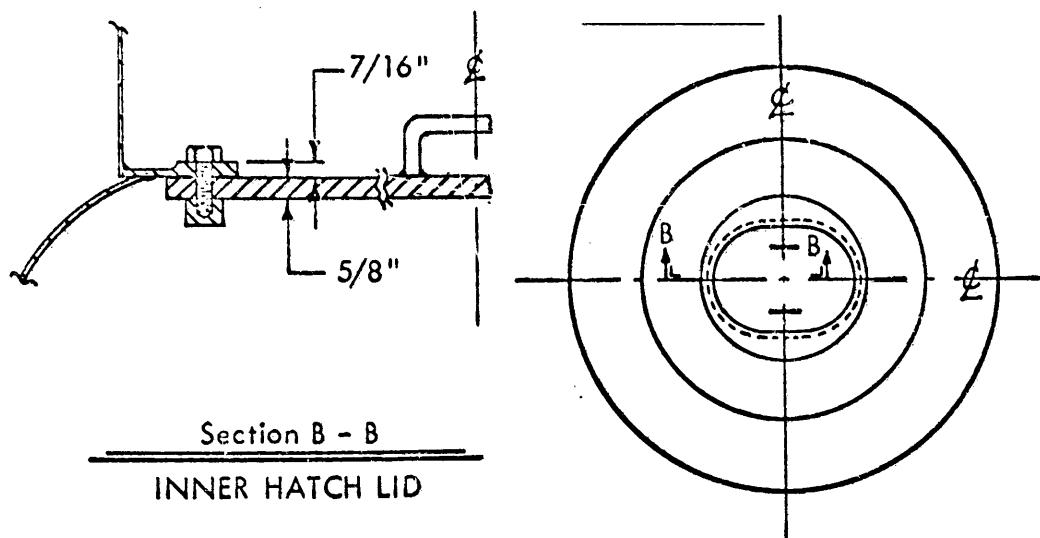


FIGURE 24 FLUID TEST SYSTEM SCHEMATIC



Front Half Of Outer Tank Omitted For Clarity

FIGURE 25 500-GALLON TEST TANK

eter. That part of the line from the storage tank through the blast wall, which separates the test area from the storage tank, is rigid; the remainder of the line is flexible. The line within the test tank annulus is effectively insulated by the annulus vacuum.

The isolation valve is opened only when liquid transfer is imminent. At all other times the valve is closed to prevent inadvertent transfer of liquid from the storage tank to the test area. In addition, it minimizes the amount of liquid outside the storage tank under non-testing conditions and thereby reduces the propellant loss due to boiloff.

The pressurant gas system is composed of the gas manifolds, transfer line, valving, and the test tank venting components as shown in Figure 24. The electrically operated valve between the manifolds and the pressure regulator is used to immediately isolate the manifolds at the end of a test run. This eliminates the loss of gas which otherwise would blow through the tanks unnecessarily. Also, it retains the residual gas so that it may be measured and thus provide a check on the amount of gas used. The manually set regulator is used to reduce the inlet pressure to the controlling regulator so that smoother action of that regulator is obtained.

The tank vent system contains three parallel elements as required to insure safe operation under all reasonable conditions. These include a rupture disc as an ultimate fail-safe device, an electrically operated on-off valve to provide fast operating low pressure-drop venting, and a pneumatically operated, variable position valve to provide fine control of tank pressure through venting.

4.6 PROPELLANT STORAGE AND SUPPLY

Liquid nitrogen required for use in the test tank was supplied from and returned to

the 6000-gallon storage tank.

Gases were supplied from standard cylinders through 6 bottle manifolds as required. The gas manifolds are in the form of saw horses to facilitate the mounting and removal of bottles and to eliminate the necessity for tying bottles in place to prevent tipping. Gas cylinders when not in use are stored in racks along the concrete wall near the place of use.

4.7 INSTRUMENTATION

The layout of sensors within the tank is shown in Figure 26, and the reasons for the particular selection and location of the sensors are discussed in this section.

Liquid level was sensed by 0.1 watt, 100 ohm carbon composition resistors used in the manner of hot wire anemometers. The technique is to pass a fixed current through the resistor and to detect the difference in ability of the liquid and the gas to remove the generated heat from the resistor.

This technique has been used quite satisfactorily in the past except for some occasions when a high level of liquid agitation resulted in a rather wide band of uncertainty. This condition did not arise in the present program.

The liquid level sensors are identified by the prefix "LL" in Figure 26. The suffix "A" indicates sensors used for recording; all other sensors are visually monitored. These sensors are positioned as required to aid the establishment of the initial liquid level and then to yield a record of the liquid level history through the period of a test.

Tank wall and pressurant gas temperatures are measured with copper-constantan thermocouples located as shown in Figure 26 by symbols prefixed by a "T" or "W".

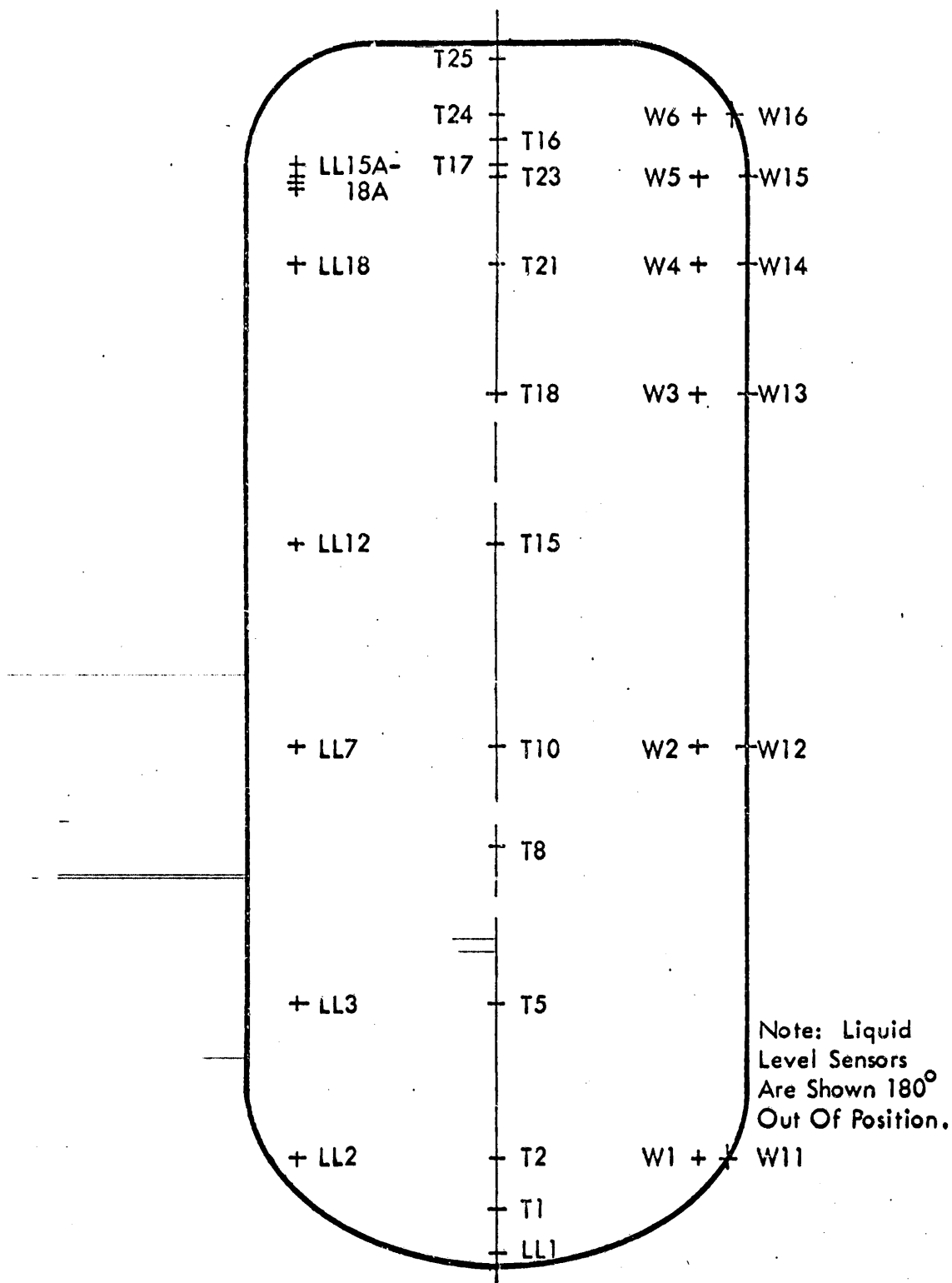


FIGURE 26 INSTRUMENTATION LAYOUT

The thermocouples along the tank centerline are used in the determination of the quantity of gas within the test tank at any time. This was accomplished by integration of the axial gas density profile within the tank (with due consideration for tank geometry and radial temperature profiles). Close spacing of the thermocouples near the initial liquid surface is required to obtain proper consideration of the more dense gas at that location.

The outboard gas temperature probe and the wall thermocouples were used to indicate the effects of wall scrubbing. In addition to that primary function of the outboard probe, it provides evidence of gross radial temperature profiles.

All thermocouple data were recorded continuously on oscillographs. The observed gas temperature variation with time provides a qualitative feel for the gas turbulence within the tank. The thermocouples were referenced to the propellant temperature so that negative galvanometer deflections were avoided.

Tank pressure was continuously recorded on the oscillograph to provide a permanent record of its history and was visually monitored on a bourdon gage for test control.

The quantity and rate of pressurant used in each test was determined by application of the equation of state corrected for gas compressibility. Gas bottle pressure was sensed by a probe extending from the interior of the bottle to a strain gage transducer. The transducer output was recorded continuously on an oscillograph. Temperature was also measured inside the gas cylinder which, except for the addition of a temperature probe down its center, was identical to the other cylinders supplying the manifold. Since this cylinder was representative of the others on the manifold in that it has the same mass, area, and initial temperature, it is expected that the gas temperature and pressure history within it represent those of the other cylinders.

Pressure in the annulus of the test tank was monitored by thermocouple-type vacuum

transducers. This is a test control measurement used only to indicate that the intended range of annulus pressure is maintained.

4.8 CALIBRATION

Each thermocouple-galvanometer unit was individually calibrated at three points by the use of baths at known temperatures. A typical calibration curve is shown in Figure 27.

In order to include the effects of temperature dependent lead resistance and of inhomogeneities of the wire in the calibration, that part of the wire which is normally submerged in the liquid during testing was submerged in the liquid during the calibration. This procedure has been found to be desirable in the calibration of any low temperature thermocouple and even more desirable when the thermocouple output is monitored by a current drawing instrument.

Liquid nitrogen boiling at atmospheric pressure which corresponds to a saturation temperature of 138.6°R was used as the reference bath. The other reference liquids were a CO_2 -trichloroethylene mixture (359.5°R) and an ice-water mixture (492.6°R). The temperatures of the latter two baths were obtained by a calibrated liquid-in-glass thermometer; the temperature of the liquid nitrogen bath was obtained from the vapor pressure curve and the known atmospheric pressure.

With the reference junctions submerged in the liquid nitrogen baths, the measuring junctions and the appropriate length of lead wire was submerged in each bath and an oscillograph record was taken after the thermocouples reached equilibrium temperature as evidenced by stability of the traces. The measuring junctions and lead wires were then removed from the bath and allowed to reach ambient temperature before being submerged in the next bath. Temperature plotted versus differences in trace deflection constitutes the calibration curves. Test data was reduced directly by the

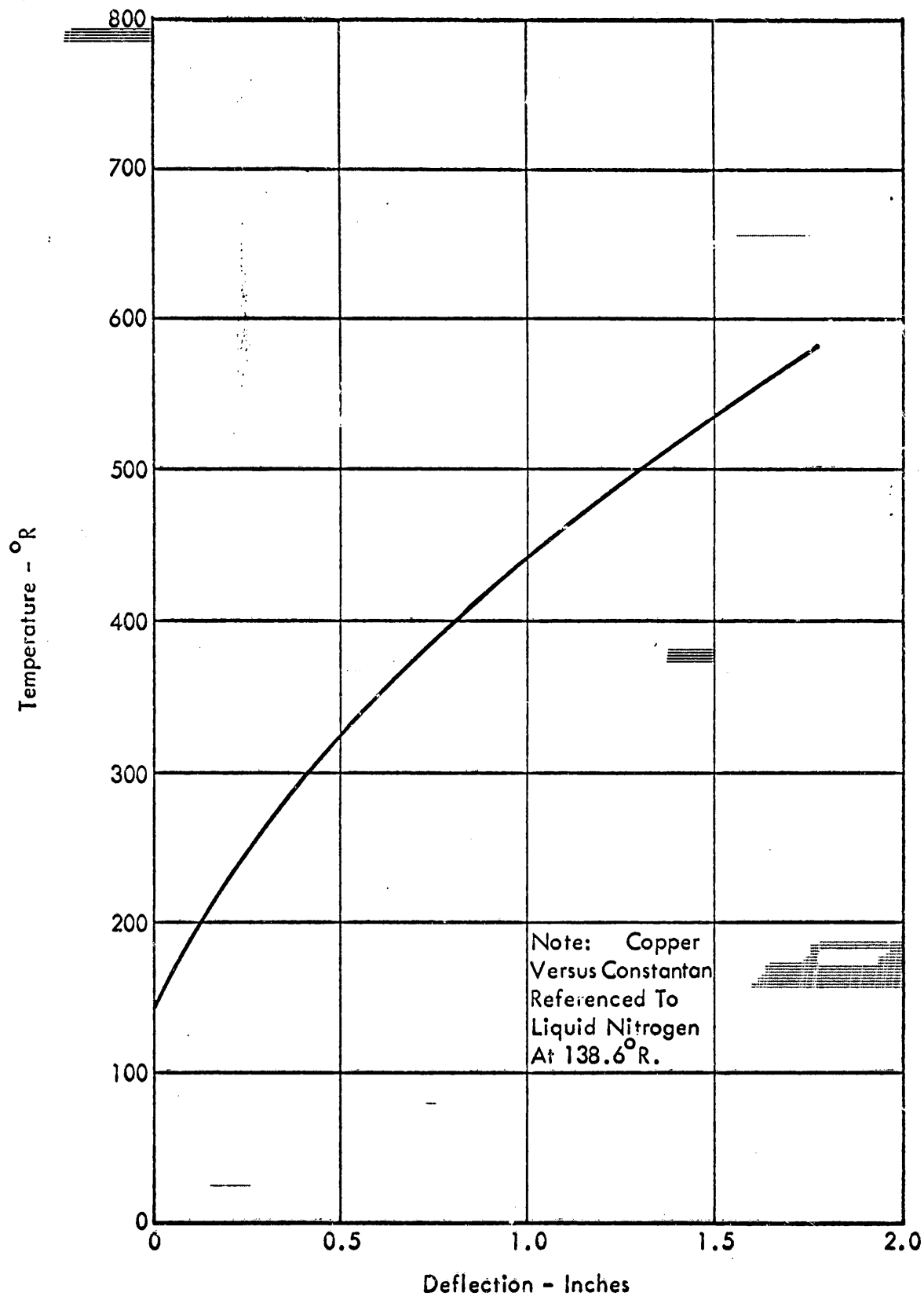


FIGURE 27 CALIBRATION, THERMOCOUPLE NO. 1

use of these curves with a correction added to account for differences in the reference junction temperature. No other correction was required since thermocouples are not subject to calibration shifts due to aging.

All other instrumentation was calibrated in accordance with the standing calibration procedures of the Instrumentation Research Laboratory Department.

4.9 TEST RESULTS

Test conditions for each of the seven cryogenic tests are given in Table 2. The first six tests employed the "good" distributor. Test number seven employed the "poor" distributor. Tables 3 through 5 contain the test data.

The poor distributor is a terminal orifice located 4.5 inches below the top of the tank and approximately 8 inches from the tank sidewall. It is aimed, horizontally and along a tank diameter, at the opposite wall. The good distributor is the 10-inch diameter plenum-and-baffle design shown in Figure 23. It was located along the tank centerline with the discharge directed axially toward the liquid surface from a plane approximately 6 inches below the top of the tank.

The extreme sensitivity of ullage pressure to pressurant inlet velocity became quite evident in the "poor distributor" configuration. Gross turbulence existed in the ullage region, and perhaps also in the upper region of liquid, as a result of high inlet gas velocities. During the initial pressurization and early part of the discharge run, the sensitivity was more pronounced as was expected due to the proximity of the inlet to the liquid surface. Low subsonic velocities were required during this phase of the test run to prevent excessive pressure collapse. Increasing the inlet velocity above some limit which appears to depend primarily upon liquid level and ullage pressure, results in massive condensation evidenced by a sudden drop in ullage pressure. The lower limit to which the pressure falls probably is a function of both the

TABLE 2 TEST CONDITIONS

Test Number	Flow Rate gpm	Initial Ullage %	Inlet Gas Temperature °R	Tank Pressure psia	Weight of Gas Used lbs.	Final Gas Weight In Tank lbs.	Time of Test sec.	Initial Gas Weight lbs.
1	138.	10.0	425	57.4	26.9	34.7	192.3	3.9
2	136.	10.4	245	61.7	45.5	52.3	187.7	8.1
3	81.5	9.0	430	36.5	17.5	25.3	324.8	2.5
4	122.	9.0	435	54.7	----	34.3	237.0	4.9
5	115.	10.2	240	56.2	----	47.2	229.0	5.9
6	111.	10.2	425	55.7	----	35.5	238.5	4.3
7	111.	33.3	425*	59.0*	----	57.4	176.3	20.8

*Estimated

TABLE 3 TEMPERATURE PROFILES

Location Inches Above Tank Bottom	T/C Number	Test 1				Test 2			
		Zero sec.	60 sec.	120 sec.	192.3 sec.	Zero sec.	60 sec.	120 sec.	187.7 sec.
96.5 Center	13	297	357	380	378	183	224	233	194
92.0	12	312	380	399	404	152	231	231	187
90.0	11	---	---	---	---	---	---	---	---
88.0	10	227	354	395	387	167	236	242	215
87.0	9	188	357	395	395	160	233	243	200
80.0	8	139	367	416	416	139	230	240	195
69.5	7	139	249	385	393	139	177	234	192
57.5	6	139	152	267	296	139	139	178	183
41.5	5	139	139	170	263	139	139	150	160
33.5	4	139	139	152	262	139	139	139	165
21.0	3	139	139	139	216	139	139	139	145
8.5	2	139	139	139	150	139	139	139	139
4.5	1	139	139	139	139	139	139	139	139
92.0 Outboard	19	253	325	353	355	166	212	219	192
87.0	18	159	306	338	339	155	204	216	192
80.0	17	139	291	326	334	139	192	208	178
69.5	16	139	250	332	338	139	168	215	183
41.5	15	139	139	187	268	139	148	178	183
8.5	14	139	139	139	144	139	139	139	139
92.0 Wall	25	227	262	280	287	168	191	200	187
87.0	24	169	245	268	272	160	189	198	179
80.0	23	139	248	272	281	194	223	233	225
69.5	22	139	219	256	269	148	189	206	194
41.5	21	139	139	171	204	139	139	165	160
8.5	20	139	139	139	139	139	139	139	139

TABLE 3 TEMPERATURE PROFILES (Continued)

Location Inches Above Tank Bottom	T/C Number	Test 3						Test 4					
		Zero sec.	60 sec.	120 sec.	180 sec.	240 sec.	324.85 sec.	Zero sec.	60 sec.	120 sec.	180 sec.	237.0 sec.	
96.5 Center	13	262	348	377	389	403	410	282	350	387	400	405	
92.0	12	256	360	391	409	422	434	298	368	402	420	427	
90.0	11	---	---	---	---	---	---	---	---	---	---	---	
88.0	10	209	320	357	378	395	411	215	345	378	397	403	
87.0	9	154	331	366	395	410	425	146	349	392	413	422	
80.0	8	139	230	385	409	433	448	139	364	409	443	446	
69.5	7	139	139	249	284	318	347	139	196	312	399	411	
57.5	6	139	139	152	193	241	272	139	139	210	282	302	
41.5	5	139	139	139	139	155	212	139	139	139	208	263	
33.5	4	139	139	139	139	139	200	139	139	139	178	258	
21.0	3	139	139	139	139	139	158	139	139	139	139	212	
8.5	2	139	139	139	139	139	139	139	139	139	139	160	
4.5	1	139	139	139	139	139	139	139	139	139	139	139	
92.0 Outboard	19	234	312	348	362	375	388	241	320	360	375	380	
87.0	18	139	283	320	339	355	376	---	300	339	360	367	
80.0	17	139	212	281	318	340	360	---	272	328	350	360	
69.5	16	139	139	233	274	306	330	---	178	300	333	353	
41.5	15	139	139	144	154	200	238	139	143	143	234	272	
8.5	14	139	139	139	139	139	148	139	139	139	139	151	
92.0 Wall	25	212	242	262	275	290	307	212	248	275	296	304	
87.0	24	145	223	245	258	275	293	145	241	265	285	293	
80.0	23	191	219	245	264	281	299	198	251	275	294	305	
69.5	22	139	160	201	230	256	283	160	185	249	279	294	
41.5	21	139	139	139	139	155	185	139	139	139	190	190	
8.5	20	139	139	139	139	139	139	139	139	139	139	139	

TABLE 3 TEMPERATURE

Location Inches Above Tank Bottom	T/C Number	Test 5		
		Zero sec.	60 sec.	120 sec.
96.5 Center	13	205	238	238
92.0	12	164	244	244
90.0	11	---	---	---
88.0	10	158	242	251
87.0	9	160	237	248
80.0	8	139	230	251
69.5	7	139	167	241
57.5	6	139	139	163
41.5	5	139	139	139
33.5	4	139	139	139
21.0	3	139	139	139
8.5	2	139	139	139
4.5	1	139	139	139
92.0 Outboard	19	188	223	230
87.0	18	148	212	224
80.0	17	139	200	216
69.5	16	139	159	215
41.5	15	139	148	148
8.5	14	139	139	139
92.0 Wall	25	187	200	212
87.0	24	160	193	201
80.0	23	198	229	235
69.5	22	139	185	211
41.5	21	139	139	139
8.5	20	139	139	139

TABLE 3 TEMPERATURE PROFILES (Continued)

Location Inches Above Tank Bottom	T/C Number	Test 7			
		Zero sec.	60 sec.	120 sec.	176.3 sec.
96.5 Center	13	153	153	184	188
92.0	12	159	152	164	164
90.0	11	---	---	---	---
88.0	10	158	158	158	175
87.0	9	154	154	154	175
80.0	8	146	146	153	160
69.5	7	145	156	166	177
57.5	6	139	152	152	167
41.5	5	139	139	156	171
33.5	4	139	139	152	159
21.0	3	139	139	139	139
8.5	2	139	139	139	139
4.5	1	139	139	139	139
92.0 Outboard	19	162	157	162	175
87.0	18	159	155	165	174
80.0	17	155	159	159	173
69.5	16	149	154	154	168
41.5	15	144	148	168	15
8.5	14	139	139	139	139
92.0 Wall	25	158	154	164	174
87.0	24	165	160	160	170
80.0	23	179	179	179	191
69.5	22	155	160	165	170
41.5	21	139	139	155	161
8.5	20	139	139	139	139

TABLE 4 TANK PRESSURE HISTORY - psia

Test Number	Time - - sec.											End Time sec.	Final Pressure psia
	0	30	60	90	120	150	180	210	240	270	300		
1	57.5	57.5	57.5	57.5	57.1	56.7						188.0	54.4
2	60.7	60.2	61.7	65.2	61.7	58.2						183.5	52.1
3	37.4	37.9	35.8	36.5	36.9	36.2	35.8	36.9	37.4	36.5	36.2	323.0	35.8
4	54.8	54.8	54.0	54.4	54.0	54.8	54.8	55.5				232.3	54.9
5	56.7	56.3	55.6	55.6	56.3	55.9	56.3	57.5				227.7	55.2
6	55.9	55.2	55.6	55.9	55.6	55.9	55.9	55.9				232.3	55.6
7*	53.0	53.0	54.0	55.0	59.0	59.0						176.3	59.0

*Pressures read from gage.

TABLE 5 MANIFOLD CONDITIONS

Test Number	Initial Pressure	Final Pressure	Number of Bottles
4	1150*	500*	6
5	1674	809	5
6	1989	1334	6
7	1910	170	11

*From Gage.

agitation and the temperature of the liquid. Ullage pressure will remain near the lower limit of a drop until either the liquid temperature is raised sufficiently to retard further condensation or the total pressure of the entering gas is reduced to a value approximating that in the ullage region. One test, after several unsuccessful attempts to avoid pressure collapse, was completed by careful manipulation of the pressurant pressure regulator. This test required approximately twice as much pressurant as its parallel in the good distributor configuration. Further testing in the poor distributor configuration would be of doubtful value since inlet velocity has already been shown to be the principal criterion of distributor design.

The extreme turbulence existing in the ullage region as a result of the poor distributor is clearly indicated by comparison of temperature gradients in Table 2. No significant ullage region temperature gradients exist in Test 7 (poor distributor) indicating that the tank wall has reached equilibrium with the gas. All other tests show temperature gradients both axially and radially in the ullage region. It is evident from this that the poor distributor results in high rates of heat transfer from the ullage gas to the tank wall and to the liquid.

Curvature of the upper tank wall probably works to the disadvantage of poor distributor. Since only gross condensation can account for the observed propellant collapse, it follows that considerable liquid turbulence must exist in the region of the liquid-vapor interface. This turbulence is governed primarily by ullage region geometry, including location of the inlet, and by the inlet stream velocity. The present tests with nitrogen indicate that velocity is the more significant consideration.

5.0 CONCLUSIONS AND RECOMMENDATIONS

The following conclusions are drawn on the basis of the analyses and experiments reported here:

- (1) High velocity impingement of condensable pressurants on the liquid surface must be avoided in order to prevent massive condensation and severe collapse of ullage pressure.
- (2) A radially discharging pressurant inlet coaxially located on a flat or slightly concave surface is characterized by a high rate of secondary fluid entrainment accompanied by a rapidly decaying maximum velocity. These characteristics are desirable in a pressurant distributor since they tend to reduce the region of influence of forced convection thereby approaching the more nearly optimum situation in which free convection dominates pressurant gas heat transfer.
- (3) The strength-to-weight ratio of Rigimesh; the woven, rolled, and sintered screen made by the Pall Corporation; is substantially higher than that of any other material considered.
- (4) Multiple radial distributors will have a lower total weight than a single distributor of the same total active area and designed for the same internal pressure. However, additional plumbing required for multiple distributors could cancel much of the apparent savings in weight.
- (5) The effects of gas flow about the liquid surface, especially when the gas impinges normal to the surface, should be investigated. Heat and mass transfer across the liquid-vapor interface involves liquid stratification as well as conditions in the gas. Perhaps, this complexity is the

reason for its avoidance. However, with a better understanding of the phenomena involved, it may become feasible to use the end surface of a radial distributor in such a manner as to reduce the total system weight by trading interface heat and mass transfer for sidewall heat transfer and distributor total area. The criteria for the initiation of massive condensation should be determined so that the possibility of encountering such a condition can better be avoided.

APPENDIX I

CALCULATION OF TURBULENT
FREE CONVECTION DATA USING
ECKERT AND JACKSON EQUATIONS

RECOMP III PROGRAM NO. L-00072

APPENDIX I

1.1 SUMMARY

This program is designed to solve the turbulent boundary layer free convection equations as derived by Eckert and Jackson (Reference 1). The program is written specifically for the Recomp III computer. However, since the program language is a form of Fortran, no difficulty should be encountered in adopting this program to another computer employing a similar language. Figure I-1 is the program listing.

The program operates as follows:

- (1) i_{max} is read from the input tape and then i_{max} sets of input data (x , tw , tb , ρ , ν , c_p , β , $cond$) are read
- (2) for each set of input data, the following quantities are calculated in order until all sets of data have been used - gr , pr , htp , u_l , and h
- (3) for each set of input data the following quantities are output under the appropriate headings - x , tw , tb , gr , htp , u_l , and h
- (4) the program is terminated

A maximum of 20 sets of input data are permitted in a single run. When more data are required multiple runs must be made.

1.2 ANALYSIS

The equations of Eckert and Jackson (Reference 1) were chosen for use because of the good agreement of the calculated heat transfer coefficients with experimental data in the range of Grashof numbers from 10^{10} to 10^{12} . This good correlation of data suggests that these equations may be valid at higher Grashof numbers.

The characteristic velocity is calculated from the following equation:

$$u_l = 1.185 \frac{v_u}{\rho \cdot x} \text{ gr}^{0.5} \left[1 + 0.0494 (\text{pr})^{2/3} \right]^{-0.5}$$

where

$$\text{gr} = \frac{32.16 \text{ beta } (t_w - t_b) x^3 \rho^2}{v_u^2}$$

$$\text{pr} = \frac{3600 v_u c_p}{\text{cond}}$$

The heat transfer coefficient is calculated from the following equation:

$$h = \frac{\text{cond}}{x} \cdot \text{htp}$$

where

$$\text{htp} = 0.0295 \cdot \text{gr}^{0.4} \cdot \text{pr}^{7/15} \left[1 + 0.0494 (\text{pr})^{2/3} \right]^{-0.4}$$

1.3 INPUT

The input data are arranged in the following order:

imax

x tw tb rho vu cp beta cond (repeated imax times)

Each of these numbers except imax may be input as either a fixed point or a floating point number. The floating point form, which permits both mixed decimal (-123.4) and exponential (-1.234e2) numbers, is recommended. A maximum of 10 characters

is permitted for each of these input quantities. The number of data points input, i_{\max} , is a positive integer and must not contain a decimal.

Any of the input devices may be used at the discretion of the operator. However, it is recommended that a tape be punched and input through the Facit tape reader when more than a few sets of data are to be handled.

1.4 OUTPUT

The output data include x , tw , and tb from the input data in addition to the desired output of gr , htp , ul , and h . These input data serve to relate the output to the input. However, since no provision is made to output all of the input data or for the output of comments, the engineer must write on the output sheet any additional identification which he requires.

The output sheet contains 7 columns each of i_{\max} entries. Each column bears the appropriate heading to identify its contents. The columns are arranged in the order:

x , tw , tb , gr , htp , ul , and h .

Data quantities are output with 4 significant figures in the exponential format ($0.2213e-01 = 0.02213$).

1.5 SAMPLE CASE

The input and output data of a sample case having 16 sets of data is presented here for reference. The fluid employed in this case is oxygen. The input data shown in Figure 1-2 were used in this case but the format of the data was different. However, the format shown is proper. Figure 1-3 is a reproduction of the actual output sheet.

FIGURE I-1 FORTRAN PROGRAM

```

dimension x(20), tw(20), tb(20), rho(20), vu(20), cp(20), beta(20), cond(20), pr(20),
      htp(20), ul(20), h(20), pr(20),

6  read input tape 2, 5, imax
   read input tape 2, 1, (x(i), tw(i), tb(i), rho(i), vu(i), cp(i), beta(i), cond(i), i=1, imax)
7  write output tape 1, 2
   do 3 i=1, imax
      gr(i)=32.16*beta(i)*(tb(i)-tw(i))*(x(i)**3)*(rho(i)**2)/(vu(i)**2)
      pr(i)=3600.*vu(i)*cp(i)/cond(i)
      htp(i)=0.0295*(gr(i)**0.4)*(pr(i)**(7./15.))*(1.+0.0494*(pr(i)**(2./3.)))**(-0.4)
      ul(i)=1.185*vu(i)/(rho(i)*x(i))*(gr(i)**0.5)*((1.+0.0494*(pr(i)**(2./3.)))**(-0.5)
      h(i)=htp(i)*cond(i)/x(i)
   write output tape 1, 4, (x(i), tw(i), tb(i), gr(i), htp(i), ul(i), h(i), i=1, imax)
4  format (7e12.4)
1  format (8e10.4)
5  format (i6)
2  format (5x, 3hX, 11x, 4hTW, 10x, 4hTB, 10x, 4hGR, 10x, 5hHTP, 10x, 4hU1, 10x, 3hH, //)
   stop
   end

```

FIGURE I-2 INPUT DATA FOR SAMPLE CASE

X	TW	TB	RHO	VU	CP	BETA	COND
3.	150.	160.	.645	4.36 E-06	.22	6.25 E-03	4.43 E-03
		190.	.517	4.91		5.26	4.9
		210.	.488	5.23		4.67	5.23
		230.	.463	5.53		4.35	5.52
		310.	.382	6.66		3.23	6.71
		410.	.314	8.02		2.44	8.14
		560.	.248	9.89		1.79	10.38
	V						
	300.	310.	.288	8.66		3.23	8.51
		340.	.275	9.02		2.94	9.37
		370.	.262	9.4		2.71	9.8
		410.	.248	9.86		2.44	10.38
		460.	.231	10.41		2.18	11.1
		500.	.220	10.9		2.	11.67
		560.	.204	11.55		1.79	12.52
	V						
	450.	460.	.193	12.11		2.18	13.13
		490.	.187	12.5		2.04	13.58
		510.	.183	12.7		1.96	13.86
V	V	560.	.173	13.2	V	1.79	14.55
					V		

FIGURE I-3 REPRODUCTION OF OUTPUT SHEET FOR SAMPLE CASE

X	TW	TB	GR	HTP	UI	H
0.3000e 01	0.1500e 03	0.1600e 03	0.1188e 13	0.1746e 04	0.2851e 01	0.2579e 01
0.3000e 01	0.1500e 03	0.1900e 03	0.2026e 13	0.2180e 04	0.5229e 01	0.3560e 01
0.3000e 01	0.1500e 03	0.2100e 03	0.2118e 13	0.2217e 04	0.6035e 01	0.3865e 01
0.3000e 01	0.1500e 03	0.2300e 03	0.2118e 13	0.2219e 04	0.6725e 01	0.4083e 01
0.3000e 01	0.1500e 03	0.3100e 03	0.1476e 13	0.1912e 04	0.8197e 01	0.4277e 01
0.3000e 01	0.1500e 03	0.4100e 03	0.8444e 12	0.1524e 04	0.9083e 01	0.4136e 01
0.3000e 01	0.1500e 03	0.5600e 03	0.4007e 12	0.1114e 04	0.9773e 01	0.3855e 01
0.3000e 01	0.3000e 03	0.3100e 03	0.3198e 11	0.4176e 03	0.2080e 01	0.1185e 01
0.3000e 01	0.3000e 03	0.3400e 03	0.9492e 11	0.6292e 03	0.3912e 01	0.1965e 01
0.3000e 01	0.3000e 03	0.3700e 03	0.1280e 12	0.7079e 03	0.4968e 01	0.2312e 01
0.3000e 01	0.3000e 03	0.4100e 03	0.1474e 12	0.7458e 03	0.5911e 01	0.2581e 01
0.3000e 01	0.3000e 03	0.4600e 03	0.1491e 12	0.7449e 03	0.6739e 01	0.2756e 01
0.3000e 01	0.3000e 03	0.5000e 03	0.1415e 12	0.7280e 03	0.7217e 01	0.2832e 01
0.3000e 01	0.3000e 03	0.5600e 03	0.1261e 12	0.6912e 03	0.7786e 01	0.2885e 01
0.3000e 01	0.4500e 03	0.4600e 03	0.4808e 10	0.1871e 03	0.1685e 01	0.8190e-00
0.3000e 01	0.4500e 03	0.4900e 03	0.1586e 11	0.3013e 03	0.3260e 01	0.1364e 01
0.3000e 01	0.4500e 03	0.5100e 03	0.2120e 11	0.3378e 03	0.3914e 01	0.1560e 01
0.3000e 01	0.4500e 03	0.5600e 03	0.2971e 11	0.3848e 03	0.5065e 01	0.1866e 01

These Data Are For Oxygen.

1.6 DESCRIPTION OF SYMBOLS

Symbol	Description	Units
x	Length of boundary layer run	ft.
tw	Wall temperature	$^{\circ}\text{R}$
tb	Bulk fluid temperature	$^{\circ}\text{R}$
rho	Specific density of fluid	lbs/ft^3
vu	Coefficient of viscosity	lbs/ft-sec
cp	Specific heat	$\text{Btu/lbs-}^{\circ}\text{R}$
beta	Coefficient of expansion	$\frac{1}{^{\circ}\text{R}}$
cond	Thermal conductivity	$\text{Btu/hr-ft-}^{\circ}\text{R}$
ul	Characteristic velocity	ft/sec
h	Heat transfer coefficient	$\text{Btu/hr-ft}^2\text{-}^{\circ}\text{R}$
pr	Prandtl number	-----
gr	Grashof number	-----
htp	Nusselt number	-----
imax	Number of input data points	-----

APPENDIX II

SCALING OF TANK
PRESSURIZATION DATA

RECOMP III PROGRAM NO. L-00090

APPENDIX II

II.1 SUMMARY

This program is designed to provide a means of correlating pressurant gas requirements data for a range of conditions which include tank size and construction and mission requirements. It is intended to be used primarily to scale requirements of flight systems down to those of test systems and to extrapolate test results up to flight systems' requirements.

The program operates as follows:

- (1) R, D, and Cp are read from the input tape.
- (2) lmax is read from the input tape and is followed by lmax sets of input data (pi, Pu, Ti, Tu, h, Time, U, Tm, Rhom, Cpm).
- (3) For each set of input data, the following quantities are computed and output under the headings A, C, E, and F, respectively:

$$\frac{W_g}{\rho_i V_t}, \frac{h \tau}{\rho_i D C_p}, \frac{t_m \rho_m C_{pm}}{h \tau}, \text{ and } \frac{\rho_i}{\rho_u} \%U.$$

The corresponding input data is output also.

- (4) The program is terminated.

A maximum of 25 sets of data are permitted in a single run.

II.2 ANALYSIS

The equation used in this scaling analysis is developed elsewhere in this report. That equation is:

$$\frac{W_g}{\rho_i V_t} = 1.135 \left(\frac{h \tau}{\rho_i D C_p} \right)^{-0.113} \left(\frac{t_m \rho_m C_{pm}}{h \tau} \right)^{-0.0675} \left(\frac{\rho_u}{\rho_i} \%U \right)^{-0.098}$$

The form of the correlating equations permits the use of this program for the computation of $\frac{W_{sg}}{\rho_i V_t}$ and $\frac{T_w}{T_g}$ merely by recompiling the program with the appropriate constants and exponents in place of the ones shown above.

The program listing is presented in Figure II-1.

II.3 INPUT

The input data are arranged in the following order:

R, D, Cp

lmax

Pi, Pu, Ti, Tu, h, Time, U, Tm, Rhom, Cpm (repeated lmax times)

Each of these numbers with the exception of lmax may be input as a fixed point or a floating point number. The floating point format (mixed decimal or exponential) is recommended. A maximum of 10 characters is permitted in each input quantity. lmax is a positive integer and must not contain a decimal.

II.4 OUTPUT

The output data include all input data, except lmax, in addition to the dimensionless terms. Data quantities are output with four significant figures in the exponential format. The output data are arranged as follows:

INPUT

R	D	Cp	Pi	Pu	Ti	Tu
xxxx	xxxx	xxxx	xxxx	xxxx	xxxx	xxxx
.
.
.
h	Time	U	Tm	Rhom	Cpm	
xxxx	xxxx	xxxx	xxxx	xxxx	xxxx	
.	
.	
.	

OUTPUT

A	C	E	F
xxxx	xxxx	xxxx	xxxx
.	.	.	.
.	.	.	.
.	.	.	.

Since no provision is made for the input/output of comments, the user must write on the output sheet any additional identification which he may require.

II.5 SAMPLE CASE

The input and output of a sample case having two sets of data are reproduced in Figures II-2 and II-3, respectively.

FIGURE II-1 PROGRAM LISTING

```

11 dimension pi(25), pu(25), ti(25), h(25), time(25), u(25), tm(25), rhom(25), cpm(25),
    c(25), c(25), e(25), f(25)
    read input tape 2, 1, r, d, cp
    read input tape 2, 9, imax
    read input tape 2, 1, (pi(i), pu(i), ti(i), h(i), time(i), u(i), tm(i), rhom(i),
        cpm(i), i=1, imax)
    do 8 i=1, imax
        c(i)=r*pi(i)*h(i)*time(i)/(pi(i)*d*cp)
        e(i)=tm(i)*rhom(i)*cpm(i)/(h(i)*time(i))
        f(i)=pu(i)*ti(i)*u(i)/(pi(i)*tu(i))
        a(i)=1.135*(c(i)**-.0.113)*(e(i)**-.0.0675)*f(i)**-.0.098)
        write output tape 1, 2
        write output tape 1, 3
        write output tape 1, 1, r(i), d(i), cp(i), pi(i), pu(i), ti(i), tu(i)
        write output tape 1, 4
        write output tape 1, 5, h(i), time(i), u(i), tm(i), rhom(i), cpm(i)
        write output tape 1, 6
        write output tape 1, 16
        write output tape 1, 7, a(i), c(i), e(i), f(i)
        continue
    format (e12.4)
    format (i6)
    format (7hINPUT,/)
    format (5x, 3hR, 11x, 3hD, 10x, 4hCp, 10x, 4hPi, 10x, 4hPu, 10x, 4hTi, 10x, 4hTu,/)
    format (5x, 2hh, 10x, 6hTime, 9x, 3hU, 11x, 4hTm, 9x, 6hRhom, 9x, 5hCpm,/)
    format (6e12.4)
    format (8hOUTPUT,/)
    format (5x, 3hA, 11x, 3hC, 11x, 3hE, 11x, 3hF,/)
    format (4e12.4)
    stop
    end

```

==

Author's address:

FIGURE II-3 SAMPLE OUTPUT

INPUT

R	D	Cp	Pi	Pu	Ti	Tu
0.7670e 03	0.3300e 01	0.2500e 01	0.9120e 04	0.2116e 04	0.5000e 03	0.4680e 02
h	Time	U	Tm	Rhom	Cpm	
0.1670e 02	0.3300e-01	0.1000e-00	0.5000e-02	0.4888e 03	0.1000e-00	

OUTPUT

A	C	E	F
0.1222e 01	0.2851e 01	0.4369e-00	0.2479e-00

II.6 DESCRIPTION OF SYMBOLS

Symbol	Description	Units
$A, \frac{W_g}{\rho_i V_T}$	Ratio of actual quantity of gas to that required if no heat or mass transfer occurred	-----
$C, c, \frac{h \tau}{\rho_i D D_p}$	Dimensionless parameter	-----
C_p, c_p	Constant pressure specific heat of gas	Btu/lb-°F
C_{pm}, c_{pm}	Specific heat of tank wall	Btu/lb-°F
D, d	Diameter of tank	ft
$E, e, \frac{t_m \rho_m C_{pm}}{h \tau}$	Dimensionless parameter	-----
$F, f, \frac{\rho_i}{\rho_u} \%U$	Dimensionless parameter	-----
h	Heat transfer coefficient in ullage region	Btu/hr-ft ² -°F
— I_{max}, i_{max}	Number of data sets input	-----
P_i, p_i	Pressure of inlet gas	lbs/ft ²
P_u, p_u	Initial ullage pressure	lbs/ft ²
R, r	Gas constant	ft/°F
R_{hom}, ρ_m	Specific weight of tank wall	lbs/ft ³
ρ_i	Specific weight of incoming gas	lbs/ft ³
ρ_u	Specific weight of initial ullage gas	lbs/ft ³
T_i, t_i	Temperature of incoming gas	°F
t_m	Thickness of tank wall	ft
T_u, t_u	Initial ullage gas temperature	°F
Time, time, τ	Emptying time of tank	hr
$U, u, \%U$	Ratio of initial ullage volume to total tank volume	-----
V_t	Total tank volume	ft ³

APPENDIX III
RADIAL DISTRIBUTOR WEIGHT DATA

APPENDIX III

III.1 SUMMARY

This appendix presents the results of a parametric weight study of a radially discharging pressurant distributor. The range of variables covered are as follows:

- (1) Aspect ratio (L/D) 0 to 10
- (2) Active surface (shell) area from 0 to 200 sq. ft.
- (3) Pressure (differential) from 0 to 100 PSI
- (4) Temperature range -473° to $+1577^{\circ}$ F.
- (5) Various head shapes:
 - (A) Hemispherical
 - (B) Dished
 - (C) Flat
- (6) Various shell (active area) materials:
 - (A) 60 X 60 X .011 screen
 - (B) 12 X 64 Rigimesh, Pall Corporation
 - (C) Perforated screen, 40 mesh
 - (D) Sintered stainless, Pall Corporation
 - (1) Type "C" - 165 micron pore size
 - (2) Type "D" - 65 micron pore size

The hemispherical head is shown to be lighter, for a given diameter and pressure differential, than either the dished head or the unstayed flat head. The flat head is considerably heavier than dished head. Non-hemispherical heads are considered only because space limitations might, in some cases, dictate their use even though a hemispherical head would be lighter.

The 12 X 64 mesh Rigimesh screen of the Pall Corporation is shown to have a strength-to-weight ratio 35 percent higher than the second best active surface material considered.

Plain woven and perforated screens have substantially equal strength-to-weight ratios which are almost an order of magnitude higher than that of the sintered powder materials.

III.2 MATERIAL SELECTION

III.2.1 Short Time Tensile Values - Values In Kips (See Figure III-1, Type 316SS(Annealed))

Temp. °F	Armco Short Time Tensile	"Design"	A.S.M.E. Code	Interpolation	- See Note
1600	22			19.4	A
1500	27		6.0	23.8	A
1400	35		9.4	30.8	A
1300	46		16.0	40.5	A
1200	56		27.2	49.5	A
1100	63		41.6	55.5	A
1000	71		56.0	62.6	A
900			64.0	64.0	B
800			<u>67.0</u>	67.0	B
700			68.0	68.0	B
600			68.4	68.5	B
500			<u>68.8</u>	69.0	B
400			70.0	70.0	B
300			<u>71.5</u>	72.0	B
200			<u>75.0</u>	75.0	B
100			75.0	75.0	B
0	85	90	75.0	75.0	C
-40		104		86.6	C
-80		<u>118</u>		98.4	C
-320		185		156.0	C
-423		210		175.0	C

- Notes:
- (A) Interpolation is ratio of "Armco" Tensile/A.S.M.E. Tensile.
 - (B) Figures are A.S.M.E. standard.
 - (C) Interpolation is ratio of "Design" Tensile/A.S.M.E. Tensile.

III.3 HEAD SELECTION

III.3.1 Dished Head Stress Calculations

Variables:

Diameter 0-96" (Reference Figure III-2)

Temperature/Stress Value

Working Pressure - 0 to 100 PSI

Find:

- (1) Thickness
- (2) Weight

Assumptions:

- (1) No safety factor.
- (2) 100% joint efficiency (one piece).
- (3) All calculations based on I.D. dimensions.
- (4) Radius of dish = to diameter.
- (5) Knuckle radius min. 6% diameter.

Formula Used:

$$t = \frac{.885 PL}{SE - .1P} \quad \text{Reference: A.S.M.E. Code}$$

t = Thickness

P = Pressure

L = Radius of Dish

E = Efficiency (100%)

S = Stress Value (See Figure III-1)

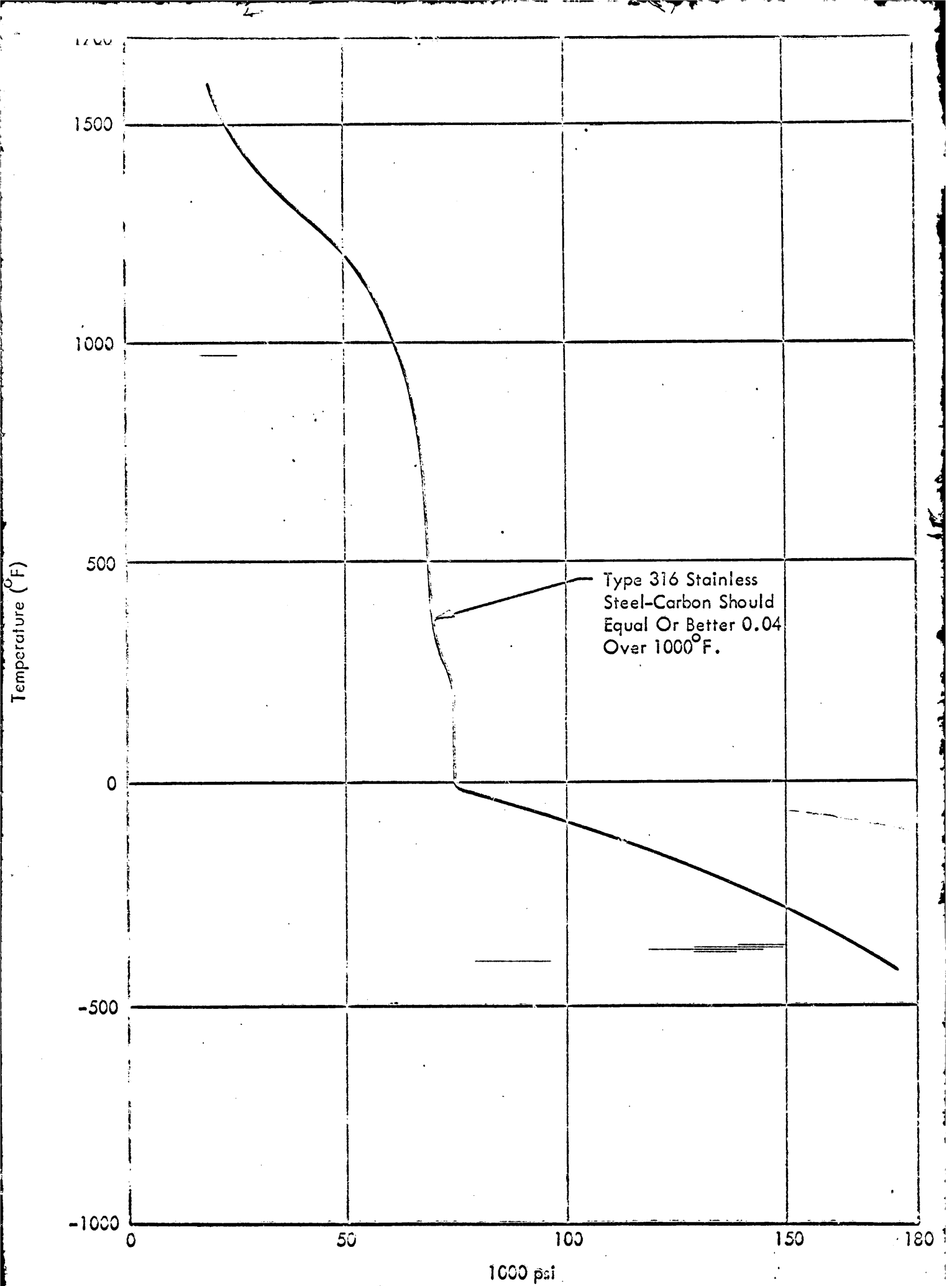


FIGURE 11-1 SHORT TIME TENSILE STRENGTH - MAXIMUM STRESS VALUE

Length In Feet (L)

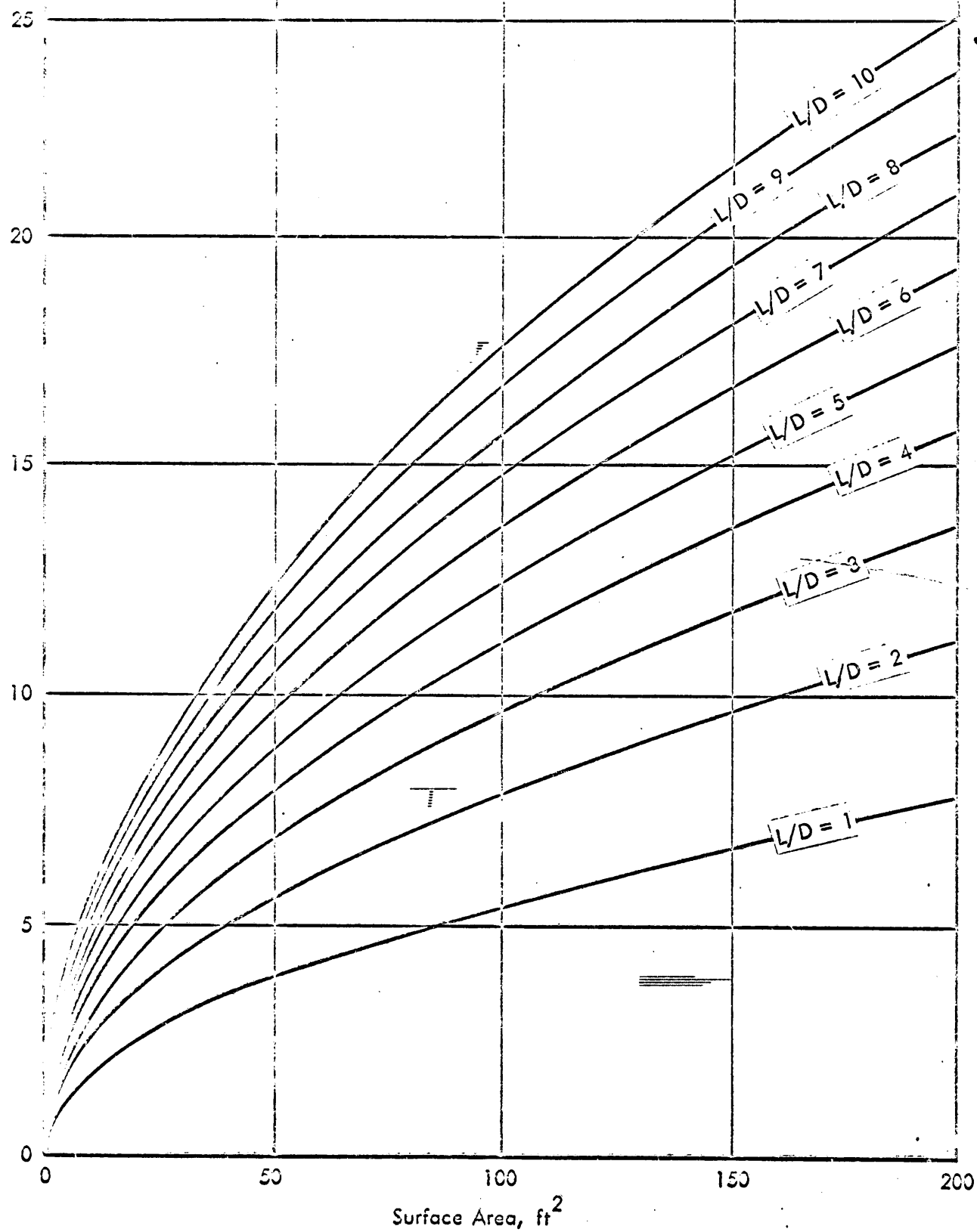


FIGURE 11-2 LENGTH RATIO FOR GIVEN AREA AND HEIGHT

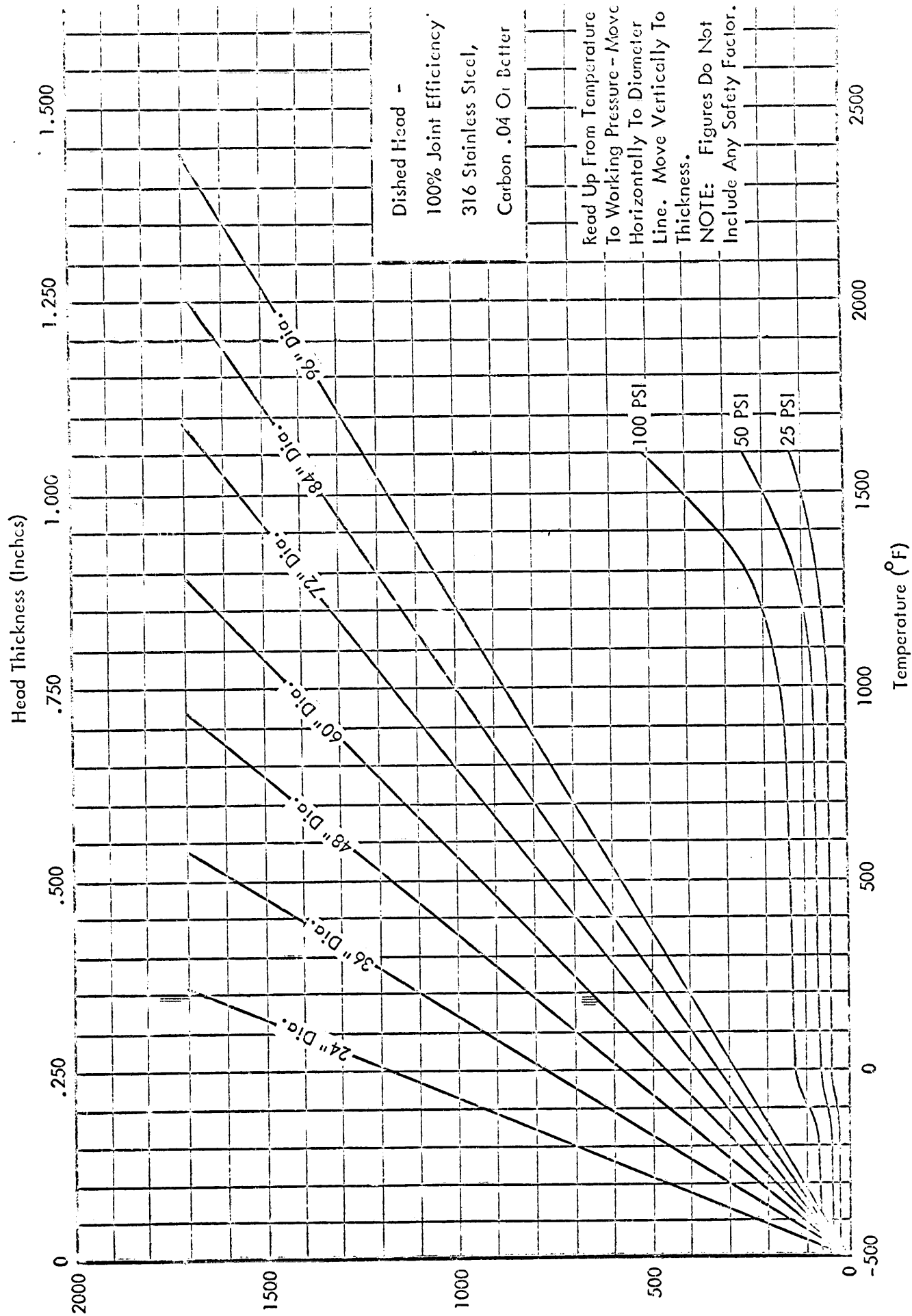


FIGURE III-3 DISHED HEAD THICKNESS

III.3.2 Hemispherical Head Stress Calculations

Variables:

Diameter - 0 to 96"

Temperature/Stress Value

Working Pressure- 0 to 100 PSI

Find:

(1) Thickness

(2) Weight

Assumptions:

(1) No safety factor.

(2) Head to shell joint 85% efficiency.

(3) All calculations based on I.D. dimensions.

Formula Used:

$$t = \frac{PL}{2SE - .2P} \quad \text{Reference: A.S.M.E. Code}$$

t = Thickness

P = Pressure

L = Radius

S = Stress Value (See Figure III-1)

E = Efficiency (85% as shell to head joint is part of this formula)

III.3.3 Flat Unstayed Heads Stress Calculations

Variables:

Diameter - 0 to 96" (Figure III-2)

Temperature/Stress Values

Working Pressure-0 to 100 PSI

Head Thickness (Inches)

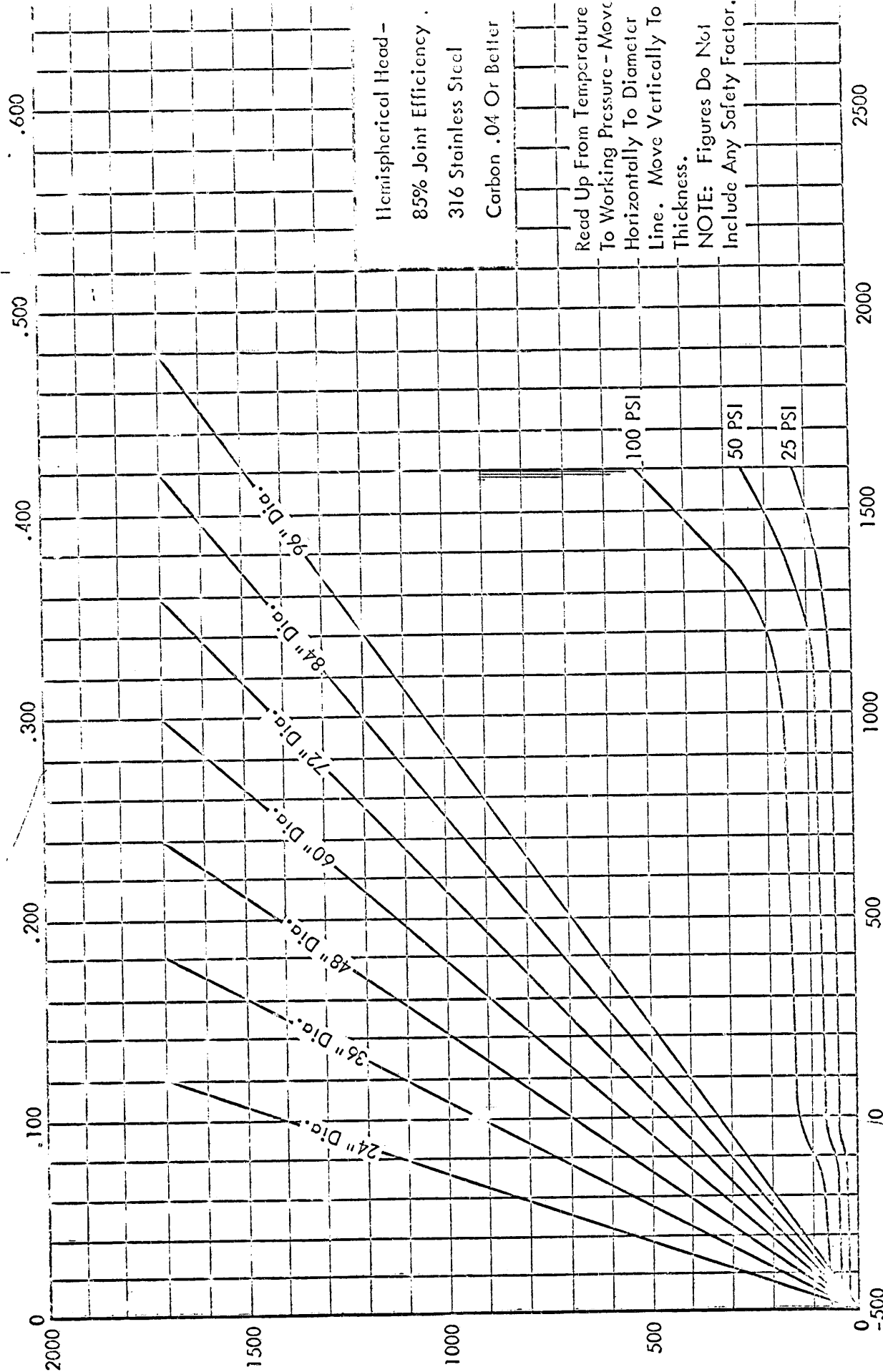


FIGURE III-4 HEMISPHERICAL HEAD THICKNESS

Find:

- (1) Thickness
- (2) Weight

Assumptions:

- (1) No safety factor.
- (2) All calculations based on I.D.
- (3) Weights will reflect the I.D. and will have to be modified according to extra diameter which will be determined by shell thickness.

Formula Used:

$$t = d \sqrt{CP/S} \quad \text{Reference: A.S.M.E. Code}$$

t = Thickness

d = Diameter

C = A factor dependent upon head; shell attachment, dimensions - figured at .5 (Reference A.S.M.E. Code, Figure U6-34-1965)

P = Pressure

S = Stress Value (Figure III-1)

III.4 SHELL SELECTION (ACTIVE AREA)

III.4.1 Shell Stress Calculations

Base problem using solid 316 S.S.

Variables:

Diameter - 0 to 96" (Reference Figure III-2)

Temperature/Stress Value (Reference Figure III-1)

Working Pressure - 0 to 100 PSI

Head Thickness (Inches)

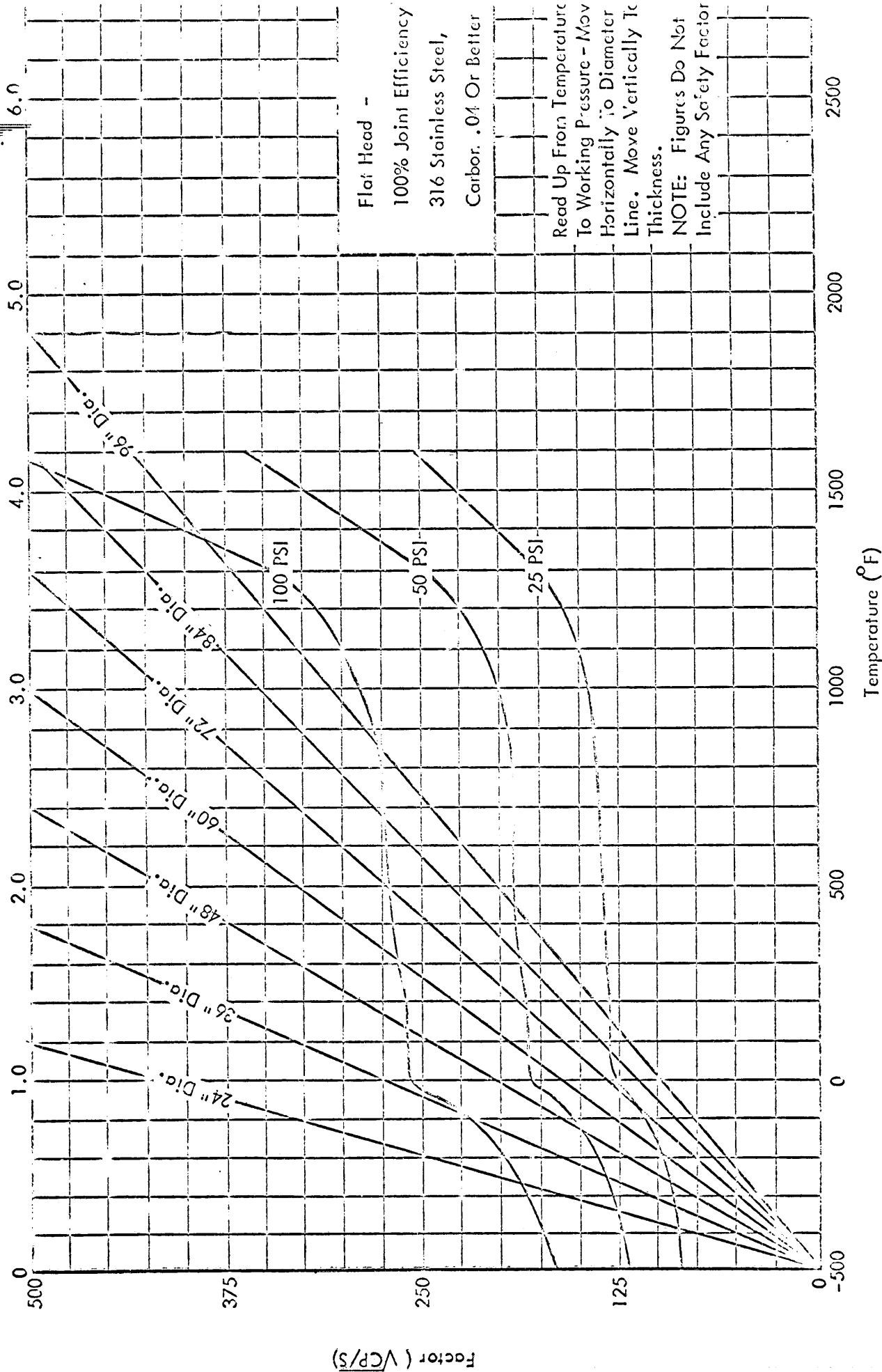


FIGURE III-6. FLAT HEAD THICKNESS VS. HEAD DIAMETER

Find:

- (1) Thickness

Assumptions:

- (1) No safety factor.
- (2) 100% joint efficiency.
- (3) All calculations based on I.D. dimensions.

Formula Used:

$$t = \frac{PR}{SE - .6P} \quad \text{Reference: A.S.M.E. Code}$$

t = Thickness

P = Pressure

R = Radius

S = Stress Value (Figure III-1)

E = Efficiency - 100%

III.4.2 Shell Material: Sintered Stainless Type 316

Reference: Pall Trinity Corporation, Cortland, Kentucky
Mr. Martin G. Kurz, Manager

Mr. Kurz furnished the following facts regarding the Type "C" and Type "D" Sintered Stainless Steels in a telephone conversation with Mr. J. Propst of Lockheed Industrial Products:

- (1) The Pall Corporation achieves an actual bond between particles due to high sintering temperatures (2400°).
- (2) The Pall Corporation states that their sintered stainless tensile strength

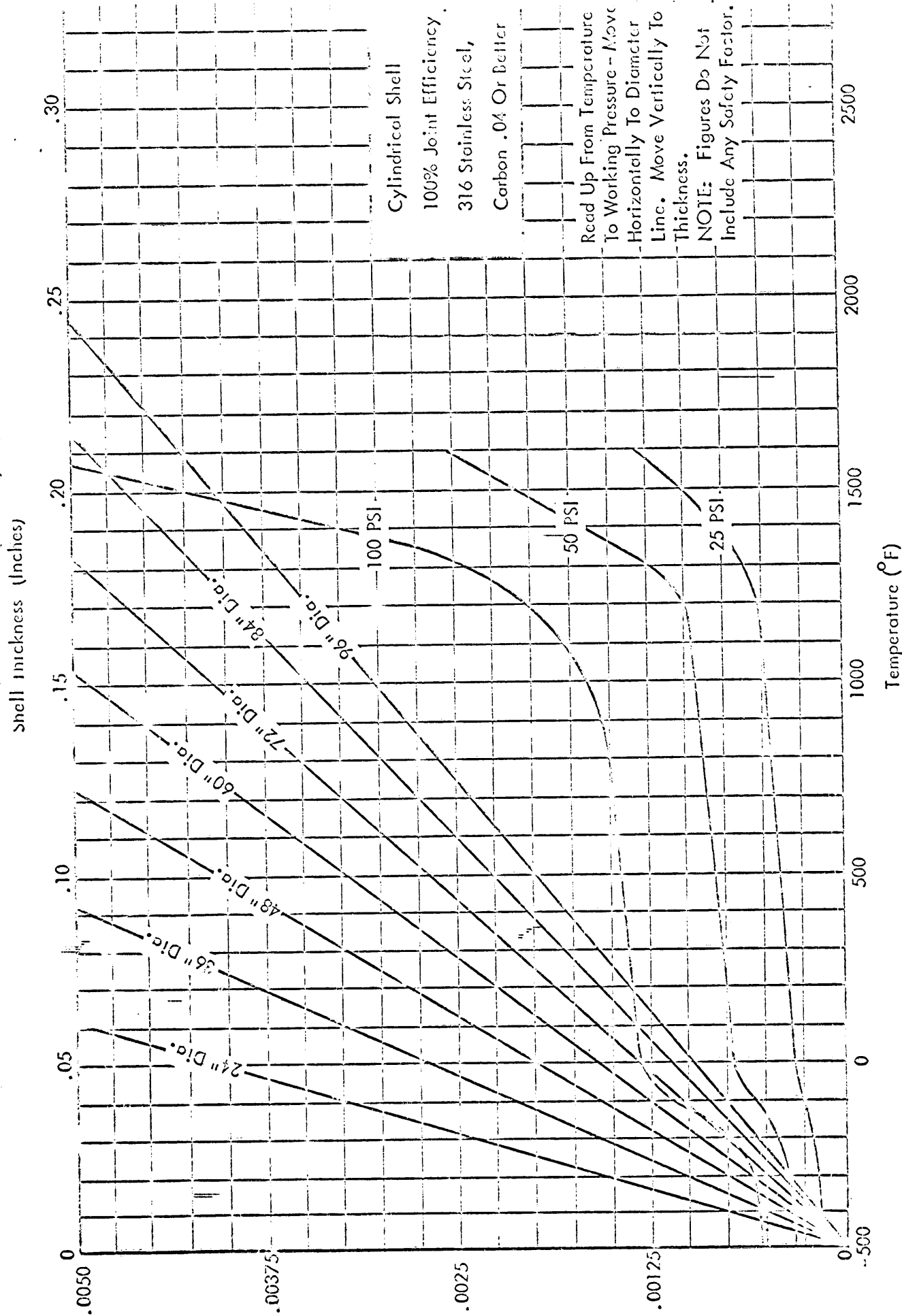


FIGURE III-6 SHELL THICKNESS FOR SOLID TYPE 316 STAINLESS STEEL - REFERENCE

values for different temperatures is almost in direct ratio to the equivalent values of type 316 stainless steel in the fully annealed condition.

(3) Tensile strength at 75°F is 7,000 PSI for Type "C" and 9,000 PSI for Type "D".

(4) Total void area is 55% for Type "C" and 50% for Type "D".

Tensile Strength:

Tensile Strength of 316 S.S. at 75°F = 75,000 PSI (See Figure III-6)

Tensile Strength of Type "C" sintered = 7,000 PSI

Tensile Strength of Type "D" sintered = 9,000 PSI

Type "C" strength ratio = 9.3%

Type "C" thickness multiplier = 10.71 times

Type "D" strength ratio = 12%

Type "D" Thickness multiplier = 8.34 times

Weight Calculations:

Type "C" weight ratio 45%

Type "D" weight ratio 50%

III.4.3 Shell Material 60 X 60 X .011 Screen, Type 316

Reference: Kays, W. M. & London, A. L., Compact Heat Exchangers; McGraw - Hill Book Co., Inc., New York, 1958.

Tensile Strength:

Total longitudinal strands per inch = 60

Total vertical strands per inch = 36

60 X 36 = 2,160 total strands/inch for best direction to stress

Shell Thickness (Inches)

3.0

2.5

2.0

1.5

1.0

.5

0

.0050

.00375

.0025

.00125

0

-500

0

500

1000

1500

2000

2500

3000

3500

4000

4500

5000

5500

6000

6500

7000

7500

8000

8500

9000

9500

10000

10500

11000

11500

12000

12500

13000

13500

14000

14500

15000

15500

16000

16500

17000

17500

18000

18500

19000

19500

20000

20500

21000

21500

22000

22500

23000

23500

24000

24500

25000

25500

26000

26500

27000

27500

28000

28500

29000

29500

30000

30500

31000

31500

32000

32500

33000

33500

34000

34500

35000

35500

36000

36500

37000

37500

38000

38500

39000

39500

40000

40500

41000

41500

42000

42500

43000

43500

44000

44500

45000

45500

46000

46500

47000

47500

48000

48500

49000

49500

50000

50500

51000

51500

52000

52500

53000

53500

54000

54500

55000

55500

56000

56500

57000

57500

58000

58500

59000

59500

60000

60500

61000

61500

62000

62500

63000

63500

64000

64500

65000

65500

66000

66500

67000

67500

68000

68500

69000

69500

70000

70500

71000

71500

72000

72500

73000

73500

74000

74500

75000

75500

76000

76500

77000

77500

78000

78500

79000

79500

80000

80500

81000

81500

82000

82500

83000

83500

84000

84500

85000

85500

86000

86500

87000

87500

88000

88500

89000

89500

90000

90500

91000

91500

92000

92500

93000

93500

94000

94500

95000

95500

96000

96500

97000

97500

98000

98500

99000

99500

100000

100500

101000

101500

102000

102500

103000

103500

104000

104500

105000

105500

106000

106500

107000

107500

108000

108500

109000

109500

110000

110500

111000

111500

112000

112500

113000

113500

114000

114500

115000

115500

116000

116500

117000

117500

118000

118500

119000

119500

120000

120500

121000

121500

122000

122500

123000

123500

124000

124500

125000

125500

126000

126500

127000

127500

128000

128500

129000

129500

130000

130500

131000

131500

132000

132500

133000

133500

134000

134500

135000

135500

136000

136500

137000

137500

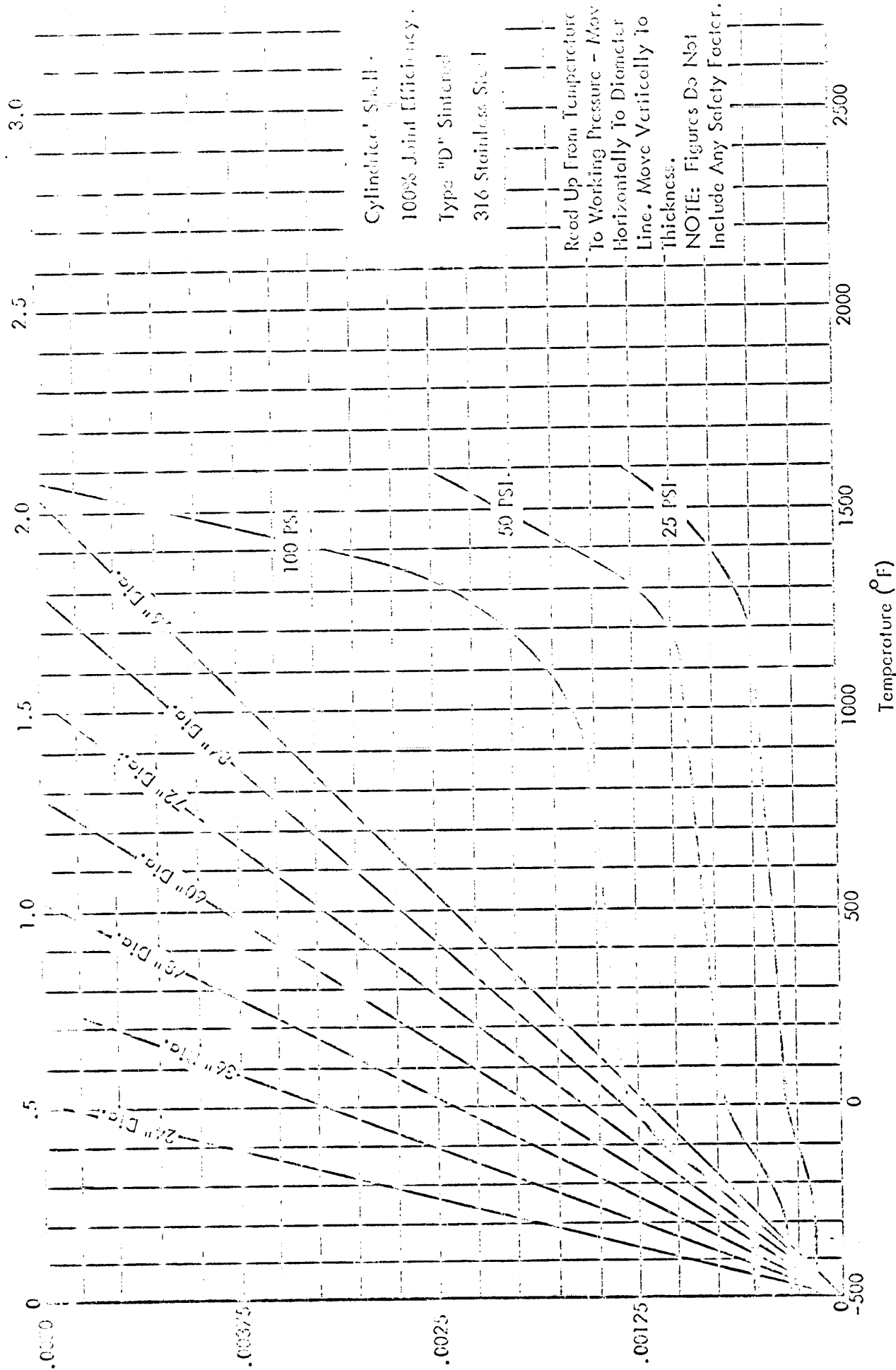
138000

138500

139000

139500

Shell Thickness (Inches)



Cylindrical Shell -
100% Joint Efficiency -
Type "D" Sintered
316 Stainless Steel

Read Up From Temperature
To Working Pressure - Move
Horizontally To Diameter
Line. Move Vertically To
Thickness.

NOTE: Figures Do Not
Include Any Safety Factor.

FIGURE III-8 SHELL THICKNESS FOR TYPE "D" POROUS STAINLESS STEEL

Wire diameter = .0105"

Wire area = $(.00525)^2 \times 3.1416 = .00003659035$ sq. inch

$.00003659035 \times 2160$ strands = .187035 sq. inch

Strength ratio = 18.7%

Thickness multiplier = 5.347

Assumptions:

All strands in direct tension

Weight Calculations:

Total longitudinal strands/inch = 60 (Best Direction)

Total vertical strands/inch = 36

Total horizontal strands/inch = 56 (Least Direction)

Cross Section:

(Best stress direction) = 2160 strands

(Least stress direction) = 2016 strands

Total wire length/cubic inch = $2160 + 2016 = 4176$ inches

Wire area = .00003659035 sq. inch

$$\frac{\text{times } 4176 \text{ inches}}{.3616013060 \text{ cubic inches}}$$

60 X 60 X .011 screen weight ratio 36.1%

III.4.4 Shell Material 12 X 64 Rigimesh - 316 S.S.

Reference: "Transpiration Cooling through Rigimesh Sintered Woven Wire Sheet,"
March 1, 1964.

Shell Thickness (Inches)

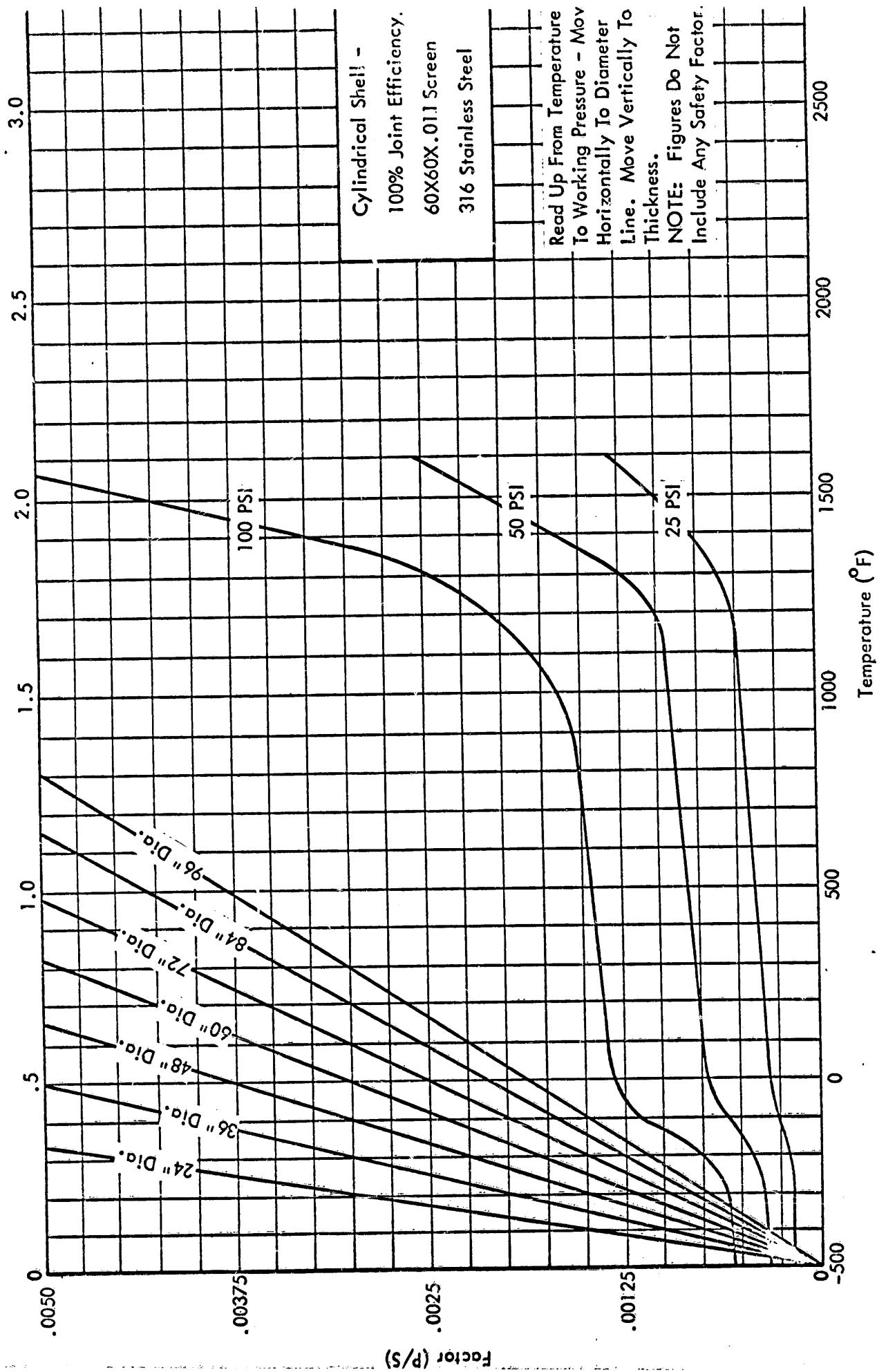


FIGURE III-9 SHELL THICKNESS FOR 60 X 60 X .011 SCREEN

Tensile Strength:

Tensile strength of 316 S.S. at 75°F = 75,000 PSI (See Figure III-6)

Tensile strength of 316 S.S. Rigimesh at 75°F = 31,400 PSI (See Bulletin)

Rigimesh strength ratio = 42%

Thickness multiplier = 2.42 times

Weight Calculations:

12 X 64 mesh .039 thick = L (Layers) X .75 lbs. (Page 4, Bulletin)

Obtain weight of 1 sq. ft., 1" thick

$1.00 \div .039 = 25.7 \text{ Layers}$

$25.7 \times .75 \text{ lbs.} = 19.29 \text{ lbs.}$

Weight of 1 sq. ft. 1" solid 316 S.S. plate = 42.58 lbs.

Weight of 1 sq. ft. 1" Rigimesh, 316 S.S. = 19.29 lbs.

Rigimesh weight ratio = 45.5%

III. 4.5 Shell Material Perforated Screen 40 Mesh

Reference: Dimensions obtained from "Design News", Page 51, January 1951.

Tensile Strength:

Effective tensile per linear inch

$.013" = \text{Tensile area}$

$\frac{.012}{.025} = \frac{\text{Open area}}{\text{Total pitch}}$

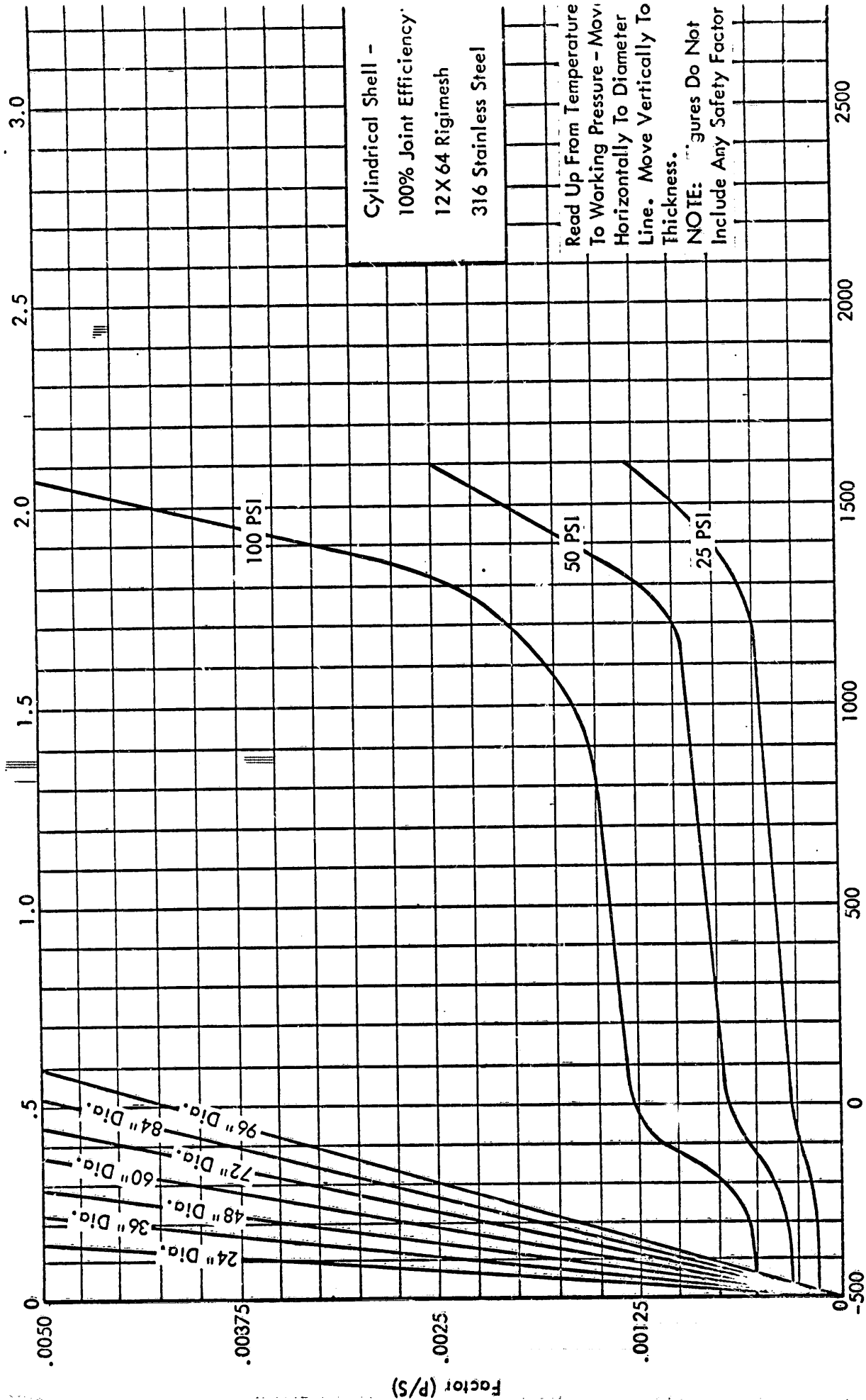
$1.00 \div .025 = 40 \text{ pitch/inch}$

$.013" \times 40 = .520 \text{ inches or tensile}$

40 Mesh strength ratio = 52%

Thickness multiplier = 1.93 times

Shell Thickness (Inches)



Cylindrical Shell -
100% Joint Efficiency
12 X 64 Rigimesh
316 Stainless Steel

Read Up From Temperature
To Working Pressure - Move
Horizontally To Diameter
Line. Move Vertically To
Thickness.

NOTE: Figures Do Not
Include Any Safety Factor

FIGURE III-10 SHELL THICKNESS FOR 12 X 64 RIGIMESH

Weight Calculations:

100% - 52% = 48% Open area each direction

.48 X .48 = 23% Open area

40 Mesh screen weight ratio = 77%

III.4.6 Shell Material Efficiency

Strength Ratio - Using solid plate at 100%

(1)	Solid 316 Stainless Steel	100%
(2)	60 X 60 X .011 Screen, Type 316	18.7%
(3)	12 X 64 Rigimesh, Type 316	42.0%
(4)	Perforated Screen, 40 Mesh Type 316	51.8%
(5)	Sintered Stainless, 316 Stainless Steel	
	Pall Type "C" (165 Micron)	9.3%
	Pall Type "D" (65 Micron)	12.0%

III.5 WEIGHT ANALYSIS

III.5.1 Weight Analysis, General

All weights based on one sq. ft. of Type 316 Stainless Steel, 1/4" thick equals 10.646 lbs.

Dished Heads:

All weights based on A.S.M.E. dished head with radius of dish equal to diameter, knuckle radius equal to 6% of dish radius and straight flanges as follows:

Up to 42", 2" wide flange
43 to 90", 3" wide flange

Shell Thickness (Inches)

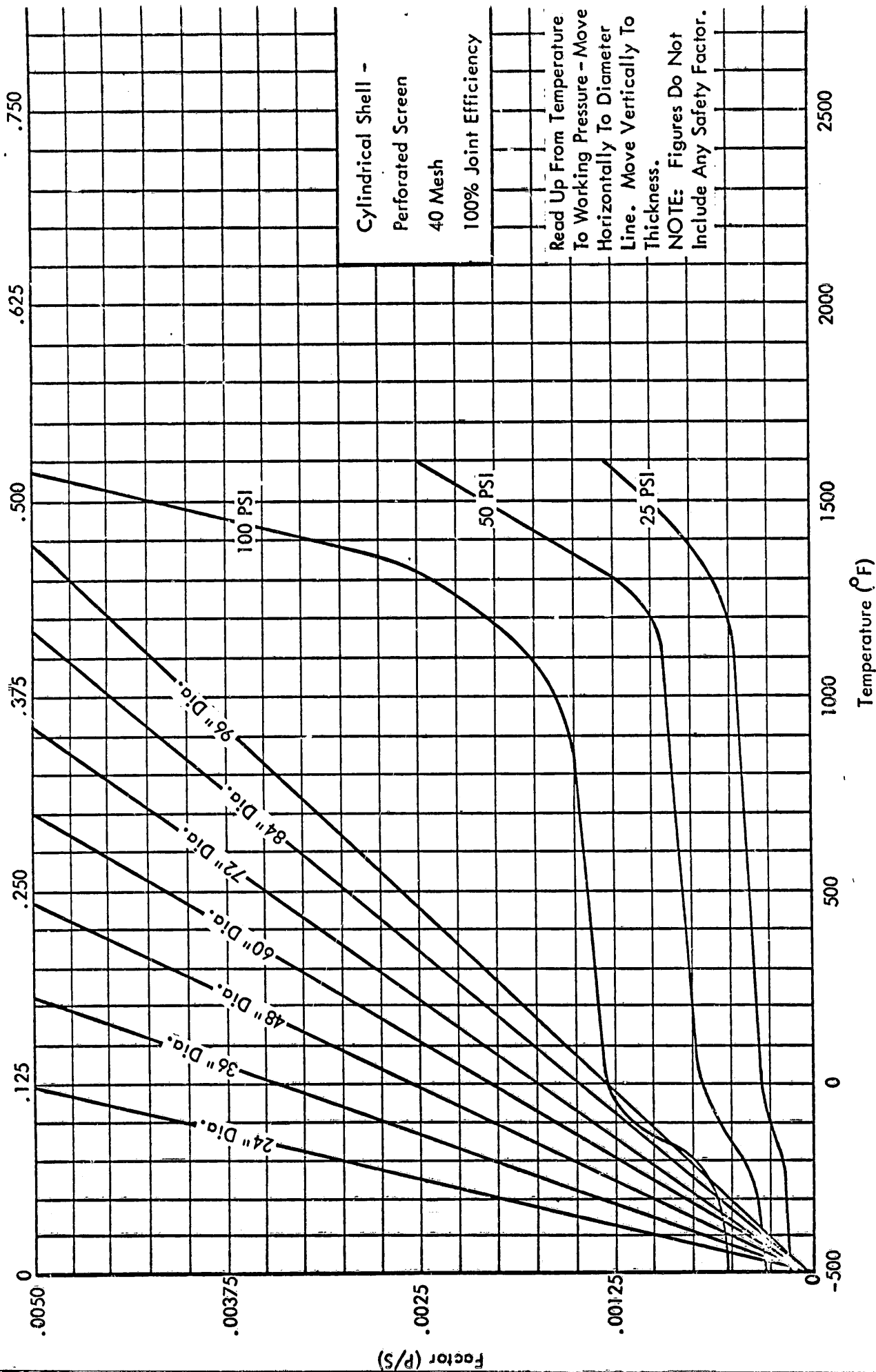


FIGURE III-11 SHELL THICKNESS FOR 40 MESH PERFORATED SCREEN

Over 90", 4" wide flange

Base Weight Reference: "Fogle's Tank and Pressure Vessel Book" for A.S.M.E.
Code, 1963 - converted from published mild steel weights to stainless steel
weights.

Hemispherical Heads:

All weights based on square footage as calculated by the formula:

$$\frac{D^2 \pi}{2}$$

Flat Heads:

All weights based on square footage determined by inside diameter. No allowance made for additional diameters required for shell to head joints.

Shell Materials:

See shell selection. Basis of weight calculations covered under each individual material.

Weight Ratios for shell materials:

(1)	Solid 316 Stainless	100%
(2)	60 X 60 X .011 Screen	36.1%
(3)	12 X 64 Rigimesh	45.5%
(4)	Perforated Screen, 40 Mesh	77.0%
(5)	Sintered Stainless	
	Pall Type "C"	45.0%
	Pall Type "D"	50.0%

III.6 STRENGTH TO WEIGHT

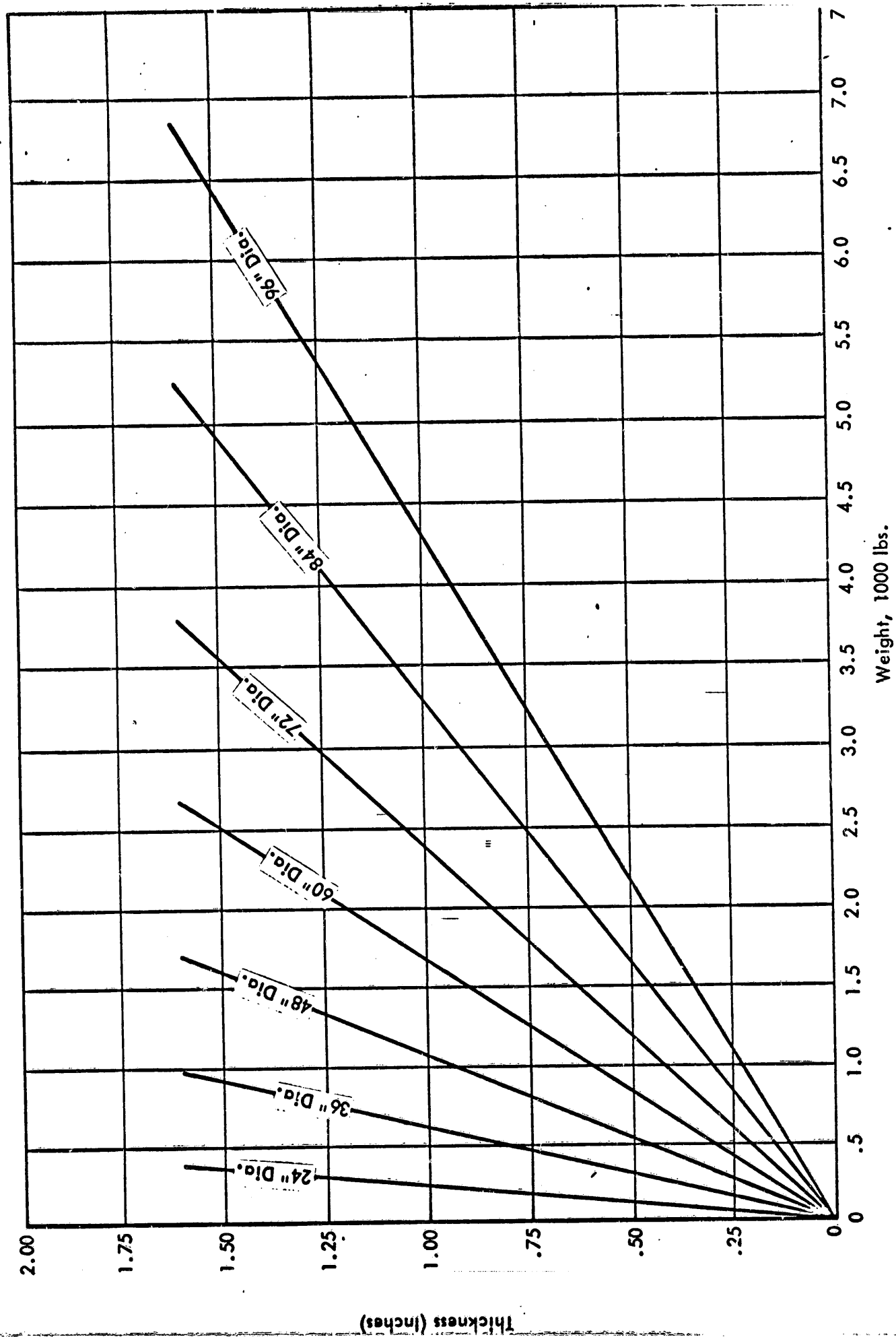
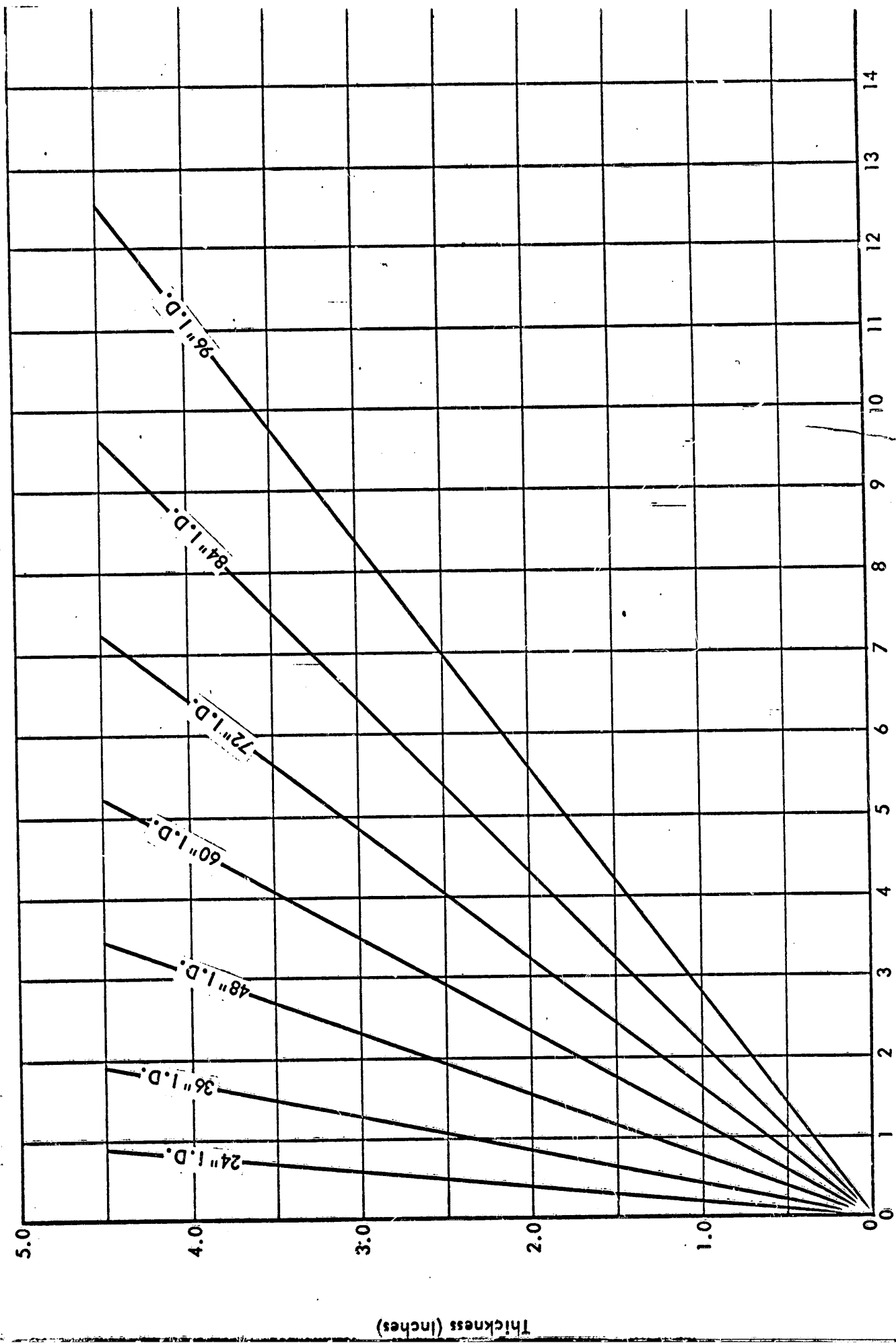


FIGURE III-12 WEIGHT OF HEMISPHERICAL HEAD



Weight, 1000 lbs.

FIGURE III-13 WEIGHT OF DISHED HEAD

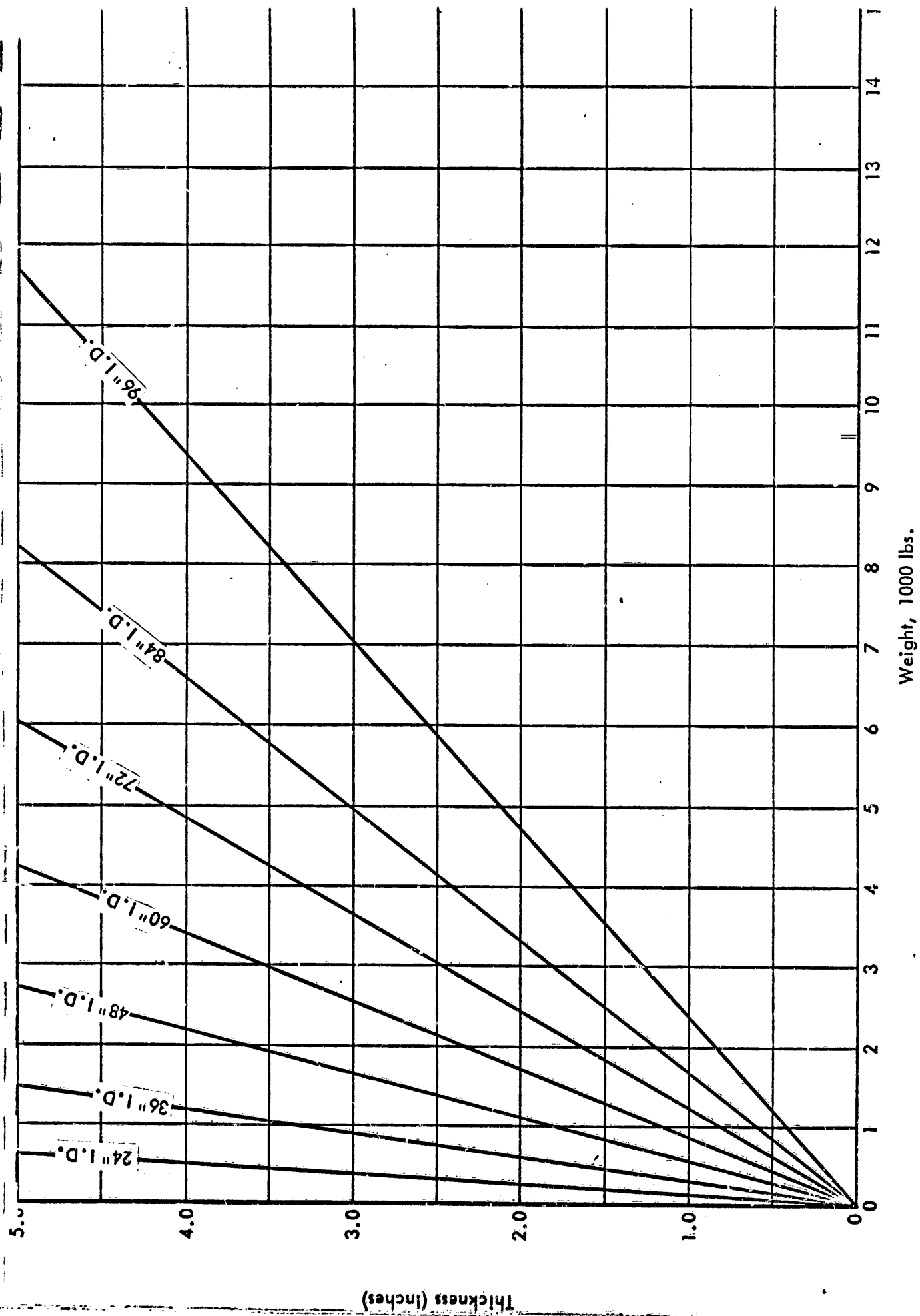


FIGURE III-14 WEIGHT OF FLAT HEAD

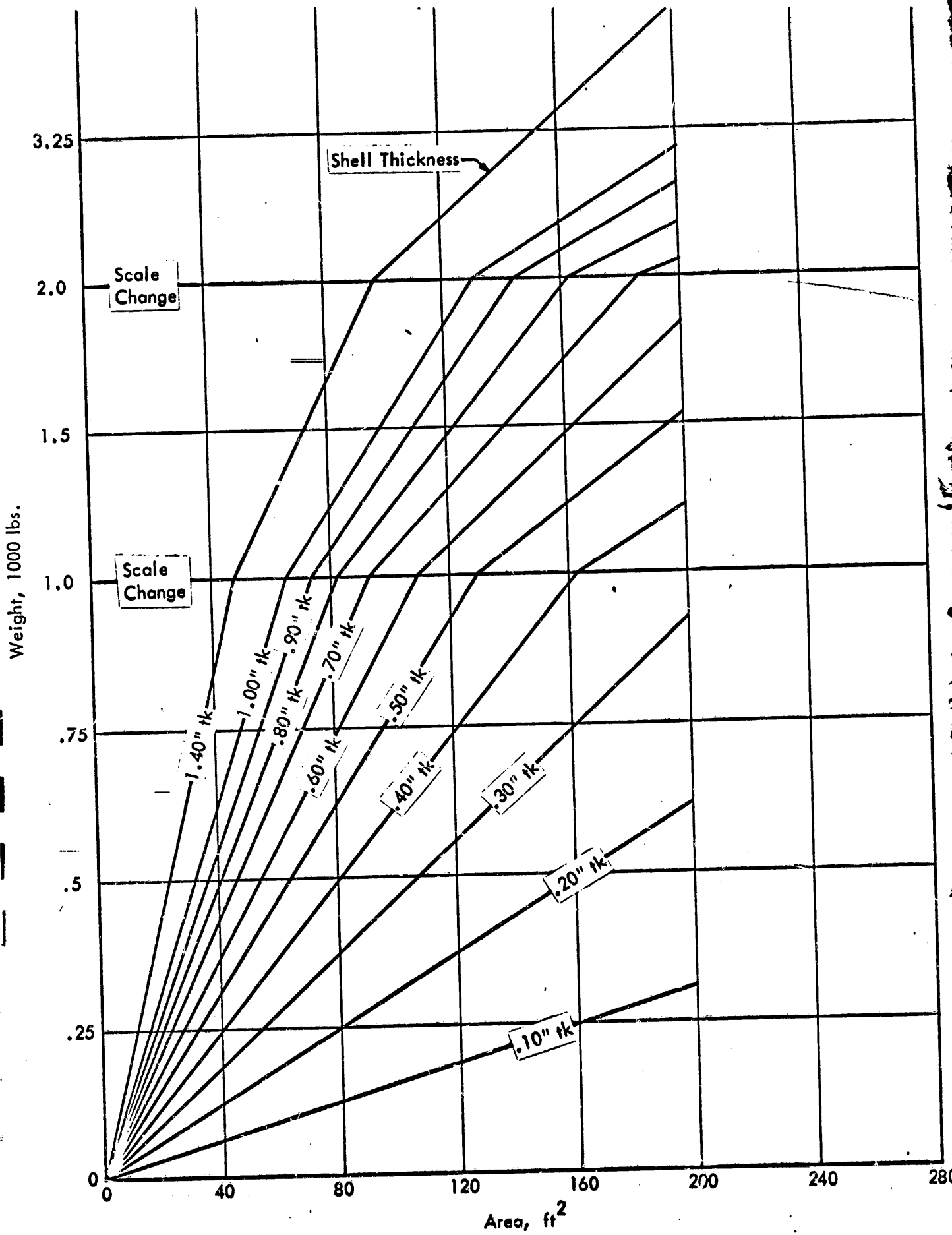


FIGURE III-15 WEIGHT OF 60 X 60 X .011 SCREEN SHELL

Weight, 1000 lbs.

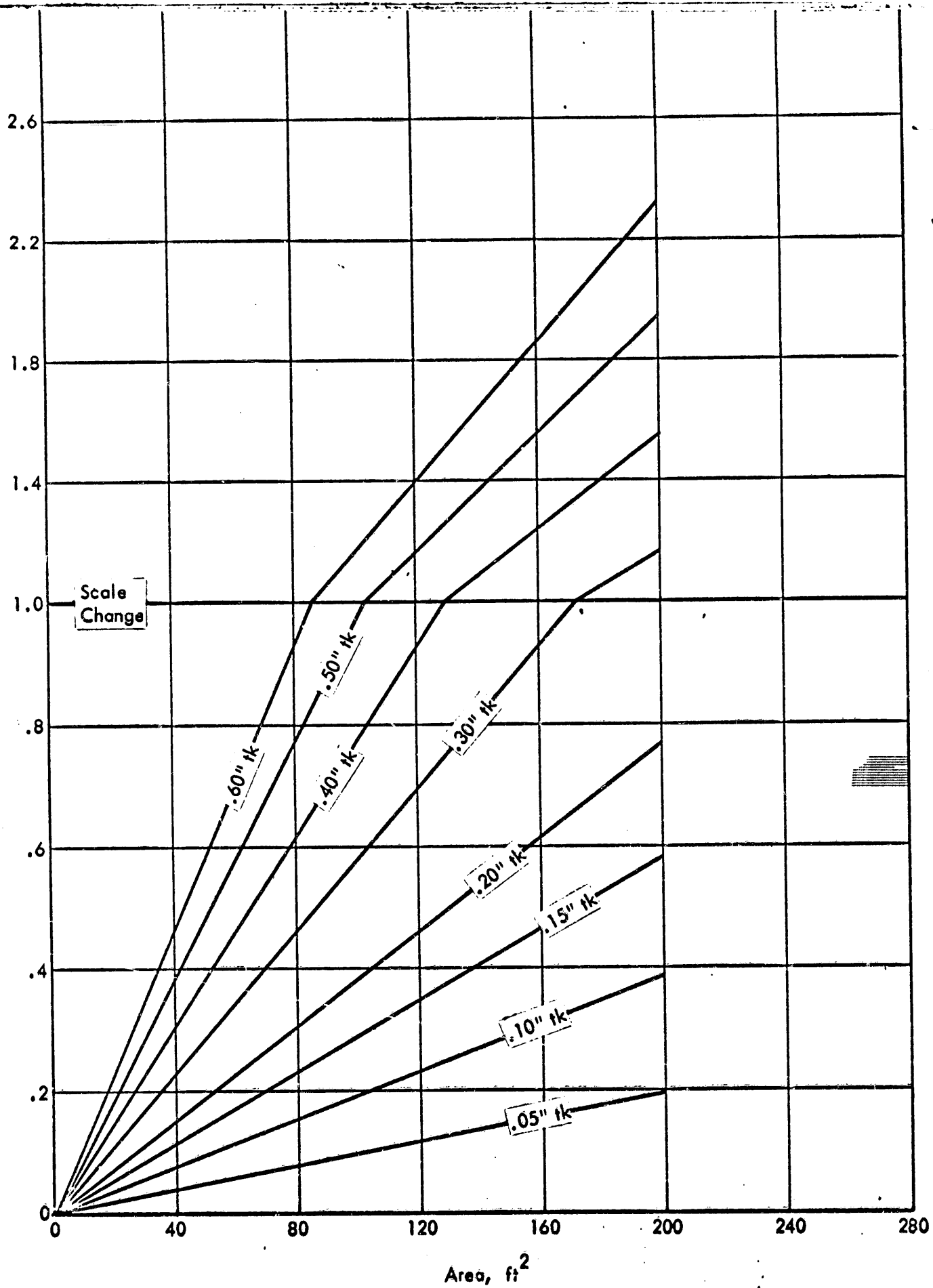


FIGURE III-16 WEIGHT OF 12 X 64 RIGIMESH SHELL

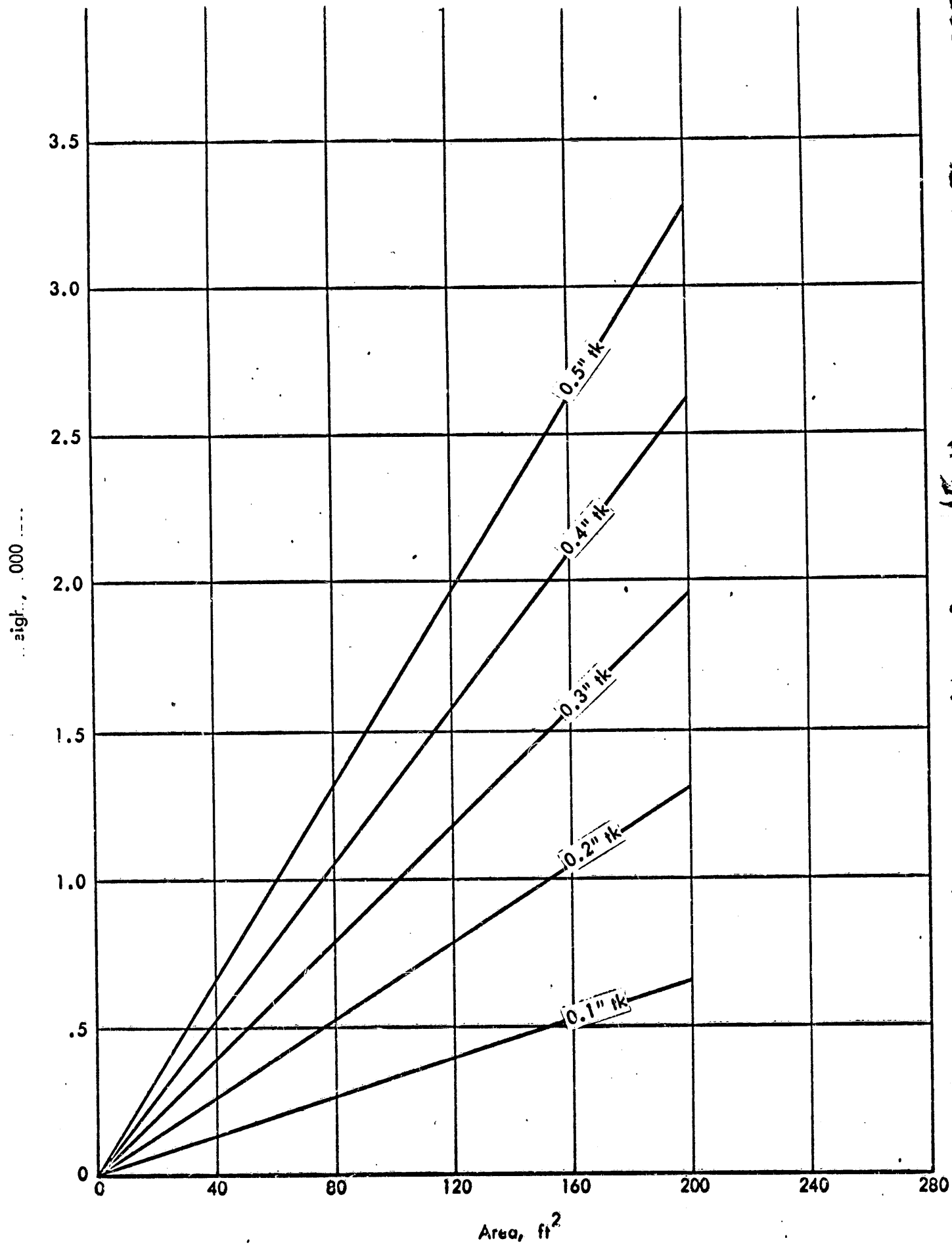


FIGURE III-17 WEIGHT OF 40 MESH PERFORATED SCREEN SHELL

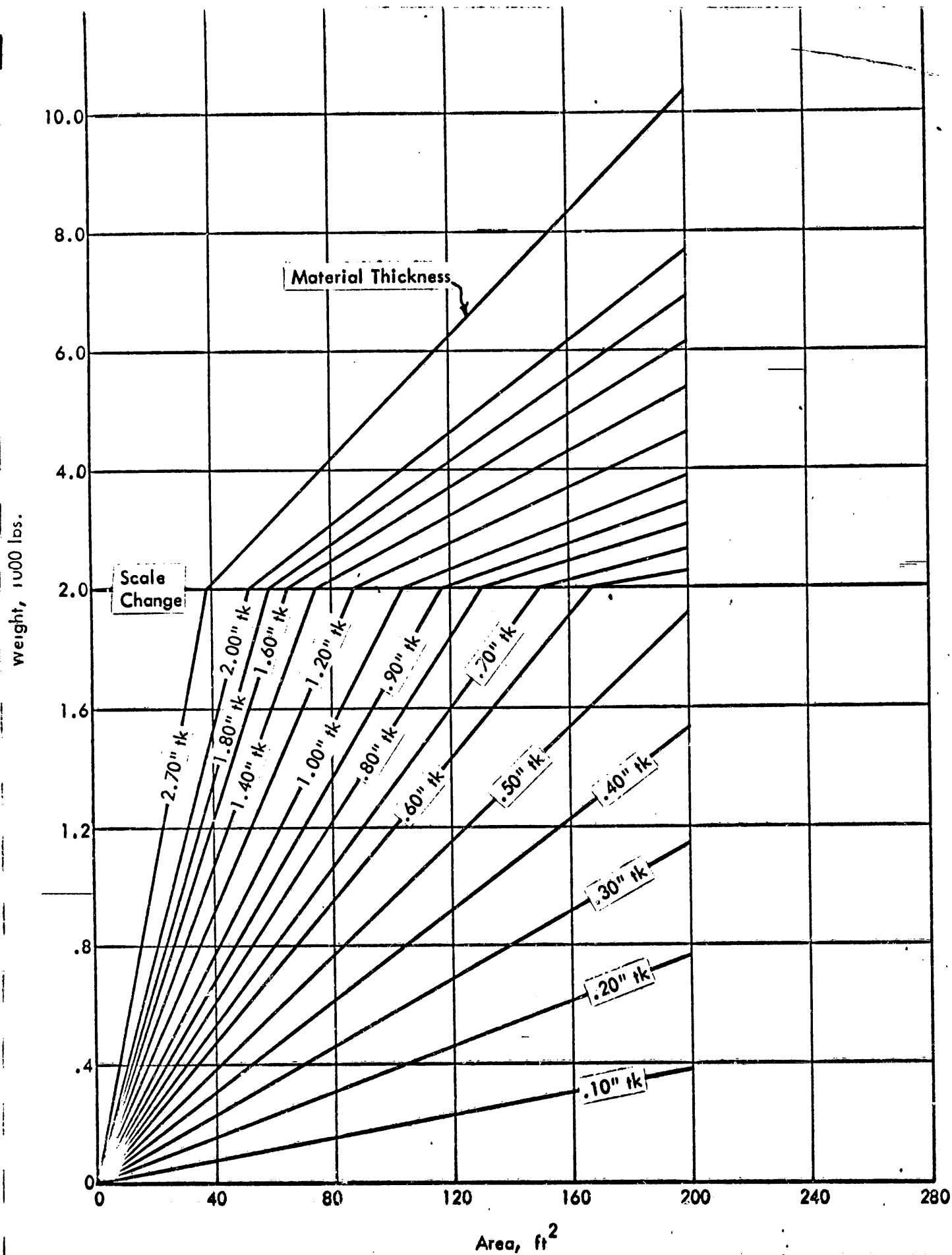


FIGURE III-18.A WEIGHT OF TYPE "C" SINTERED SHELL

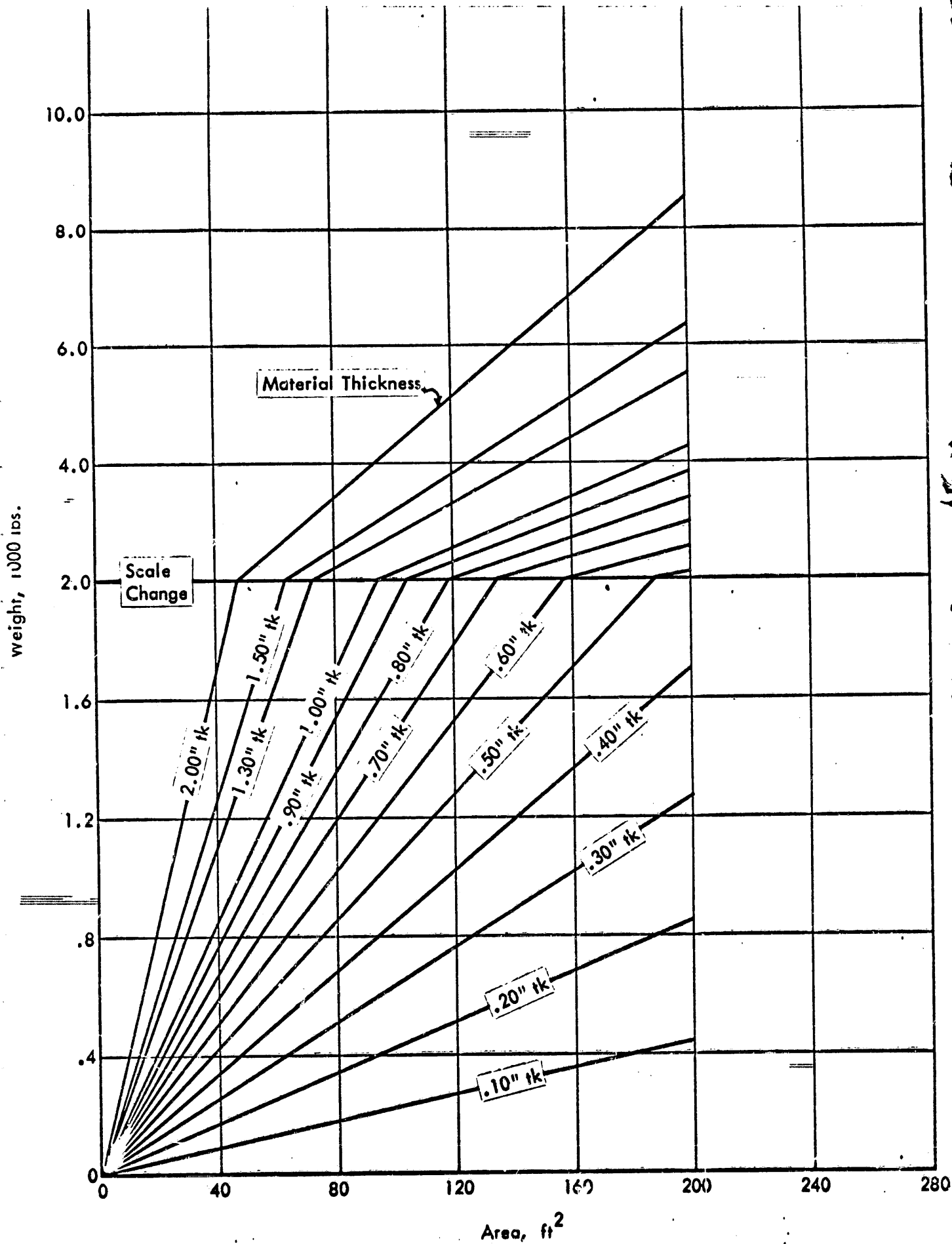


FIGURE III-18.B WEIGHT OF TYPE "D" SINTERED SHELL

III.6.1 Strength To Weight - General

Shell Size:

Aspect ratio L/D does not matter for weight selection. The only factor to consider here is for minimum total weight, the aspect ratio should be as high as possible as this will keep the head diameter to a minimum.

Shell Material:

For the ultimate in weight saving, a material with as high a strength to weight ratio as possible should be selected. The respective ratios are as follows:

(1)	Solid Stainless, 316	100% (Base)
(2)	60 X 60 X .011 Screen	68%
(3)	12 X 64 Rigimesh	92%
(4)	Perforated Screen, 40 Mesh	67%
(5)	Sintered Stainless	
	Pall Grade "C"	21%
	Pall Grade "D"	24%

Head Shape:

Head shape is a large factor to weight for a given thickness or pressure.

Hemispherical - Lightest Weight

Dished - Intermediate Weight

Flat - Heaviest Weight

Weight Examples:

Heaviest Design - Aspect ratio = 1, Head shape = Flat.

Lightest Design - Aspect ratio = 10, Head shape = Hemispherical.

III.7 DIMENSIONS

III.7.1 Dimensions, General

Shell:

Determine aspect ratio (L/D) from Figure III-2. Divide overall length by aspect ratio to obtain diameter.

Heads:

- (1) Hemispherical - Overall height is equal to $1/2$ the diameter plus the thickness.
- (2) Dished - Refer to Figure III-19. Please note that heads have straight flanges as follows:
 - Up to and including 42" diameter = 2"
 - Up to and including 90" diameter = 3"
 - Over 90" diameter = 4"
- (3) Flat - Overall height = to thickness.

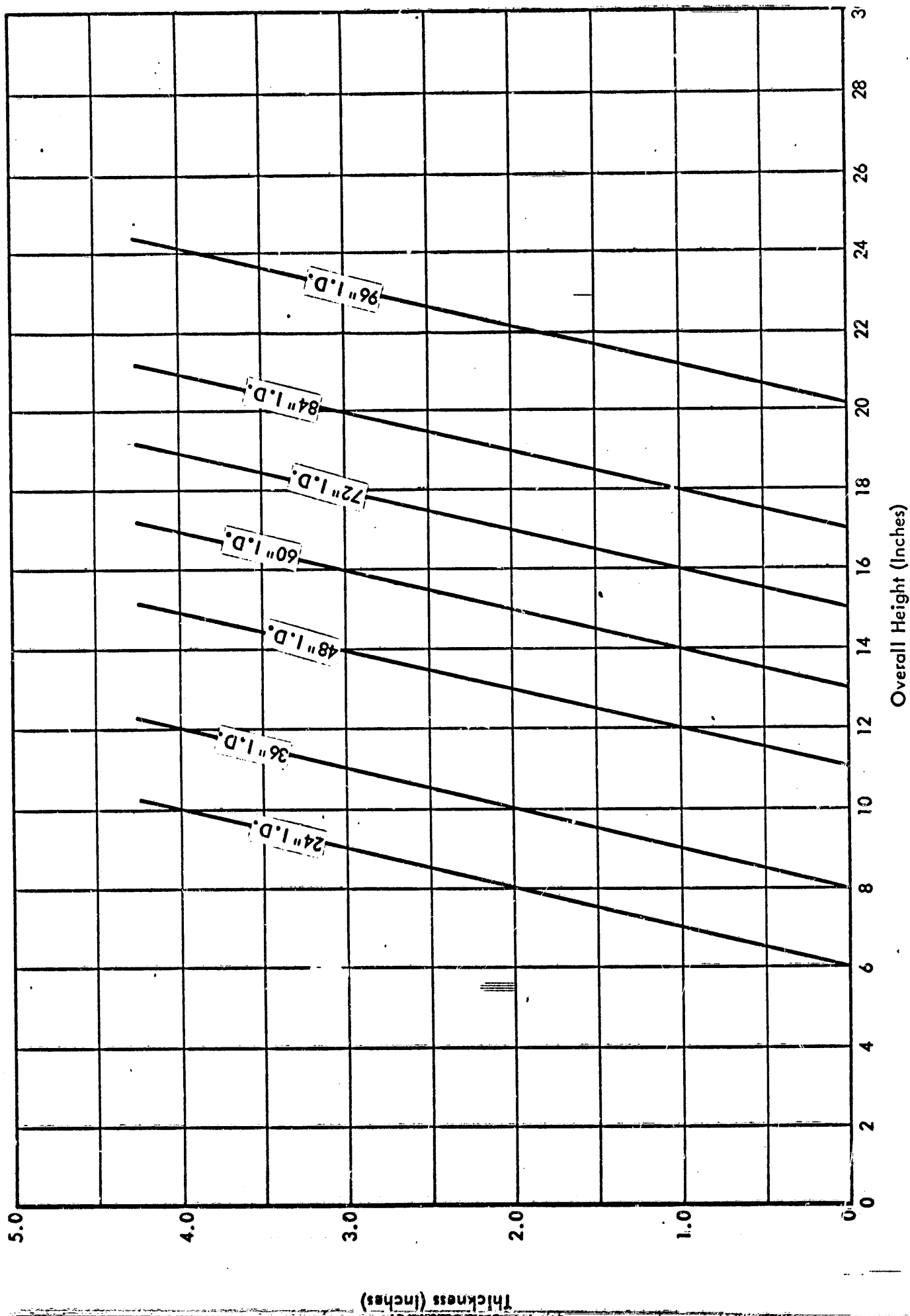


FIGURE III-19 HEIGHT OF FLANGED AND DISHED HEAD

REFERENCES

1. Eckert, E. R. G., and Thomas W. Jackson: "Analysis of Turbulent Free-Convection Boundary Layer on Flat Plate, " NACA TR 1015, 1951.
2. Cornell Aeronautical Laboratory, Inc.: "Theoretical and Experimental Studies of Impinging Uniform and Non-Uniform Jets, " TRECOM TR 64-42, August 1964.
3. Kurz, M. G.: "Transpiration Cooling Through Rigimesh Sintered Woven Wire Sheet, " APM-FSR-18A, Aircraft Porous Media, Inc., November 1964.
4. Pall Trinity Micro Corporation: "PSS Sintered Stainless Steel Filters and Other Porous Metals, " Bulletin M201A, 1963.
5. Repko, L. L.: "Pressure Drop Across Various Commercial Screens, " Design News, January 1951.
6. Kays, W. M., and A. L. London: Compact Heat Exchangers, McGraw-Hill Book Co., Inc., New York, 1958.
7. Lockheed-Georgia Company: "Main Propellant Tank Pressurization System Study and Test Program, Volume IV, Computer Program, " Lockheed-Georgia Company ER-5296, SSD-TR-61-21 Volume IV, December 1961.
8. Klinkenburg, A., and H. H. Mooy: "Chemical Engineering Progress, " 44:17 (1948).
9. Knudsen, J. G., and D. L. Datz: Fluid Dynamics and Heat Transfer, McGraw-Hill Book Co., Inc., New York, 1958.